AUGUST 2020 Ph.D. in Electrical and Electronics Engineering MUHAMMAD UMAIR KHAN

REPUBLIC OF TURKEY

GAZİANTEP UNIVERSITY

GRADUATE SCHOOL OF NATURAL & APPLIED SCIENCES

ROBUST ADAPTIVE TYPE-2 NEURAL FUZZY SLIDING MODE CONTROL OF A CLASS OF NONLINEAR SYSTEMS

Ph.D. THESIS

IN

ELECTRICAL AND ELECTRONICS ENGINEERING

BY

MUHAMMAD UMAIR KHAN

AUGUST 2020

ROBUST ADAPTIVE TYPE-2 NEURAL FUZZY SLIDING MODE CONTROL OF A CLASS OF NONLINEAR SYSTEMS

Ph.D. Thesis

in

Electrical and Electronics Engineering

Gaziantep University

Supervisor

Assoc. Prof. Dr. Tolgay KARA

by

Muhammad Umair KHAN

August 2020

I hereby declare that all information in this document has been obtained and presented in accordance with academic rules and ethical conduct. I also declare that, as required by these rules and conduct, I have fully cited and referenced all material and results that are not original to this work.

Muhammad Umair KHAN

ABSTRACT

ROBUST ADAPTIVE TYPE-2 NEURAL FUZZY SLIDING MODE CONTROL OF A CLASS OF NONLINEAR SYSTEMS

KHAN, Muhammad Umair
Ph.D. in Electrical and Electronics Engineering
Supervisor: Assoc. Prof. Dr. Tolgay KARA
August 2020
101 pages

This study aims to develop an adaptive control scheme for the control of a class of flexible multi-body nonlinear systems with infinite dimensions and extremely coupled dynamics. The finite-dimensional model is obtained by the assumed modes method (AMM) but there are uncertainties in the truncated model, which makes the system a challenging control problem. The proposed adaptive control scheme is the hybrid of the sliding mode control (SMC) and the type-2 neural fuzzy system (NFS). A newly modified conjugate gradient (CG) algorithm is used to optimize the NFS parameters, thus enhancing its self-adapting capabilities. The control law of the proposed control scheme requires the estimation of the unknown system functions, which is provided by the adaptive NFS. The stability of the control scheme is guaranteed by the Lyapunov stability theorem. Several other intelligent control schemes have also been tested to provide a comparison with the proposed control scheme. The simulation results clearly show that the proposed control scheme improves tracking efficiency while managing the inherent deflections of the system, making it an appropriate adaptive control technique for the class of flexible multi-body nonlinear systems.

Key Words: Neural Fuzzy Systems, Assumed Mode Method, Steepest Descent, Conjugate Gradient, Flexible Nonlinear Systems, Sliding Mode Control

ÖZET

BİR DOĞRUSAL OLMAYAN SİSTEMLER SINIFININ GÜRBÜZ UYARLANIR TİP-2 SİNİRSEL BULANIK KAYAN KİPLİ KONTROLÜ

KHAN, Muhammad Umair
Doktora Tezi, Elektrik ve Elektronik Mühendisliği
Danışman: Doç. Dr. Tolgay KARA
Ağustos 2020
101 sayfa

Bu çalışmanın amacı aşırı birleşik dinamikleri ve sonsuz sayıda boyutu olan, esnek çok elemanlı doğrusal olmayan sistemler sınıfının kontrolü için bir uyarlamalı kontrol şeması tasarlamaktır. Modların süperpozisyonu yöntemiyle (AMM) sonlu sayıda boyutlu bir model elde edilir, ancak kesilmiş modelde sistemi zor bir kontrol problemi haline getiren belirsizlikler mevcuttur. Önerilen uyarlamalı kontrol şeması kayan kipli kontrol (SMC) ile tip-2 sinirsel bulanık sistemin (NFS) melezidir. NFS parametrelerini optimize etmek için yeni değiştirilmiş eşlenik gradyan (CG) algoritması kullanılmıştır, böylece kendi kendini uyarlama yetenekleri geliştirilmiştir. Önerilen kontrol şemasının kontrol kuralı belirsiz sistem fonksiyonlarının tahminini gerektirir ki bunlar uyarlamalı NFS tarafından sağlanır. Kontrol sisteminin kararlılığı Lyapunov kararlılık teoremi kullanılarak sağlanmıştır. Önerilen kontrol şemasıyla karşılaştırmak amacıyla çeşitli diğer akıllı kontrol şemaları da test edilmiştir. Benzetim sonuçları açık biçimde önerilen kontrol şemasının sistemin doğal sapmalarını yönetmenin yanı sıra takip verimliliğini de iyileştirdiğini, bu nedenle doğrusal olmayan esnek çok elemanlı sistemler sınıfı için güvenilir bir teknik olduğunu açıkça ortaya koymuştur.

Anahtar Kelimeler: Sinirsel Bulanık Sistemler, Modların Süperpozisyonu Yöntemi, En Dik Iniş, Eşlenik Gradyan, Esnek Doğrusal Olmayan

"Dedicated to my family"

ACKNOWLEDGEMENTS

First and foremost, I would like to thank God Almighty for providing me with the capability, knowledge, and motivation to carry out this research study and to complete it successfully.

I would like to express my special appreciation and gratitude to my supervisor, Dr. Tolgay Kara, for supporting me in my study, for encouraging my research and for inspiring me to develop as a research scientist. His advice and support for both research and my career have been priceless. I would like to thank Prof. Dr. Arif Nacaroğlu and Dr. Hasari Karci for serving as my thesis monitoring committee members and later being the part of my thesis defense jury. Their valuable suggestions and comments on my reports and thesis have helped me improve the quality of the thesis. I am also thankful to Dr. Alkan Alkaya and Dr. Sema Kayhan for being part of my thesis defense jury. Their appreciation and advice have given me inspiration and motivation for my future research.

I am grateful to Turkiye Bursları, Turkey Government Scholarships, for providing me with a scholarship to complete my education.

My sincere thanks to my colleagues for their support on a number of occasions, and above all, I would like to thank my family for their endless love, patience, prayers, and emotional support.

TABLE OF CONTENTS

LIST OF TABLES

Page

LIST OF FIGURES

Page

LIST OF SYMBOLS

b_{ij}	consequent variables
Λ_{ij}	fuzzy membership function vectors
A_i	rigid transformation matrix
$\overline{\delta}_{\gamma'}$	generalized coordinates for the appendage
K_S	stiffness matrix for the satellite system
Q_S	input weighting matrix for the satellite system
r_i	absolute point along $\left\{\hat{X}_0, \hat{Y}_0\right\}$
$(\hat{\cdot})$	unit vector
$\left\{\hat{X}_i, \hat{Y}_i\right\}$	*ith* link flexible body moving coordinate frame
ρ	mass density of the appendages
J_t	rotary inertia of the *ith* tip mass
K	stiffness matrix
M_S	mass matrix for the satellite system
m_{tip}	mass density of the *ith* payload
w_s	generalized coordinates for the satellite system
$(MD)_i$	contribution of masses of distal links
α	learning rate
$\overline{\mu}_i$ & $\underline{\mu}_i$	upper and lower firing strengths
$\overline{p}_i$ & $\underline{p}_i$	upper and lower normalized DoF
χ	measurable states vector
χ_n & χ_{dn}	actual and desired trajectory
$\hat{f}$ & $\hat{g}$	estimated functions

$\{X_i, Y_i\}$	*ith* link rigid body moving coordinate frame
$\{\hat{X}_o, \hat{Y}_o\}$	inertial coordinate frame
φ	gradient vector
$\{\hat{b}_1, \hat{b}_2, \hat{b}_3\}$	body-fixed axis for satellite system
$\{n_1, n_2, n_3\}$	inertial reference axis for satellite system
${}^i r_{i+1} = {}^i p_i(l_i)$	position of origin of frame
c_i	consequent output parameters
C_T	vector of centrifugal and Coriolis forces for TLFM
$d(t)$	unknown bounded disturbance
e	error between the desired and actual trajectory
h	vector of centrifugal and coriolis forces
I_{hub}	rotary inertia of hub
K_T	stiffness matrix for TLFM
M	inertia positive definite matrix
m_{tip}	tip mass
Q	input weighting matrix
Q_T	input weighting matrix for TLFM
$u(t)$	control input variable
w_i	coordinate of a typical mass element measured along the undeformed ith beam
w_T	generalized coordinates for TLFM
d_i	distance of center of mass of link *i* from joint *i*
J_{oi}	inertia of link *i*
m_i	mass of link *i*
Q_R	input weighting matrix for the spacecraft system

T_p	kinetic energies associated with payload
v_{ij}	deformation moment of order 0 of mode *j* of link *i*
ω_{ij}	natural frequency of vibration
$C_{1,ij}$	coefficients in TLFM
J_{Li}	actual moment of inertia at the end of link *i*
l_i	*ith* link length
m_p & J_p	payload mass and moment of inertia
T_{hi}	KE associated with hubs
$(\dot{.})$	partial derivative with respect to time
$(.'')$	second partial derivative with respect to the w_i
$(.')$	partial derivative with respect to w_i
λ_{n-1}	Hurwitzian polynomial
$\phi_i(w)$	spatial mode shapes (or eigen function)
θ_S	rigid hub rotation angle
υ_{ij}	variance vector of the membership function
Ξ_{ij}	required parameter needed to be updated
ζ_{ij}	mean vector of the membership function
E	mean squared error
EI	appendage flexural rigidity of the *ith* beam
F	generalized force
$f(\chi,t)$ & $g(\chi,t)$	unknown non-linear bounded functions
L	Lagrangian
L_i	length of the *ith* appendage
M_T	inertia positive definite matrix for TLFM
r	hub radius

S	sliding surface
T	total KE
U	total PE
u^* & u_{des}	actual and desired output
V	Lyapunov function
x_j	input vectors
$z(w,t)$	elastic displacements
$\delta_i(t)$	time varying variables associated with spatial mode shapes
K_R	stiffness matrix for the spacecraft system
M_R	mass matrix for the spacecraft system
m_{hi} & J_{hi}	hub mass and moment of inertia
v_i	velocity of the deformed point
w_R	generalized coordinates for the spacecraft system
β_{ij}	frequency coefficients
$\dot{\alpha}_i$	absolute angular velocity
μ_i	firing strengths
ρ_i	uniform density
θ_i	*ith* joint angle
E_i	flexible link rotation matrix
M_{Li}	actual mass at the end of link *i*
p_i	inertial position vector
T_{app}	KE of appendages
T_{hub}	KE of hub
T_{li}	KE associated to link *i*

T_{tip}	KE of appendage payloads
$z_i(w_i)$	*ith* link flexible transversal deflection

LIST OF ABBREVIATIONS

AMM	assumed modes method
ANFC	adaptive neural fuzzy control
ANFCT2	type-2 adaptive neural fuzzy control
BP	backpropagation
CG	conjugate gradient
DoF	degree of fulfillment
FEM	finite element method
FLC	fuzzy logic controller
GA	Genetic algorithm
HZ	Hager and Zang
IAE	integral absolute error
ISE	integral squared error
ITAE	integral time absolute error
ITSE	integral time squared error
KE	kinetic energy
LM	Levenberge-Marquardt
LPM	lumped parameter method
LQR	linear quadratic regulator
MHS	modified Hestenes-Stiefel
MIMO	multiple input multiple output
MSE	mean square error
NFS	neural fuzzy system
NN	neural network
PE	potential energy

RSFFA	rotating spacecraft with four flexible appendages
RSTFA	rotating satellite with two flexible appendages
SD	steepest descent
SMANFC-1	hybrid of SMC and type-1 ANFC
SMANFC-2	hybrid of SMC and type-2 ANFC
SMC	sliding mode control
SMNFC	hybrid of SMC and ANFC
TLFM	two link flexible manipulator
TSK	Takagi Sugeno Kang

CHAPTER 1

INTRODUCTION

This chapter discusses the motivation, objectives, and literature review of research. In addition, the contribution of this study and the organization of the thesis are discussed in this chapter.

1.1 Literature Review

Many physical systems have a high level of uncertainty and nonlinearity, making it difficult to control them. This has led to considerable efforts by researchers in recent years to improve the behavior of nonlinear systems by designing appropriate control schemes. These are model predictive control [3], H_∞ control [4, 5], fuzzy logic controller (FLC) [6,7], neural network (NN) control [8,9], SMC [10,11], and many other nonlinear control techniques [12–15].

The vast amount of uncertainty in some nonlinear systems complicates the development of an accurate mathematical model for such systems. This motivates the need for control schemes that are robust against uncertainties. SMC introduced by Utkin [16] is preferred in the literature because of its simplicity, better disturbance rejection, and robustness against parameter uncertainties [17]. The desired tracking of the trajectory is achieved in two phases in the SMC; the approaching phase during which the system states are controlled to approach the predefined sliding surface, and the sliding phase in which the trajectories reside on the sliding surface. Conventional SMC has the drawback that the control requires infinite switching to maintain the dynamics of the system on the sliding surface. This

phenomenon known as chattering is more likely in practical implementations due to the limitations of the actuator and signal delays. The conventional methods for dealing with this phenomenon are the use of integral sliding control [18], saturation approximation [19] and boundary layer technique [20]. These methods may mitigate the chattering effect, but most often there is a trade-off between tracking performance and start-up control, or between the time response and the thickness of the boundary layer [21]. Other well-known control techniques can be used in conjunction with the SMC to resolve the issues of the method. The FLC is effective in mitigating the limitations of the SMC [22,23]. In recent years, many researchers have used FLC and SMC combinations to develop a robust controller for nonlinear systems [24–27].

The FLC, originally introduced by Zadeh [28], is capable of approximating any continuous function on a compact set to a defined precision due to its universal approximation capability [29, 30]. It is useful when an accurate mathematical description of the system is unavailable, ill-modeled, or unachievable. Type-1 FLC has limitations that it has not been able to address larger numerical and linguistic uncertainties, while type-2 FLC is capable of handling uncertainties more effectively by taking into account uncertainties in membership functions. The interval type-2 FLC has many applications in the literature where it deals better with uncertainties [31–34]. A comparative analysis between type-1 FLC and type-2 FLC is presented in the literature [35, 36]. Compared to FLC, a NN controller is logically difficult to comprehend, but has strong learning capabilities [37].

The NFS offers the benefits of both schemes, such as superior learning skills, good interpretation, and integration of prior knowledge [38]. Usually, the steepest descent (SD) method is used to update the NFS parameters. SD method is widely known to have a slow learning speed when the search space is complex. It lacks global convergence and has poor convergence rate. The efficiency of the method

relies on the correct choice of the initial weights, and even a small difference in the parameters affects the outcome of the algorithm [39–41]. Lin, Le and Huynh have established an autonomous type-2 NFS for nonlinear identification and control of time-varying plants [42]. The parameters of the control system are modified using the SD method and the stability is established by the Lyapunov function approach. In recent years, many researchers have designed optimization algorithms to overcome the drawback of the conventional SD algorithm. Han, Lin, and Qiao have introduced an adaptive gradient algorithm to overcome the drawback of the traditional SD method in order to optimize the NFS parameters for nonlinear system modeling [43]. C. Juang and K. Juang have introduced a type-2 NFS scheme with the antecedent and consequent parts having the type-2 membership functions and the Takagi Sugeno Kang (TSK) rules, respectively [44]. Mai, Yang, and Qiao have proposed a new SD algorithm for the NN [45]. Their algorithm has a higher convergence rate and a better predictive precision. Lin and Le have developed a self-organizing interval type-2 NFS control for the anti-locking braking system [46]. The parameters are updated with the gradient descent algorithm. To optimize the algorithm, the particle swarm optimization method is used in determining the weights of all parameters. Khanesar and Kayacan have proposed a FLC-based type-2 scheme using the Levenberge-Marquardt (LM) algorithm, which offers the advantages of the SD and the Gauss-Newton theorem [47]. Their algorithm has a mechanism to avoid the computational burden normally seen in the traditional LM algorithm due to the inverse matrix problem. The results reveal an increased speed of the algorithm while the efficiency has remained relatively the same compared to the traditional LM algorithm. Mathew et al. have illustrated that the NFS if tuned by using a hybrid algorithm generates more accurate estimates than the LM algorithm or any other traditional algorithm [48].

1.2 Motivation and Methodology

The literature review explains the need for a robust, fast-tracking, and self-tuning hybrid control scheme. The SMC and type-2 NFS hybrid control scheme for robust control of a class of nonlinear systems is presented in this paper as a solution to the aforementioned problems. The hybrid control scheme delivers the benefits of both schemes and overcomes their shortcomings. In addition, an improved algorithm is used for the efficient tuning of type-2 NFS parameters. The proposed algorithm adjusts the search directions, thus achieving stable and faster operations, and has global convergence properties that are lacking in other conventional optimization methods, such as SD. Type-2 NFS with its self-tuning novel optimization algorithm (referred to hereafter as type-2 adaptive neural fuzzy control (ANFCT2)) estimates the parameters of the system and provides them to SMC control law. In order to make the system states reach the sliding surface more efficiently and to avoid the chattering problem in SMC, a separate ANFCT2 scheme is also used instead of the typically used switching control function. The ANFCT2 is therefore used for both identification and control purposes. Finally, the stability of the proposed control scheme is verified by the Lyapunov stability theory.

1.3 Aims and Objectives

The main aim of the research is to develop a self-tuning adaptive control strategy for the control of a class of nonlinear systems. These systems are a combination of rigid and elastic interconnected bodies attributed to the family of multi-body distributed parameter systems. They are highly nonlinear, infinite-dimensional, highly coupled systems described by hybrid coordinate systems of ordinary, partial, and integral differential equations. Three systems belonging to the such class of nonlinear systems are studied. The objectives covered during this research are:

- Studying a dynamic mathematical model of the studied systems belonging to the same class of nonlinear systems.
- Implementing these systems in Matlab/Simulink.
- Design of the control system that is robust and has an exceptional self-tuning mechanism.
- Integrating the proposed control scheme with the studied nonlinear systems.
- Comparative analysis and results discussion of the systems.

1.4 Organization of Thesis

The thesis is coordinated into six different chapters. The following is a general idea of what each chapter covers:

- Chapter 1 discusses the motivation, objectives, and literature review of research.
- Chapter 2 discusses the mathematical design and implementation of the proposed control scheme.
- Three nonlinear systems that belong to the same class of nonlinear systems are studied during this study. These three nonlinear systems are presented in two different chapters. Chapter 3 presents the mathematical modeling and discussion of the first two nonlinear systems.
- Chapter 4 discusses the mathematical modeling and discussion of the third nonlinear system.
- Chapter 5 presents simulation results, discussions, and a thorough analysis of all the nonlinear systems with the proposed control scheme.
- A brief overview of the research is provided in Chapter 6.

- Proofs of theorems associated with the proposed control scheme and its stability analysis are presented in the appendices.

CHAPTER 2

CONTROL SCHEME

2.1 Literature Review

Control schemes can mostly be categorized as: model-free or model-based. The model-based types are mostly feed-forward control strategies. Physical properties and vibrational effects must be carefully considered for the proper design of these types of control strategies. The disadvantage of these strategies is that they cannot give good results for changes and uncertainties in the systems. Model-free control strategies have feedback mechanisms usually measured from sensor and observer mechanisms. They are simpler techniques and can be efficient even in the case of uncertainties in the system. Furthermore, some model-free control schemes lie in the category of intelligent and robust schemes. Literature work related to all of these control schemes is provided in the following subsections.

2.1.1 Model-based Control Strategies

Optimal control and predictive control are examples of a model-based control strategy. Heidari, Korayem, Haghpanahi, and Batlle have used the optimal control technique for single-link flexible manipulator control [49]. The optimal control technique is the powerful model-based technique, which finds out the optimal control law for the dynamic system, to minimize the certain performance index or cost function. Non-minimum phase system problem in the flexible manipulator causes undershoot or time delay. This problem is handled by some researchers by using a model-based predictive control scheme. The controller predicts the

future changes in the output and by using these predictions the desired control input can be generated. Pradhan and Subudhi [50] have developed an adaptive model predictive control strategy for vibration and position control of a two-link flexible manipulator (TLFM). AMM is used for modeling the dynamics of TLFM. System identification is carried out with ARMAX technique.

2.1.2 Model-free Control Strategies

In the literature, more focus is being put on model-free control strategies to better address system uncertainties.

End-point acceleration feedback [51], velocity feedback control [52], and positive position feedback are some examples of the model-free control strategy. PID control is the most well-known, simple model-free control technique. Mahamood and Pedro [53] have used PID control strategy on two link flexible manipulator (TLFM) based on AMM model. The performance of the controller is evaluated on the basis of input tracking and vibration suppression capability. PID control strategy is not capable of adapting to changes in process parameters.

Intelligent Control Strategies

In real practice, uncertainties and disturbances can largely affect the system. Robust control, such as SMC, $H\infty$ control, and adaptive control, have the ability to perform better even in the presence of uncertainties in the system.

$H\infty$ is a model-free robust control scheme. The controller is robust to model uncertainties and is insensitive to parameter variations. In the literature, $H\infty$ is used along with other techniques, such as adaptive control [54] and PID [55], to give better performance. The drawback of the scheme is that the controller order should be at least equal to or greater than that of the process model. That is not

practical for real system implementation, as it complicates the computation.

Genetic algorithm (GA) is an intelligent model-free control scheme. GA is used together with SMC [56] and FLC [57] to improve the performance of the TLFM system. The disadvantage of GA is that it has a slower convergence rate.

SMC is the intelligent model-free popular control strategy. It is a nonlinear control strategy that can change the dynamics of the nonlinear system by the application of the discontinuous control signal, which ensures the system to slide along the system normal behaviors. This technique is efficient in dealing with modeling uncertainties, thus maintaining stability and consistent performance. The drawback is that more often it has a chattering problem, energy loss and can lead to plant damage. In the literature, a combination of SMC with other control strategies on a flexible manipulator has been applied. In [58], the neural fuzzy sliding mode is designed for a flexible manipulator system. Sanz and Etxebarria [59] have proposed a hybrid strategy comprising linear quadratic regulator (LQR) and SMC for TLFM. In order to overcome the disadvantages of SMC and to gain advantages, a combination of SMC and other intelligent control strategies is very beneficial.

With all the uncertainties in the system, the development of accurate mathematical modeling is a cumbersome task. Consequently, the use of self-tuning adaptive control strategies like FLC and NN have highly attracted the attention of recent researchers.

FLC is a model-free intelligent technique based on human expertise and knowledge. The general structure of the FLC consists of four components: these are rule-based, inference mechanism, fuzzification and defuzzification. The rule base component comprises rules to provide better action for the control of the system. In the fuzzification process, the crisp external input is converted into fuzzy input so that later on fuzzy related operations can be applied onto it. In the inference

engine, the best rule is selected to provide the desired response for the control of the system. Defuzzification then converts the fuzzified output value to the crisp value again, for the system to consider as an input. In the literature, FLC is used in combination with other control strategies for the control of flexible manipulators. Pradhan and Subudhi [60] have used the adaptive and FLC combination for the tip trajectory control of TLFM. Varying payloads are taken into consideration for checking the robustness of the control strategy. The drawback of FLC is that it is too dependable on human knowledge. If too many changes or uncertainties occur then there is a risk of failure of the FLC system and there is a need of changing the rules of the FLC system. To overcome this problem, an adaptive FLC system can be used. It has the ability to change the rule adaptively, to better deal with uncertainty. Li, Tong, and Lu have designed adaptive FLC for the control of a single flexible manipulator [61]. The designed controller is based on the TSK based modeling and linear matrix inequality analysis. The backstepping technique is used for tuning the parameters.

NN is a model-free intelligent control technique. It can be trained by using the input-output relation of the process system. The NN consists of three layers: input, hidden and output layer. NNs are of two types: feedforward and recurrent networks. In a feedforward network, signals move in one direction only from input to output. The network may already be tuned by offline learning. In recurrent networks, feedback connections are present. Recurrent networks are more popular because of their learning capability that can be used for better control of the uncertain systems. Parameters in recurrent NN can be updated online using the error that is fed back. Zhihong and Khorasani [62] have used the NN controller for a single-link flexible manipulator. The feedback error signal is used to tune the NN structure. Neto, Goes, and Nascimento have used multiple NNs for the control of a flexible manipulator [63]. Multiple NNs provides the opportunity of ensuring the proper tuning, but it is time-consuming and it needs much computation for tuning. Zhang, Yang, and Sun have developed the fusion

of SMC and NN for the control of TLFM [64].

To achieve more advantages, researchers are combining FLC and NN control, which provides better control and deals well with uncertainties. FLC can provide better interpretation of human knowledge in mathematical form, while NN can provide better training strategies for updating the parameters. Further details about FLC, NN and NFS can be found in [65–67]. Tinkir, Önen, and Kalyoncu have used NFS control for single-link flexible manipulator [68] . From the input-output data of a single-link flexible manipulator, tuning of the controller is achieved later the control is applied. Önen, Kalyoncu, Tinkir, and Botsali have designed NFS controller based on type-2 FLC system [69]. Tracking and vibration control of a flexible manipulator is taken out efficiently. Subudhi and Morris [70] have developed NFS control strategy. NN is based on radial basis functions. AMM is used for the dynamic modeling of TLFM. The performance of the controller is compared with PD, adaptive control, and fuzzy controller.

Proposed Control Mechanism

Literature work presented in the earlier sections shows researchers' trend of working on control strategies to make it more robust. Researchers use hybrid control techniques, so to make the control strategies robust and to tune the parameters more quickly.

NFS gained huge popularity among researchers because of their ability to train its parameters quickly from the input-output data. Backpropagation (BP) is the most popular and common training algorithm for NFS. It is established on the basis of SD algorithm. SD is widely known to have a poor convergence rate and it is dependent on parameters specified by the user, since no theoretical technique for choosing these parameters exists. The algorithm thoroughly depends on the appropriate selection of these parameters such as learning rate and initial weights.

Even a slight deviation in these values can make a difference in algorithm performance between the best or worse [71]. This results in a slow convergence rate, so even for simple problems, many iterations are needed to train a small network. This is why the BP algorithm occasionally is slow and convergence is not always upright. Some examples of NFS that have used BP algorithms based on SD are developed in [72, 73].

Newton method has better and faster convergence compared to first-order SD based techniques. Although, the Newton method requires complex computations with the increase of the number of parameters and is less efficient if the function is non-quadratic. Newton method requires a lot of information to compute the Hessian matrix that is a difficult task for larger systems. To deal with this problem, variable metric techniques can be used. The variable metric method tries to obtain estimates of the Hessian matrix by using its algorithm using information from current iterations. Fletcher and Powell [74] have developed the Davidon variable metric technique, also known as the quasi-Newton method for the first time. The reviews regarding various optimization techniques to improve the training efficiency are present in the literature [75,76]. Some of these methods are Fletcher-Reeves [77], Hestenes and Stiefel [78], Broyden-Fletcher-Goldfarb-Shano method and Polak-Ribiere method.

By using these optimization techniques or by using other such explored optimization techniques rather than SD in NFS system, new better control strategies could be developed. The new strategies can improve the efficiency of network training by adaptively adjusting the initial search direction. Consequently, better fast training methodologies could be achieved, which will be able to achieve a faster and more stable response. This motivated this study to use the novel optimization methodology that has global convergence properties and that provides better training of the NFS. SMC and NFS integration provides a robust control scheme, which has fast convergence.

2.2 Control Scheme

This section introduces a control scheme for the control of the above-mentioned class of nonlinear systems. Consider the general class of ηth order nonlinear system, expressed as (2.1), which covers a wide range of physical systems, including the systems discussed in the previous section [79].

$$\chi^{(\eta)} = f(\chi, t) + g(\chi, t)u(t) + d(t) \tag{2.1}$$

where, $\chi \in R^n$ is a vector of measurable states, $d(t)$ is unknown bounded disturbance such that $|d(t)| < D < \infty$ and D is the upper bound of external disturbance, $u(t) \in R^m$ is control input variable, $f(\chi, t) \in R^n$ and $g(\chi, t) \in R^{n \times m}$ are unknown nonlinear bounded functions.

Assumption 2.2.1. *Without loss of generality, it is assumed that* $g(\chi, t) > 0$*, and the system* (2.1) *is controllable.*

2.2.1 Control Law

The objective of the control scheme is to ensure that the system follows the specified trajectory. The tracking error is,

$$e = \begin{Bmatrix} e_1 \\ e_2 \\ . \\ . \\ . \\ e_n \end{Bmatrix} = \begin{Bmatrix} \chi_1 - \chi_{d1} \\ \chi_2 - \chi_{d2} \\ . \\ . \\ . \\ \chi_n - \chi_{dn} \end{Bmatrix} \tag{2.2}$$

where χ_n and χ_{dn} are the actual and desired trajectory, and e is the error between the desired and actual trajectory. Also

$$\dot{e}_i = e_{i+1}, \qquad i = 1, \ldots, n-1$$

A sliding surface is defined in (2.3).

$$S = e_n + \lambda_1 e_{n-1} + \ldots + \lambda_{n-1} e_1 \tag{2.3}$$

where the coefficients $\lambda_1 \ldots \lambda_{n-1}$ are the coefficients of the Hurwitzian polynomial [80]. A Lyapunov function (2.4) is defined, so to design the control law.

$$V = \frac{1}{2} S^2 \tag{2.4}$$

Derivative of V along the error trajectories is

$$\dot{V} = S\dot{S} = S\left[\dot{e}_n + \lambda_1 \dot{e}_{n-1} + \ldots + \lambda_{n-1}\dot{e}_1\right] \tag{2.5}$$

From (2.2) and (2.3), (2.5) can be written as

$$\dot{V} = S\left[\dot{\chi}_n - \dot{\chi}_{dn} + \lambda_1 e_n + \ldots + \lambda_{n-1} e_2\right] \tag{2.6}$$

or equivalently

$$\dot{V} = S\left[f(\chi) + g(\chi)\, u + d - \dot{\chi}_{dn} + \sum_{i=1}^{n-1} \lambda_i e_{n-i+1}\right] \tag{2.7}$$

To achieve the reaching condition, the control law (2.8) is derived from (2.7).

$$u = \frac{1}{\hat{g}(\chi)}\left[-\hat{f}(\chi) - \sum_{i=1}^{n-1} \lambda_i e_{n-i+1} + \dot{\chi}_{dn} + \Upsilon\right] \tag{2.8}$$

whereas, Υ in (2.8) is a function that helps system dynamics to reach the sliding phase. $\hat{f}$ and $\hat{g}$ are estimated functions since actual functions in (2.7) are unknown. These functions are estimated with type-2 adaptive neural fuzzy control (ANFCT2) in next section.

Remark 2.2.1. *The control law in* (2.8) *has no dynamic parameters, which makes it a model-free scheme.*

Remark 2.2.2. *The ANFCT2 estimates the unknown functions in the control law* (2.8)*. Furthermore, an another ANFCT2 produces the* Υ *term in order to mitigate the chattering phenomenon.This integration of SMC and ANFCT2 offers robustness as well as a fast-tracking response that is verified by the simulation results in the upcoming chapter.*

The ANFCT2 is presented in the next section. The stability analysis of the control scheme is presented in the Appendix A.

2.2.2 ANFCT2 Control

This section presents the proposed ANFCT2 scheme. The ANFCT2 structure is shown in Figure 2.1. It comprises many layers in which all the operations are performed. The ANFCT2 ith rule is described as [81–83]:

$$if\ x_1\ is\ \Lambda_{i1}(x_1) \ldots and\ x_n\ is\ \Lambda_{in}(x_n)\ THEN\ c_i = b_{i0} + b_{i1}x_1 + \ldots + b_{in}x_n \quad (2.9)$$

where x_j is the input vector, Λ_{ij} is fuzzy membership function, c_i is the output parameter, b_{ij} is the variable in the consequent part, $j = 1, \ldots, n$, $i = 1, \ldots, r$, and n and r are the number of inputs and number of rules, respectively. As the rule in (2.9) illustrates, the antecedent part of the ANFCT2 encompasses the input-output region by a fuzzy set and the mathematical functions are used in the consequent part to define the region. The fuzzification process takes place in the second layer, where the membership functions transform crisp values into fuzzy values. For fuzzification, fuzzy sets can be triangular, trapezoidal, sigmoidal, sinc and many other functions. Mitaim and Kosko [84] have used different membership functions and have achieved fast function approximations with the sinc membership function. The sinc membership function is defined as,

$$\Lambda_{ij}(x_j) = \frac{\sin\left(\dfrac{x_j - \zeta_{ij}}{\upsilon_{ij}}\right)}{\left(\dfrac{x_j - \zeta_{ij}}{\upsilon_{ij}}\right)} \quad (2.10)$$

$$= N(\zeta_{ij}, \upsilon_{ij}, x_j), \quad \zeta_{ij} \in [\zeta_{ij1}, \zeta_{ij2}] \quad (2.11)$$

where $i = 1, \ldots, r$, $j = 1, \ldots, n$, r denotes the number of rules, n denotes the number of inputs, $x_j \in R^n$ is the input vector, $\zeta_{ij} \in R^{r \times n}$ is the mean vector and $\upsilon_{ij} \in R^{r \times n}$ is the variance vector of the membership function. Fuzzy type-2 membership functions are taken into account with uncertain means and fixed

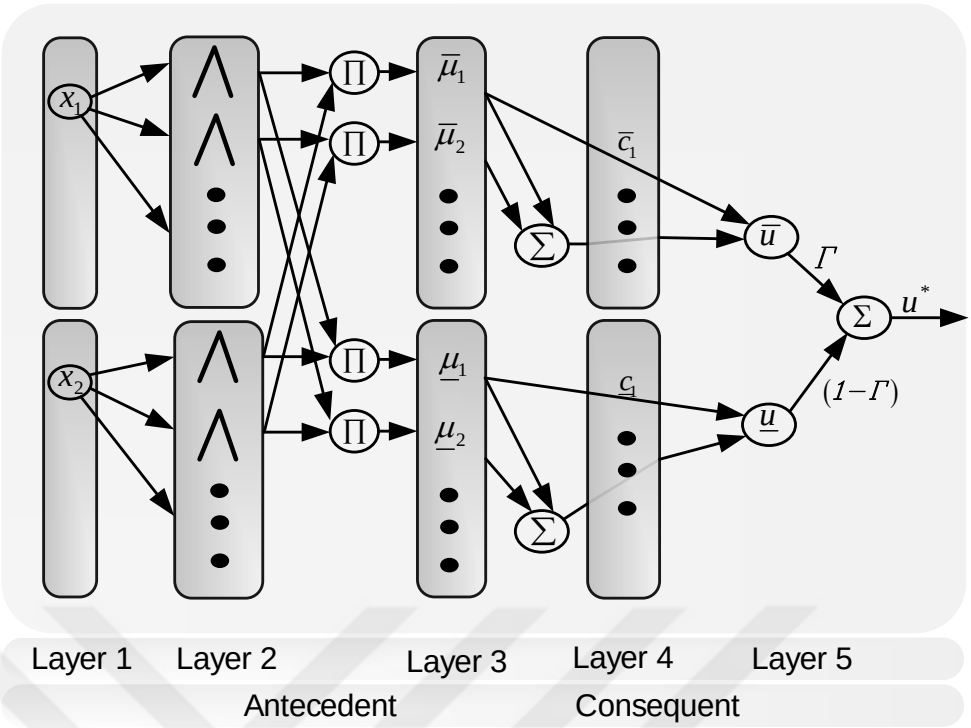

Figure 2.1 ANFCT2 structure

variances. Type-2 membership function is represented by upper (2.12) and lower (2.13) part.

$$\bar{\Lambda}_{ij}(x_j) = \begin{cases} N\left(\zeta_{ij1}, \upsilon_{ij}; x_j\right), & x_j < \zeta_{ij1} \\ 1 & \zeta_{ij1} \leq x_j \leq \zeta_{ij2} \\ N\left(\zeta_{ij2}, \upsilon_{ij}; x_j\right), & x_j > \zeta_{ij2} \end{cases} \tag{2.12}$$

$$\underline{\Lambda}_{ij}(x_j) = \begin{cases} N\left(\zeta_{ij2}, \upsilon_{ij}; x_j\right), & x_j \leq \frac{\zeta_{ij1}+\zeta_{ij2}}{2} \\ N\left(\zeta_{ij1}, \upsilon_{ij}; x_j\right), & x_j > \frac{\zeta_{ij1}+\zeta_{ij2}}{2} \end{cases} \tag{2.13}$$

The firing strengths $\mu_i \in \left[\underline{\mu}_i, \bar{\mu}_i\right]$ of the ANFCT2 rules are calculated in the third layer by multiplying the outputs of the previous layer; thus, the lower firing strengths ($\underline{\mu}_i \in R^r$) and the upper firing strengths ($\bar{\mu}_i \in R^r$) are calculated in this layer.

$$\bar{\mu}_i = \prod_{j=1}^{n} \bar{\Lambda}_{ij}(x_j), \quad \underline{\mu_i} = \prod_{j=1}^{n} \underline{\Lambda}_{ij}(x_j) \tag{2.14}$$

Consequent parameters $c_i \in [\underline{c}_i, \bar{c}_i]$ defined in (2.9) are in the fourth layer. The centroid defuzzification method is used to calculate the output (2.15) in the final layer.

$$u^* = (\Gamma)\bar{u} + (1 - \Gamma)\underline{u} \tag{2.15}$$

In (2.15), the ratio of the upper ($\bar{u} = \sum_i \bar{p}_i \bar{c}_i$) and lower output ($\underline{u} = \sum_i \underline{p}_i \underline{c}_i$) is adjusted by the scalar Γ, where $\bar{p}_i \in R^r$ and $\underline{p}_i \in R^r$, defined in (2.16), are normalized degree of fulfillment (DoF), and depict the normalized weights of individual firing rules.

$$\underline{p}_i = \frac{\underline{\mu}_i}{\sum_{j=1}^{r} \underline{\mu}_j}, \quad \bar{p}_i = \frac{\bar{\mu}_i}{\sum_{j=1}^{r} \bar{\mu}_j} \tag{2.16}$$

Self-Tuning Algorithm

The parameters in the antecedent and consequent layers are needed to be optimized. The cost function namely mean square error (MSE) (2.17) is used to optimize these parameters.

$$E = \frac{1}{2}(u^* - u_{des})^2 \tag{2.17}$$

where u^* and u_{des} in (2.17) are the actual and desired output respectively. The objective of the algorithm is to minimize the cost function by optimizing the parameters. The CG method is used for tuning of the parameters, which requires the gradient of the required parameters to be evaluated. BP method is used to find out the gradient vectors of the required parameters. The gradient vectors are the derivatives of MSE with respect to the required updated parameters. A general form of the gradient of MSE with respect to the antecedent membership function mean is defined by the chain rule as:

$$\frac{\partial E}{\partial \zeta_{ij}} = \frac{\partial E}{\partial u^*} . \frac{\partial u^*}{\partial \mu_i} . \frac{\partial \mu_i}{\partial \zeta_{ij}} \tag{2.18}$$

The gradient of MSE with respect to the antecedent membership function variance is,

$$\frac{\partial E}{\partial \upsilon_{ij}} = \frac{\partial E}{\partial u^*}.\frac{\partial u^*}{\partial \mu_i}.\frac{\partial \mu_i}{\partial \upsilon_{ij}} \tag{2.19}$$

The gradient of MSE with respect to the consequent parameters are,

$$\frac{\partial E}{\partial b_{i0}} = \frac{\partial E}{\partial u^*}.\frac{\partial u^*}{\partial c_i}.\frac{\partial c_i}{\partial b_{i0}} \tag{2.20}$$

$$\frac{\partial E}{\partial b_{ij}} = \frac{\partial E}{\partial u^*}.\frac{\partial u^*}{\partial c_i}.\frac{\partial c_i}{\partial b_{ij}} \tag{2.21}$$

The gradient of MSE with respect to Γ is,

$$\frac{\partial E}{\partial \Gamma} = \frac{\partial E}{\partial u^*}.\frac{\partial u^*}{\partial \Gamma} \tag{2.22}$$

where $\frac{\partial u^*}{\partial c_i} = \frac{\mu_i}{\sum\limits_j \mu_j(x_j)}$, $\frac{\partial u^*}{\partial \mu_i} = \frac{c_i - u^*}{\sum\limits_j \mu_j(x_j)}$, $\frac{\partial c_i}{\partial g_{i0}} = 1$, $\frac{\partial u^*}{\partial \Gamma} = (\bar{u} - \underline{u})$, $\frac{\partial E}{\partial u^*} = e$, and $\frac{\partial c_i}{\partial b_{ij}} = x_j$. The derivations for the particular mean and variance of upper and lower membership functions are determined as:

$$\frac{\partial \bar{\mu}_i}{\partial \zeta_{ij1}} = \frac{\partial \bar{\mu}_i}{\partial \bar{\Lambda}_{ij}(x_j)} \frac{\partial \bar{\Lambda}_{ij}(x_j)}{\partial \zeta_{ij1}} \tag{2.23}$$

$$= \begin{cases} \left[\bar{\Lambda}_{ij}(x_j) - \cos\left(\frac{x_j - \zeta_{ij1}}{\upsilon_{ij}}\right)\right] \frac{1}{x_j - \zeta_{ij1}}, & x_j \leq \zeta_{ij1} \\ 0, & otherwise \end{cases} \tag{2.24}$$

$$\frac{\partial \bar{\mu}_i}{\partial \zeta_{ij2}} = \frac{\partial \bar{\mu}_i}{\partial \bar{\Lambda}_{ij}(x_j)} \frac{\partial \bar{\Lambda}_{ij}(x_j)}{\partial \zeta_{ij2}} \tag{2.25}$$

$$= \begin{cases} \left[\bar{\Lambda}_{ij}(x_j) - \cos\left(\frac{x_j - \zeta_{ij2}}{\upsilon_{ij}}\right)\right] \frac{1}{x_j - \zeta_{ij2}}, & x_j > \zeta_{ij2} \\ 0, & otherwise \end{cases} \tag{2.26}$$

$$\frac{\partial \underline{\mu}_i}{\partial \zeta_{ij1}} = \frac{\partial \underline{\mu}_i}{\partial \underline{\Lambda}_{ij}(x_j)} \frac{\partial \underline{\Lambda}_{ij}(x_j)}{\partial \zeta_{ij1}} \tag{2.27}$$

$$= \begin{cases} \left[\underline{\Lambda}_{ij}(x_j) - \cos\left(\frac{x_j - \zeta_{ij1}}{\upsilon_{ij}}\right)\right] \frac{1}{x_j - \zeta_{ij1}}, & x_j > \frac{\zeta_{ij1} + \zeta_{ij2}}{2} \\ 0, & otherwise \end{cases} \tag{2.28}$$

$$\frac{\partial \underline{\mu}_i}{\partial \zeta_{ij2}} = \frac{\partial \underline{\mu}_i}{\partial \underline{\Lambda}_{ij}(x_j)} \frac{\partial \underline{\Lambda}_{ij}(x_j)}{\partial \zeta_{ij2}} \tag{2.29}$$

$$= \begin{cases} \left[\underline{\Lambda}_{ij}(x_j) - \cos\left(\frac{x_j - \zeta_{ij2}}{\upsilon_{ij}}\right)\right] \frac{1}{x_j - \zeta_{ij2}}, & x_j \leq \dfrac{\zeta_{ij1} + \zeta_{ij2}}{2} \\ 0, & otherwise \end{cases} \tag{2.30}$$

$$\frac{\partial \bar{\mu}_i}{\partial \upsilon_{ij}} = \frac{\partial \bar{\mu}_i}{\partial \bar{\Lambda}_{ij}(x_j)} \frac{\partial \bar{\Lambda}_{ij}(x_j)}{\partial \upsilon_{ij}} \tag{2.31}$$

$$= \begin{cases} \frac{1}{\upsilon_{ij}} \left[\bar{\Lambda}_{ij}(x_j) - \cos(\frac{x_j - \zeta_{ij1}}{\upsilon_{ij}})\right], & x_j \leq \zeta_{ij1} \\ \frac{1}{\upsilon_{ij}} \left[\bar{\Lambda}_{ij}(x_j) - \cos(\frac{x_j - \zeta_{ij2}}{\upsilon_{ij}})\right], & x_j > \zeta_{ij2} \\ 0, & otherwise \end{cases} \tag{2.32}$$

$$\frac{\partial \underline{\mu}_i}{\partial \upsilon_{ij}} = \frac{\partial \underline{\mu}_i}{\partial \underline{\Lambda}_{ij}(x_j)} \frac{\partial \underline{\Lambda}_{ij}(x_j)}{\partial \upsilon_{ij}} \tag{2.33}$$

$$= \begin{cases} \frac{1}{\upsilon_{ij}} \left[\underline{\Lambda}_{ij}(x_j) - \cos(\frac{x_j - \zeta_{ij2}}{\upsilon_{ij}})\right], & x_j \leq \frac{\zeta_{ij1} + \zeta_{ij2}}{2} \\ \frac{1}{\upsilon_{ij}} \left[\underline{\Lambda}_{ij}(x_j) - \cos(\frac{x_j - \zeta_{ij1}}{\upsilon_{ij}})\right], & x_j > \frac{\zeta_{ij1} + \zeta_{ij2}}{2} \end{cases} \tag{2.34}$$

Hager and Zang (HZ) algorithm [85] is an updated version of the Hestenes and Stiefel algorithm known as HS [86]. Dong, Liu, Xu and Yang have developed modified CG algorithms by modifying the HZ algorithm [87]. Motivated by this, the HZ algorithm has been modified in this study in a slightly different way and a new modified optimization algorithm has been developed which is called the modified Hestenes–Stiefel (MHS) algorithm. The general CG algorithm has the form,

$$\Xi_{ij}(\kappa + 1) = \Xi_{ij}(\kappa) + \alpha(k)\eta(\kappa) \tag{2.35}$$

where Ξ_{ij} is any required parameter that is needed to be updated, and α is the learning rate. The search direction for the MHS algorithm is,

$$\eta(\kappa) = \begin{cases} -\varphi(\kappa) & \left|\varphi(\kappa)^T \psi(\kappa - 1)\right| \geq \rho \left\|\varphi(\kappa)\right\| \\ -\varphi(\kappa) + \beta(\kappa)\eta(\kappa - 1) & \left|\varphi(\kappa)^T \psi(\kappa - 1)\right| < \rho \left\|\varphi(\kappa)\right\| \end{cases} \tag{2.36}$$

whereas,

$$\beta(\kappa) = \max\left\{0,\ \frac{\varphi(\kappa)^T\psi(\kappa-1)}{\eta(k-1)^T\psi(\kappa-1)} - \iota\frac{\varphi(\kappa)^T\eta(\kappa-1)}{\|\eta(\kappa-1)\|^2}\right\} \tag{2.37}$$

where $\varphi(\kappa) = \frac{\partial E}{\partial \Xi_{ij}(\kappa)}$ is the gradient vector, $\psi(\kappa-1) = (\varphi(\kappa) - \varphi(\kappa-1))$, and ι and ρ are the constants.

Figure C.9 shows ANFCT2 internal structure. Figure C.10 shows sinc membership function simulation module. Membership functions' switching module, mean variable update module, variance variable update module, consequent variable update module, and algorithm module are shown in Figures C.11, C.12, C.13, C.14 and C.15, respectively. Variable names may differ from what is presented in the main text of the thesis.

Assumption 2.2.2. *The general assumptions for the convergence analysis of the CG method are considered [88]. The set* $\Delta = \{\,\bar{z} \in R^n |\, E(\bar{z}) \leq E(\bar{z}_0)\}$ *is bounded, where* $\bar{z}_0$ *is a given point. In some region* Δ_o *of* Δ*, E function is continuously differentiable, and its gradient* φ *is Lipschitz continuous. Moreover, a constant* $\bar{s} > 0$ *exists, so that*

$$\|\varphi(\bar{z}_1) - \varphi(\bar{z}_2)\| \leq \bar{s}\,\|\bar{z}_1 - \bar{z}_2\|\,,\ \forall\ \bar{z}_1, \bar{z}_2 \in \Delta_o \tag{2.38}$$

Theorem 2.2.1. *Consider the proposed algorithm defined by* (2.35) *and* (2.36) *with the* β_k *variable specified by* (2.37)*. Then*

$$\eta(\kappa)^T\varphi(\kappa) \leq -\left(1 - \frac{1}{4\iota}\right)\|\varphi(\kappa)\|^2 \tag{2.39}$$

The algorithm is required to meet the necessary descent condition which is $\eta(\kappa)^T\varphi(\kappa) \leq -\bar{c}\|\varphi(\kappa)\|^2$, where $\bar{c} > 0$ [89, 90]. This theorem demonstrates that this requirement is fulfilled by the proposed algorithm. Sufficient descent condition proof is given in the Appendix B.1.

Theorem 2.2.2. *Let $\Xi(\kappa)$ and $\eta(\kappa)$ are obtained by the algorithm discussed in the Section 2.2.3. If $\|\varphi(\kappa)\| \geq \varepsilon$, where $\varepsilon > 0$ is a constant, then there exists a constant $\bar{o} > 0$ such that*

$$\|\eta(\kappa)\| \leq \bar{o}\,\|\varphi(\kappa)\| \;\; \forall\, \kappa \in N \tag{2.40}$$

The Zoutendijk condition [91], which is often used to show the global convergence [85,92,93], has been used to prove the global convergence of the proposed scheme. Global convergence proof is given in the Appendix B.2.

Theorem 2.2.3. *Let $\Xi(\kappa)$ is obtained by the algorithm discussed in the Section 2.2.3. Then*

$$\lim_{\kappa \to \infty} \inf \|\varphi(\kappa)\| = 0 \tag{2.41}$$

This theorem demonstrates the convergence result of the proposed method. Proof of the theorem is given in the Appendix B.3.

Remark 2.2.3. *The estimation error is smaller than any positive number based on the fuzzy universal approximation theorem, Theorem 2.2.2 and Theorem 2.2.3. It is therefore concluded that $|f - \hat{f}|$ and $|g - \hat{g}|$ are less than any positive number.*

2.2.3 Algorithm of the Proposed Control Scheme

As stated above, the aim of the control scheme is to maintain control of the angular positions of the nonlinear highly flexible structures while also regulating the inherent deflections. This is accomplished by the control system by generating the required control operations. The control scheme and the nonlinear system are incorporated into a closed-loop system as shown in the block diagram in Figure 2.2 and simulation model in Figure C.6.

- The control law (2.8) indicates that the indirect control method is used, where the estimates $\hat{f}$ and $\hat{g}$ are to be estimated by the ANFCT2 and then given to the control law.

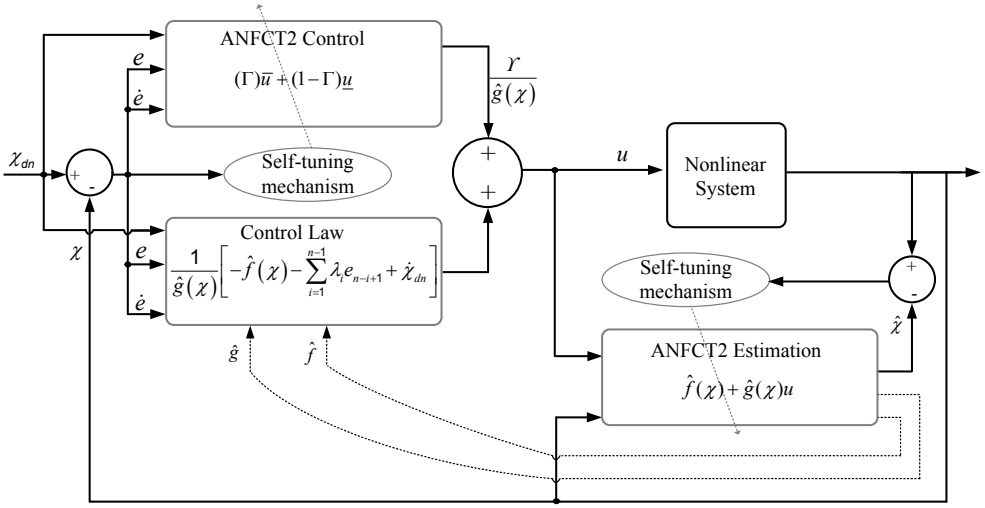

Figure 2.2 Block diagram of the proposed control scheme with a nonlinear system

- As it is presumed that the nonlinear system is in the form of (2.1), the estimation is taken into account as follows.

$$\hat{\chi} = \hat{f}(\chi) + \hat{g}(\chi)u \tag{2.42}$$

where $\hat{f} = (1-\Gamma)\underline{u}_f + (\Gamma)\bar{u}_f$ and $\hat{g} = (1-\Gamma)\underline{u}_g + (\Gamma)\bar{u}_g$ gives the estimation output (2.42).

- As shown in the block diagram in Figure 2.2, the ANFCT2 estimation self-tuning algorithm works on the basis of the error between the estimated output and the actual output of the nonlinear system. The operating procedure of the ANFCT2 is given below.

- The identification module estimates the nonlinear system and the estimated functions $\hat{f}$ and $\hat{g}$ from the ANFCT2 are then provided to the control law. The control law and identification module are shown in Figures C.7 and C.8, respectively.

- In addition, another ANFCT2 scheme u^* (2.15) is used for the Υ function in (2.8), which provides direct control and ensures that the system states reach the sliding surface more quickly and efficiently. The parameters of

this scheme are optimized on the basis of an error between the desired and actual trajectories of the nonlinear system.

- The controller delivers a smooth adaptable output rather than an abrupt immutable output normally provided by traditional methods and overcomes the chattering problem. To ensure the stability of the proposed control scheme by the Lyapunov stability theorem, which is presented in Appendix A, the Υ function in the control law is calculated as $\Upsilon = -K\ |u^*|\ sgn(S)$. The final control output u (2.8) is then fed to the nonlinear system.

Operating procedure of the ANFCT2 scheme

Step 1 Initially, each parameter is randomly defined and the output (2.15) is determined.

Step 2 The error is determined and returned to the previous ANFCT2 layers.

Step 3 The appropriate control action is executed on the basis of the error by optimizing all the required ANFCT2 parameters Ξ_{ij} (2.35).

Step 4 The search direction is updated with the algorithm using $\eta(\iota)$ (2.36), $\beta(\iota)$ (2.37) and the gradients (2.18)-(2.34), in order to ensure $\|\varphi(\iota)\| \leq \bar{\varepsilon}$, where $\bar{\varepsilon} \in (0, 1)$.

Step 5 The next iteration is executed and the process is repeated from *Step 2*.

2.3 Summary

The proposed control scheme, hybrid of SMC and type-2 ANFC (SMANFC-2), is presented in this chapter for the control of the class of nonlinear systems. The SMANFC-2 offers the advantage of both SMC and adaptive neural fuzzy control (ANFC), and overcomes their limitations. The control scheme is model-free and does not rely on the dynamic parameters of the system, allowing it to operate on

a variety of nonlinear systems. The new CG algorithm, named MHS, has global convergence properties and a better search direction, which enhances ANFC self-tuning abilities. Estimates of unknown functions from the system are given to the SMC control law, and another ANFC system helps to overcome the chattering problem normally seen in SMC. Thus, ANFC plays an important role in estimating and controlling at the same time. The stability analysis of the proposed control scheme is ensured by the Lyapunov stability theorem. Furthermore, its global convergence and stability properties are mathematically demonstrated in this thesis.

CHAPTER 3

THE STUDIED CLASS OF NONLINEAR SYSTEMS (PART 1)

3.1 Introduction

The proposed control scheme is designed for the class of nonlinear systems which have the form (2.1). Flexible satellites, multi-link robotic systems, and many similar large flexible systems belong to the same class of nonlinear systems [94]. The control of such a class of nonlinear flexible multi-body systems is a challenging task. Such systems can be regarded as a combination of rigid and elastic interconnected bodies attributed to the family of multi-body distributed/discrete parameter systems. If no assumptions and constraints are ascribed to the body's geometry and link deflections, then the resulting model consists of a hybrid coordinate system of ordinary, partial, and integral differential equations. The rigid body movements of the system are defined by the time-varying coordinates, while elastic movements are characterized by the time and space-varying coordinates. These systems have significant coupling between rigid and elastic movements. The coupled partial differential equations are difficult to analyze analytically and computationally. The solution of these equations requires an infinite set of eigenvalues and corresponding eigenfunctions, so the distributed parameter systems are infinite-dimensional. Developing a finite-dimensional solution from the distributed infinite-dimensional system is a non-trivial process involving the approximation methodology. There are three most used methodologies for the dynamic modeling of the system: those are finite element method (FEM) [95], AMM [96], and lumped parameter method (LPM) [97]. The most used model between them is AMM because of having many advantages like flexibility in the choice of choos-

ing proper boundary conditions, computational efficiency, and model accuracy.

LPM method uses a lump of masses and massless springs for modeling of system. This method is the simplest method among others but gives inaccurate results [98]. LPM is not being widely used because of its inability to handle complexity and nonlinearity in a better manner.

FEM is the second most popular among researchers after AMM. In this method, each flexible link is depicted as a combination of an infinite number of elements. The complete link acts as an entity by ensuring displacements to be compatible and internal forces to be in equilibrium at certain points called nodes. The displacement at any point of the continuous element is expressed by polynomial interpolation functions multiplied by finite numbers of displacements at the nodal points. Next, the equation of motion for the system, in general, is obtained by first deriving the equations of motion for a typical element, and then assembling equations for all the elements [99]. This method has the ability to handle irregular geometries and can handle nonlinear conditions with ease [100]. However, flexibility approximation often results in an overestimated stiffness matrix. This results in numerous state-space equations, consequently increasing the simulation time for computation [101, 102].

AMM represents a flexible manipulator dynamic model with a truncated finite modal series. It comprises eigenmode functions and time-varying mode amplitudes. In this model, the flexible dynamics is represented by vibration modes rather than its natural modes. For boundary conditions, selecting a suitable set of assumed modes can be valuable. If sufficient modes are taken into account in AMM, this can result as close as a model estimated by a partial differential [103]. The model derived from AMM has a lower order and its final output matrix structure allows the system to be transformed into the state-space model [104]. This can create more simplicity for control-related problems [105]. Korayem and Rahimi used both FEM and AMM for dynamic manipulator modeling and pre-

sented the advantages/disadvantages of both modeling techniques [106].

The aim of this chapter is to provide the two studied nonlinear systems, and the third studied nonlinear system is provided in the next chapter.

3.1.1 Literature Review

The first two studied nonlinear systems, which belong to the class of nonlinear systems, comprise flexible orbital space systems, such as satellite and spacecraft systems. Modern satellites have lightweight appendages like solar arrays and antennas connected to them. These are necessary parts for remote sensing, communication, and a variety of space-related equipment. These flexible structures provide advantages like low launch costs and ensure sustainable energy for the satellite. On the other hand, these flexible structures are more susceptible to vibrations. Low-frequency vibration modes in these flexible appendages are more excited during satellite maneuvering. These vibrations affect the normal operation of the satellite and can alter its orbit position. The big challenging task is to suppress these induced vibrations and provide precise attitude control of the satellite. It is not an easy task as the model parameters of the satellite are not accurately known and unknown disturbance torques act on the satellite. Attitude maneuvering and vibration suppression of the rotating satellite are an active research area and many researchers have shown interest in this field.

A control scheme based on feedback linearization is designed for the satellite system by Karray, Grewal, Glaum and Modi [107]. LQR based robust control technique has been designed for the satellite system by Grewal and Modi [108]. Nonlinear input shaping technique was designed by Gorinevsky and Vukovich [109] for spacecraft reorientation maneuvering. Using high gain observer robust control of a spacecraft with flexible appendages has been implemented by Singh and Zhang [110]. Adaptive control strategies have also been implemented for the con-

trol of satellite/spacecraft systems [111–114]. The control of flexible spacecraft with NN has been considered in [115] by Nayeri, Alasty, and Daneshjou. $L1$ adaptive control system has been implemented in [116, 117] for the satellite. The control scheme includes state predictors, to better predict the uncertain parameters and disturbances in the system, in order to provide better control of the satellite. In a real environment, there can be uncertainties because of unknown torques acting on the satellite. To deal with this problem, robust and disturbance rejection control strategies have been designed also for satellite applications. SMC scheme has been implemented by many researchers for satellite/spacecraft systems [118–121].

These nonlinear systems are presented in the following sections.

3.2 The First Studied Nonlinear System

The first studied nonlinear system that is considered is rotating satellite with two flexible appendages (RSTFA). A RSTFA is often modeled as a rigid hub with flexible beam like appendages. The model is defined by coupled systems of integro-partial differential equations [1, 122–124]. The planar vibrational/rotational dynamics of a RSTFA system consists of a rigid hub with two identical cantilevered flexible appendages and tip masses are shown in Figure 3.1.

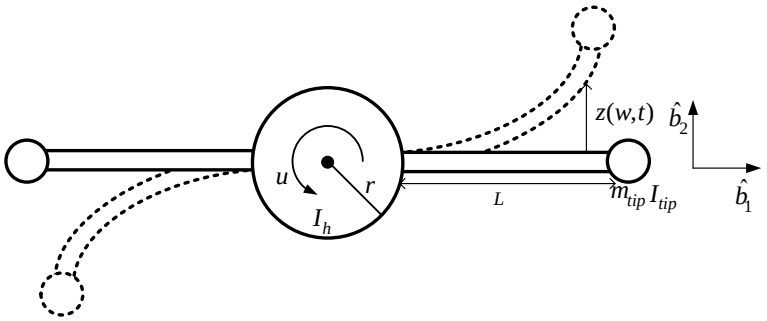

Figure 3.1 Satellite with two flexible appendages

3.2.1 Mathematical Modeling

Complete modeling and detailed equations of motion of the RSTFA system can be found in [125–127].

Assumption 3.2.1. *For dynamic kinematic modeling, certain assumptions are considered. For the flexible appendages, the Euler-Bernoulli beam model is used, therefore cross-sectional rotary inertia and shear deformations are neglected. The opposing appendages are constrained to deflect antisymmetrically, such that the deformed system's mass center coincides with the hub center. The two appendages are considered to have the same deflection profiles. The control system is assumed to generate torque u acting on the hub of the satellite. In addition, the control actuator is modeled as a massless, concentrated, and torque generating device.*

To derive the equation of motion, consider one of the flexible appendage that is shown in Figure 3.1 with tip mass m_{tip}. Let $\{n_1, n_2, n_3\}$ be the right-handed inertial reference axis and $\{\hat{b}_1, \hat{b}_2, \hat{b}_3\}$ be the right-handed body-fixed axis. The inertial position vector p_i of a typical deformed point in the ith appendage is given by (3.1).

$$p_i = (w_i + r)\,\hat{b}_1 + z_i\hat{b}_2 \tag{3.1}$$

where $(\hat{.})$ denotes the unit vector, r is the hub radius, w_i is the coordinate of a typical mass element measured along the undeformed ith beam, and z_i is the local deformation measured perpendicular to the b_1 axis. The velocity of the deformed point is

$$v_i(t, w_i) = \dot{p}_i + \breve{w} \times p_i \tag{3.2}$$

where $\breve{w} = \dot{\theta} \times \hat{n}_3$ is the angular velocity of the hub-fixed frame relative to the inertial frame.

$$v_i = \dot{z}_i\hat{b}_2 + \dot{\theta}\hat{b}_3 \times \left[(w_i + r)\,\hat{b}_1 + z_i\hat{b}_2\right] \tag{3.3}$$

The kinetic energy (KE) for the model is combination of KEs of satellite hub, two appendages of satellite and two payloads attached at the end of the flexible

appendages.

$$T = T_{hub} + 2T_{app} + 2T_{tip} \tag{3.4}$$

$$T_{hub} = \frac{1}{2} I_{hub} \dot{\theta}^2 \tag{3.5}$$

$$T_{app} = \frac{1}{2} \int_0^L \rho v_i . v_i dx_i \tag{3.6}$$

$$T_{tip} = \frac{1}{2} \left[m_{tip} v_i(L) . v_i(L) + J_t \left\{ \dot{\theta} + \dot{z}'(L) \right\}^2 \right] \tag{3.7}$$

where I_{hub} is the rotary inertia of the hub, J_t is the rotary inertia of the ith tip mass, ρ is the mass density of the appendage, m_{tip} is the mass of the ith tip or payload, L_i is the length of the ith appendage, $(\dot{.})$ denotes the partial derivative with respect to time and $(.')$ denotes the partial derivative with respect to w_i. Substituting (3.5)-(3.7) into (3.4) give total KE of the model (3.8).

$$\begin{aligned} T = \frac{1}{2} I_{hub} \dot{\theta}^2 + \int_0^L \rho \left(\dot{z} + (w + r) \dot{\theta} \right)^2 dx + m_{tip} \left((r + L) \dot{\theta} + \dot{z}(L) \right)^2 \\ + I_{tip} \left(\dot{\theta} + \dot{z}'(L) \right)^2 \end{aligned} \tag{3.8}$$

The total potential energy (PE), under the Euler-Bernoulli assumption is

$$U = \int_0^L EI (z'')^2 dx \tag{3.9}$$

where EI is the appendage flexural rigidity of the ith beam and $(.'')$ denotes second partial derivative with respect to the w_i.

Generalized coordinates are introduced that locate uniquely all the mass in the system. Using the AMM, these coordinates are the amplitudes of the chosen base functions. The elastic displacements (3.10) are modeled as series.

$$z(w, t) = \sum_{i=1}^{N} \delta_i(t) \phi_i(w) \tag{3.10}$$

where, $\delta_i(t)$ is generalized coordinate, $\phi_i(w)$ denotes set of comparison functions whose linear combination approximates the actual appendage mode shapes, and

N denotes the number of modes. The admissible function (3.11) satisfies the geometric and physical boundary conditions of the given system and is found to be the excellent admissible functions for clamped-free appendages.

$$\phi_i(w) = 1 - \frac{\cos(i\pi w)}{L} + \frac{1}{2}(-1)^{i+1}\left(\frac{i\pi w}{L}\right)^2 \tag{3.11}$$

The Lagrangian equation (3.12) is used to obtain the finite-dimensional ordinary differential equations of motion.

$$\frac{d}{dt}\left(\frac{\partial T}{\partial \dot{w}}\right) - \frac{\partial T}{\partial w} + \frac{\partial U}{\partial w} = F \tag{3.12}$$

where $w = \{\theta\, \delta_j\}^T$ and $j = 1, ..., N$. F is the generalized force that can be determined by finding the virtual work associated with control torque. Substituting (3.10)-(3.11) in (3.8)-(3.9) and using Lagrangian equation (3.12), closed form equations of motion are derived and represented in the matrix form as

$$\begin{bmatrix} I_2 & M_{\theta\delta}^T \\ M_{\theta\delta} & M_{\delta\delta} \end{bmatrix} \ddot{w} + \begin{bmatrix} 0 & 0 \\ 0 & K_{\delta\delta} \end{bmatrix} w = \begin{bmatrix} u \\ 0 \end{bmatrix} \tag{3.13}$$

where unknown terms in (3.13) are given in (3.14)-(3.16).

$$I_2 = I_{hub} + 2m_{tip}(r+L)^2 + 2I_{tip} + 2\int_0^L \rho(r+w)^2 dx \tag{3.14}$$

$$[M_{\theta\delta}]_i = 2\left[\rho\int_0^L (r+w)\,\phi_i(w)\,dx + m_{tip}\,(r+L)\,\phi_i(L) + I_{tip}\phi'_i(L)\right] \tag{3.15}$$

$$[K_{\delta\delta}]_{ij} = 2\left[EI\int_0^L \phi''_i(w)\,\phi''_i(w)\,dx\right] \tag{3.16}$$

where $[.]_i$ denotes the ith element of the vector $[.]$ and $[.]_{ij}$ denotes the (i,j) element of the matrix $[.]$.

The RSTFA system's detailed closed form of equations of motion (3.13) can be written in the generalized form of equation in accordance with this study as

$$M_S\ddot{w}_S + K_S w_S = Q_S u \tag{3.17}$$

where $w_S = \{\theta_S\ \bar{\delta}_1\ \ldots\ \bar{\delta}_{\gamma'}\}^T$; θ_S is rigid hub rotation angle, and $\bar{\delta}_{\gamma'}$ are the generalized coordinates for the appendage. Furthermore, in (3.17): $M_S \in R^{\Gamma'\times\Gamma'}$,

$w_S \in R^{\Gamma' \times 1}$, $K_S \in R^{\Gamma' \times \Gamma'}$, $Q_S \in R^{\Gamma' \times 1}$ and $u \in R^{1 \times 1}$. The control system generates the torque u that operates at the rigid hub of the satellite. In addition, $\Gamma' = 1 + \gamma'$, and γ' represents the modes considered for appendages.

3.3 The Second Studied Nonlinear System

The second nonlinear system that has been studied is rotating spacecraft with four flexible appendages (RSFFA). The system comprises a rigid hub and four identical cantilevered flexible appendages with tip masses. The RSFFA system has included actuators on the appendages along with an actuator on the hub of spacecraft, to further reduce the fluctuations. This makes the task of the control schemes more complex, and therefore the system is an appropriate example. Figure 3.2 shows the RSFFA system. The system has many control actuators as seen in Figure 3.2a. Figure 3.2b is effective for the mathematical modeling of the system.

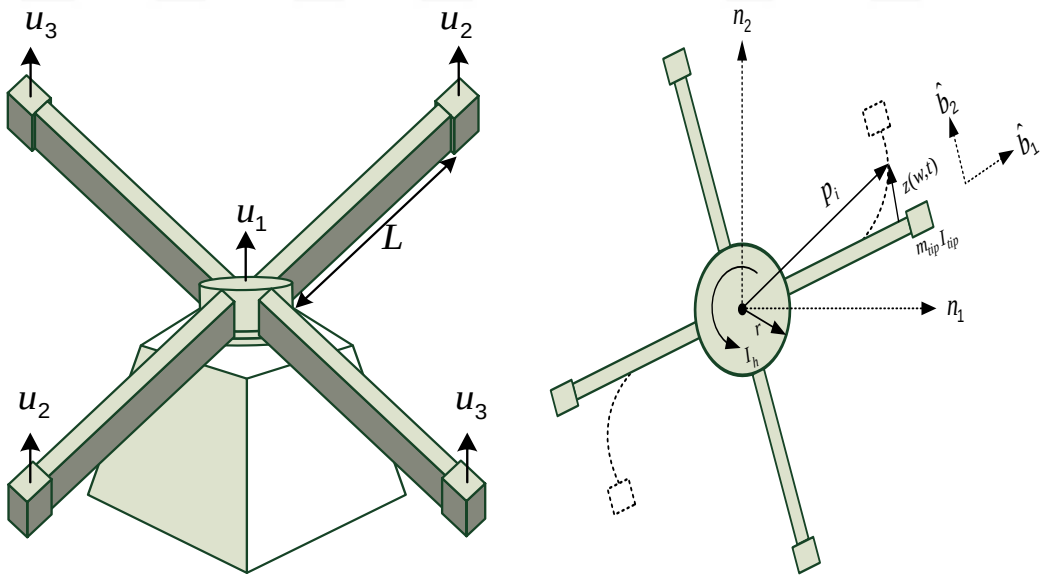

(a) Perspective view **(b)** Top view

Figure 3.2 Spacecraft with four flexible appendages

3.3.1 Mathematical Modeling

Complete modeling and detailed equations of motion of the RSFFA system can be found in [128, 129].

Assumption 3.3.1. *The following assumptions are considered when modeling the RSFFA system. The Euler-Bernoulli beam model is used to represent flexible appendages, hence the beam's shear deformation and sectional rotary inertia are not taken into account. The antisymmetric deformation assumption is taken into consideration in such a way that the opposite appendages, appendages 1 and 3 (set 1), have the same deflection profile and, likewise, appendages 2 and 4 (set 2), have the same deflection profile. The control system is assumed to generate torque u_1 acting on the hub of the spacecraft, u_2 acting on the end of set 1 appendages, and u_3 acting on the end of set 2 appendages. Control actuators are considered to be massless torque generating devices.*

To derive the equation of motion, consider one of the flexible appendage that is shown in Figure 3.2b with tip mass m_{tip}. Let $\{n_1, n_2, n_3\}$ be the right-handed inertial reference axis and $\{\hat{b}_1, \hat{b}_2, \hat{b}_3\}$ be the right-handed body-fixed axis. The inertial position vector p_i is given as (3.1) and the velocity of the deformed point is given as (3.2). Then

$$v_i(t, w) = -\dot{\theta} z_i \hat{b}_1 + \left[\dot{z}_i + \dot{\theta}\,(r + w_i)\right] \hat{b}_2 \tag{3.18}$$

The KE for the model is combination of KEs of spacecraft's hub, two appendages of spacecraft and two payloads attached at the end of the flexible appendages.

$$T = \frac{1}{2} I_{tot} \dot{\theta}^2 + \sum_{i=1}^{2} \left[\begin{array}{l} \int_0^{L_i} \rho \dot{z}_i^2 dw_i + m_{tip} (\dot{z}_i\,(L))^2 + I_{tip} (\dot{z}'\,(L))^2 \\ +2\dot{\theta} \left(\begin{array}{l} \int_0^{L_i} \rho\,(r + w_i)\,\dot{z}_i dw_i + \\ m_{tip}\,(r + L)\,\dot{z}_i\,(L) + I_{tip}\,(\dot{z}'\,(L)) \end{array} \right) \end{array} \right] \tag{3.19}$$

The total PE, under the Euler-Bernoulli assumption is

$$U = \int_0^L EI(z'')^2 dx \tag{3.20}$$

It is important to evaluate the generalized force that can be evaluated by finding the virtual work associated with the three torques u_1, u_2, and u_3. The total work of the three torques is expressed as

$$W = \int_{w_1}^{w_2} u_1\, d\theta + 2\left[u_2\left\{d\theta + dz'_1\,(L)\right\} + u_3\left\{d\theta + dz'_2\,(L)\right\}\right] \tag{3.21}$$

where w_1 and w_2 are the arbitrary initial and final parameters of the system. The appendage deflections are represented by the AMM as

$$z_i(t, w_i) = \sum_{j=1}^{r} \delta_{ji}(t)\vartheta_j(w_i) \tag{3.22}$$

where r is the number of modes, $\delta_{ji}(t)$ is the time-varying modal displacements and $\vartheta_j(w_i)$ is the spatial mode shape functions.

Using the virtual variation and (3.22), (3.21) can be written as

$$\Delta W = \left[u_1 + 2u_2 + 2u_3\right]\Delta\theta + 2\sum_{j=1}^{N}\left[u_2\phi'_j\,(L)\,\Delta\delta_{j1} + u_3\phi'_j\,(L)\,\Delta\delta_{j2}\right] \tag{3.23}$$

or

$$\Delta W = F_\theta\delta\theta + \sum_{j=1}^{N}\left[F_{j1}\Delta\delta_{j1} + F_{j2}\Delta\delta_{j2}\right] \tag{3.24}$$

Using (3.24), the generalized force can be written in the matrix form as

$$F = \begin{Bmatrix} F_\theta \\ F_{11} \\ \vdots \\ F_{\underline{N}1} \\ F_{12} \\ \vdots \\ F_{\underline{N}2} \end{Bmatrix} = \begin{bmatrix} 1 & 2 & 2 \\ 0 & 2\phi'\,(L) & 0 \\ 0 & 0 & 2\phi'\,(L) \end{bmatrix} \begin{bmatrix} u_1 \\ u_2 \\ u_3 \end{bmatrix} \tag{3.25}$$

where $\underline{N}$ represents the number of modes considered for appendages. The elastic displacements are modeled by (3.22) and the admissible function considered is given in (3.11). Substituting (3.19), (3.20) and (3.25) into Lagrangian equation (3.12), a finite-dimensional system of ordinary differential equations of motion (3.26) is derived.

$$\begin{bmatrix} I & M_{\theta\delta_1}^T & M_{\theta\delta_2}^T \\ M_{\theta\delta_1} & M_{\delta_1\delta_1} & 0 \\ M_{\theta\delta_2} & 0 & M_{\delta_2\delta_2} \end{bmatrix} \ddot{w} + \begin{bmatrix} 0 & 0 & 0 \\ 0 & K_{\delta_1\delta_1} & 0 \\ 0 & 0 & K_{\delta_2\delta_2} \end{bmatrix} w = F \tag{3.26}$$

where unknown terms in (3.26) are given in (3.27)-(3.30), and F is given in (3.25).

$$I = I_{hub} + 4m_{tip}(r+L)^2 + 4I_{tip} + 4\int_0^L \rho(r+w)^2 dx \tag{3.27}$$

$$[M_{\theta\delta_1}]_i = [M_{\theta\delta 2}]_i = 2\begin{bmatrix} \rho\int_0^L (r+w)\,\phi_i(w)\,dx + m_{tip}\,(r+L)\,\phi_i(L) + \\ I_{tip}\phi'_i(L) \end{bmatrix} \tag{3.28}$$

$$[M_{\delta_1\delta_1}]_{ij} = [M_{\delta_2\delta_2}]_{ij} = 2\begin{bmatrix} \rho\int_0^L \phi_i(w)\,\phi_j(w)\,dx + m_{tip}\phi_i(L)\,\phi_j(L) + \\ I_{tip}\phi'_i(L)\,\phi'_j(L) \end{bmatrix} \tag{3.29}$$

$$[K_{\delta_1\delta_1}]_{ij} = [K_{\delta_2\delta_2}]_{ij} = 2\left[EI\int_0^L \phi''_i(w)\,\phi''_i(w)\,dx\right] \tag{3.30}$$

where, $[.]_i$ denotes the ith element of the vector $[.]$ and $[.]_{ij}$ denotes the (i,j) element of the matrix $[.]$.

The RSFFA system detailed closed form of equations of motion (3.26) can be written in the generalized form of equation in accordance with this study as

$$M_R\ddot{w}_R + K_R w_R = Q_R u \tag{3.31}$$

where $w_R = \{\theta_R\ \underline{\delta}_{11}\ldots\underline{\delta}_{\gamma 1}\ \underline{\delta}_{12}\ldots\ \underline{\delta}_{\gamma 2}\}^T$, θ_R is the spacecraft hub rotation angle, $M_R \in R^{\grave{\Gamma}\times\grave{\Gamma}}$ is the mass matrix, $K_R \in R^{\grave{\Gamma}\times\grave{\Gamma}}$ is the stiffness matrix, Q_R is the input weighting matrix, and u is the input vector. In addition, $\grave{\Gamma} = 1 + \sum_i \grave{\gamma}_i$, and $\grave{\gamma}_i$ represents the modes considered for each set of appendages.

3.4 Summary

This chapter introduces two nonlinear systems, RSTFA and RSFFA, belonging to the same class of nonlinear systems. The systems are highly nonlinear, infinite-dimensional, highly coupled systems described by the hybrid coordinate systems of ordinary, partial, and integral differential equations. The discretization technique AMM is used to convert the dynamical system to a finite-dimensional system. Mathematical modeling of both systems are presented in the chapter.

CHAPTER 4

THE STUDIED CLASS OF NONLINEAR SYSTEMS (PART 2)

4.1 The Third Studied Nonlinear System

The third nonlinear system which is considered in this study is the flexible manipulator. It comprises highly nonlinear, lengthy and coupled dynamic equations because of the flexible nature of the system [106]. A flexible manipulator is a popular subject of study among researchers due to its complexity. Some of the work on TLFM is discussed in Chapter 2. There are several complexities associated with flexible manipulators, as well as previously studied structures belonging to the same class of nonlinear flexible systems, such as: non-minimum phase problem, non-collocation, under-actuation problems, uncertainties due to the truncated model, and factors like control and observation spillover.

Non-minimum phase in the manipulator is because of two reasons. Firstly, this is due to non-collocated actuation and sensing. This means that the actuator and sensors are located at various locations. The transfer function between the torque inputs to the end-effector is non-minimum phase. Secondly, the input torque voltages at the joints exhibit non-minimum phase properties [130]. The effects of non-minimum phase systems can cause the inaccuracy problem in position control of end-effectors.

The under-actuation problem originates if the robot has fewer actuators than the number of joints [131]. The problem can cause the failure of actuators. Using a few actuators provides advantages like energy saving and lightweight, but requires enhanced control techniques for superior control of manipulators.

Practically, robot manipulators are considered to pick up the payload from one place to another place. Carrying the payload by manipulator further increases the complexity since the dynamic behavior of manipulators changes with the varying payload [132].

Flexible manipulator has distributed parameter properties, since flexible manipulator has rigid as well as flexible components. This causes problems because of their highly coupled time-varying nonlinear multi-input multi-output (MIMO) system properties [133]. To define a finite-dimensional dynamical model, truncation takes place that causes unmodeled dynamic problems [134]. During the modeling of manipulators, the chosen number of vibration modes are taken into consideration. The control action that is selected can excite the part of output that is not included in the set. This phenomenon is known as control spillover. On the other hand, measurements from sensors could be taken that comprise part of the output not presented in the set. This results in corruption of the control action. This phenomenon is known as observation spillover. These phenomena can cause the system to be unstable [135].

All these complexities of the flexible manipulator demonstrate that the system is a challenging example of nonlinear MIMO systems to validate the robustness of the control system and to analyze how the controller can respond to uncertainties. The flexible nature and dynamic characteristics of manipulator while constructing a dynamic suitable model is considered. Section 4.1.1, presents the kinematic modeling of n-link flexible manipulator. Section 4.1.2, presents dynamic modeling of n-link flexible manipulator.

4.1.1 Kinematic Modeling

Complete modeling and detailed equations of motion of the TLFM can be found in [2].

Assumption 4.1.1. *The following assumptions are considered when modeling the TLFM [136]. Links are slim and long, as well as assumed to move only in the horizontal plane, and the effects of cross-shearing and rotary inertia are insignificant. In addition, the links are assumed to have uniform material with continuous cross-section area and deflections are assumed to be small. The backlash in the motor and the friction effects are ignored. The links are serially cascaded and actuated by joints with individual motor.*

In this section, flexible manipulator kinematics modeling has been described. The kinematics of n-link cascaded connected flexible manipulators have been described. A planar flexible manipulator is shown in Figure 4.1.

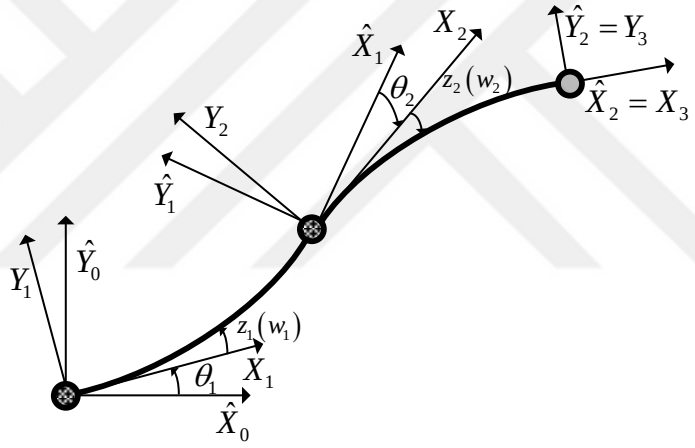

Figure 4.1 Two link flexible manipulator

The following coordinates frames have been created: $\left\{\hat{X}_0, \hat{Y}_0\right\}$ is the inertial coordinate frame, $\{X_i, Y_i\}$ is the ith link rigid body moving coordinate frame, whereas $\left\{\hat{X}_i, \hat{Y}_i\right\}$ is the ith link flexible body moving coordinate frame. Rigid motion is defined by joint angles θ_i , ith link flexible transversal deflection is defined by $z_i(w_i)$, where $0 \leq w_i \leq l_i$ and l_i is the ith link length.

When a motion of manipulator with revolute joint over a two-dimensional plane is considered, the rigid transformation matrix A_i from $\{X_{i-1}, Y_{i-1}\}$ to $\{X_i, Y_i\}$ is written as follows:

$$A_i = \begin{bmatrix} \cos\theta_i & -\sin\theta_i \\ \sin\theta_i & \cos\theta_i \end{bmatrix} \tag{4.1}$$

The flexible link rotation matrix E_i is defined as:

$$E_i = \begin{bmatrix} 1 & -z'_{ie} \\ z'_{ie} & 1 \end{bmatrix} \tag{4.2}$$

where $z'_{ie} = \left({}^{\delta z_i}/_{\delta w_i}\right)_{w_i=l_i}$. This is based on the assumption made earlier that each link has small deflections. Consequently, all second order terms are ignored. The absolute position vector is defined as:

$$p_i = r_i \ + W_i {}^i p_i, \quad r_{i+1}{=}r_i{+}W_i \ {}^i r_{i+1} \tag{4.3}$$

Here, ${}^i p_i\,(w_i) = (w_i \ z_i\,(w_i))^T$ is the point on deflected link i with respect to frame $\{X_i, Y_i\}$ and p_i is the same point absolute position along $\left\{\hat{X}_0, \hat{Y}_0\right\}$. Similarly, r_i is the absolute point along $\left\{\hat{X}_0, \hat{Y}_0\right\}$ and ${}^i r_{i+1} = {}^i p_i\,(l_i)$ is the position of origin of frame $\{X_{i+1}, Y_{i+1}\}$ with respect to $\{X_i, Y_i\}$. W_i is transformation matrix from $\left\{\hat{X}_0, \hat{Y}_0\right\}$ to $\{X_i, Y_i\}$ that obeys the recursive equation as shown below:

$$W_i = W_{i-1}E_{i-1}A_i = \hat{W}_{i-1}A_i, \quad \hat{W}_o = I \tag{4.4}$$

The above relations completely describes the kinematics at any point of the link. Next step is to find out the derivatives of these kinematic terms, since later sections will need these terms to be placed in energy formulas. The absolute angular velocity is defined as [2]:

$$\dot{\alpha}_i = \sum_{j=1}^{1} \dot{\theta}_j + \sum_{k=1}^{i-1} \dot{z}'_{ke} \tag{4.5}$$

Here, upper dot donates derivative with respect to time and upper prime donates derivative with respect to space. The linear absolute velocity of link is:

$$\dot{p}_i = \dot{r}_i + \dot{W}_i^i p_i + W_i^i \dot{p}_i \tag{4.6}$$

where,

$$\dot{W}_i = \dot{\hat{W}}_{i-1} A_i + \hat{W}_{i-1} \dot{A}_i, \qquad \dot{\hat{W}}_i = \dot{W}_i E_i + W_i \dot{E}_i$$

4.1.2 Dynamic Modeling and AMM

The kinematic relations derived in Section (4.1.1) are needed to be used for deriving dynamic modeling of n-link flexible manipulators. The total energy related to flexible manipulator using above-mentioned relations are computed that can be later plugged into the Lagrangian equation for the derivation of dynamic equations. So total KE (i.e. T) and PE (i.e. U) are needed to be computed for the formation of Lagrangian i.e. $L = T - U$.

The KE of flexible manipulator is sum of contributions of KEs associated with hubs, links and payload.

$$T = \sum_{i=1}^{n} T_{hi} + \sum_{i=1}^{n} T_{li} + T_p \tag{4.7}$$

The KE associated to hub for the rigid body having mass m_{hi} and moment of inertia J_{hi} is

$$T_{hi} = \frac{1}{2} m_{hi} \dot{r}_i^T \dot{r}_i + \frac{1}{2} J_{hi} \dot{\alpha}_i^2 \tag{4.8}$$

The KE associated to link i having uniform density ρ_i is

$$T_{li} = \frac{1}{2} \int_0^{li} \rho_i \left(w_i\right) \dot{p}_i^T \left(w_i\right) \dot{p}_i \left(w_i\right) dw_i \tag{4.9}$$

The KE associated to payload located at the end of link having mass m_p and moment inertia J_p is

$$T_p = \frac{1}{2} m_p \dot{r}_{n+1}^T \dot{r}_{n+1} + \frac{1}{2} J_p \left(\dot{\alpha}_n + \dot{z}_{ne}^{'}\right)^2 \tag{4.10}$$

It is assumed that motion is along horizontal direction so ignoring the effect of

gravity, the PE of the manipulator is

$$U = \sum_{i=1}^{n} U_i = \sum_{i=1}^{n} \frac{1}{2} \int_{0}^{li} (EI)_i(w_i) \left[\frac{d^2 z_i(w_i)}{dw_i^2} \right]^2 dw_i \tag{4.11}$$

where U_i is the elastic energy stored in the link i and $(EI)_i$ is the flexural rigidity of the link.

The discretization of the flexible manipulator had not been made until this point. As a result of the above expression, the Lagrangian has an unlimited dimensional model with limited use for simulation and control purposes. Therefore, hereafter, a finite-dimensional representation of a flexible link manipulator has been presented. Euler-Bernoulli beams theory is used to model link with uniform density ρ_i, flexural rigidity $(EI)_i$ and deflection $z_i(w_i, t)$ [137].

$$(EI)_i \frac{\partial^4 z_i(w_i, t)}{\partial w_i^4} + \rho_i \frac{\partial^2 z_i(w_i, t)}{\partial t^2} = 0, \quad i = 1, \ldots, n \tag{4.12}$$

To solve this equation, boundary conditions are needed at the base and end of each link. Details about boundary conditions that are used for flexible manipulator are given in references [138, 139]. Boundary conditions at the base are:

$$z_i(0, t) = 0, \qquad z_i^{'}(0, t) = 0, \qquad i = 1, \ldots, n \tag{4.13}$$

In the flexible manipulator system, one valid assumption is that the inertia of the link is small compared to the inertia of the hub. It is observed that clamped mass boundary conditions have better results for the system having inertia of link small compared to inertia of hub [2, 140, 141]. In clamped mass boundary conditions, it is considered that the end of the link is independent of dynamic constraints, because it is difficult to take into consideration unknown or time-varying inertias and masses. Clamped mass boundary conditions at the end of the link are:

$$
\begin{aligned}
(EI)_i \frac{\partial^2 z_i(w_i,t)}{\partial w_i^2}|_{w_i=l_i} &= -J_{Li}\frac{d^2}{dt^2}\left(\frac{\partial z_i(w_i,t)}{\partial w_i}|_{w_i=l_i}\right) - (MD)_i \frac{d^2}{dt^2}\left(z_i(w_i,t)|_{w_i=l_i}\right) \\
(EI)_i \frac{\partial^3 z_i(w_i,t)}{\partial w_i^3}|_{w_i=l_i} &= M_{Li}\frac{d^2}{dt^2}\left(z_i(w_i,t)|_{w_i=l_i}\right) + (MD)_i \frac{d^2}{dt^2}\left(\frac{\partial z_i(w_i,t)}{\partial w_i}|_{w_i=l_i}\right) \\
i &= 1,\ldots,n
\end{aligned}
\tag{4.14}
$$

where J_{Li} and M_{Li} are the actual moment of inertia and actual mass at the end of link i. Furthermore, $(MD)_i$ is the contribution of masses of distal links. For the finite-dimensional solution of (4.12), the AMM technique is used [2,136,139,142], which separates the solution into time and space functions. The link deflection is expressed as:

$$
z_i\left(w_i,t\right) = \sum_{j=1}^{m_i} \phi_{ij}\left(w_i\right)\delta_{ij}(t) \tag{4.15}
$$

The *ith* link has assumed spatial mode shapes (or eigenfunctions) i.e. $\phi_{ij}\left(w_i\right)$ that defines natural mode shape of vibrations of that link and $\delta_{ij}(t)$ that defines the time-varying variables associated with aforementioned spatial mode shapes. There are rules for the selection of assumed mode shapes [137, 138]. These are:

- They need to establish a complete coordinate basis, i.e. it should be possible to express any link with the assumed modes.
- Boundary conditions of the system should be applicable on them.
- They should be at least n time differentiable over defined domain. n depicts the degree of partial differential equation that defines the modeling of flexible link.
- These modes shapes should hold orthogonality properties with respect to each other. The orthogonality properties of mode shapes bring in simplicity for the design of system by reducing some cross coupled equations between the modes.

Putting (4.15) in (4.12), so that the separation of time and spatial function is achieved.

$$(EI)_i \frac{\partial^4 \sum_{j=1}^{m_i} \phi_{ij}(w_i)\delta_{ij}(t)}{\partial w_i^4} + \rho_i \frac{\partial^2 \sum_{j=1}^{m_i} \phi_{ij}(w_i)\delta_{ij}(t)}{\partial t^2} = 0 \tag{4.16}$$

From (4.16),

$$(EI)_i \frac{\partial^4 \sum_{j=1}^{m_i} \phi_{ij}(w_i)\delta_{ij}(t)}{\partial w_i^4} = -\rho_i \frac{\partial^2 \sum_{j=1}^{m_i} \phi_{ij}(w_i)\delta_{ij}(t)}{\partial t^2} \tag{4.17}$$

Achieving time and space separability parts from (4.17),

$$(EI)_i \frac{\partial^4 \sum_{j=1}^{m_i} \phi_{ij}(w_i)}{\phi_{ij}(w_i)\rho_i \partial w_i^4} = -\frac{\partial^2 \sum_{j=1}^{m_i} \delta_{ij}(t)}{\delta_{ij}(t)\partial t^2} \tag{4.18}$$

$$(EI)_i \frac{d^4\phi_{ij}(w_i)}{\phi_{ij}(w_i)\rho_i dw_i^4} = -\frac{d^2\delta_{ij}(t)}{\delta_{ij}(t)dt^2} \tag{4.19}$$

$$(EI)_i \frac{d^4\phi_{ij}(w_i)}{\phi_{ij}(w_i)\rho_i dw_i^4} = -\frac{d^2\delta_{ij}(t)}{\delta_{ij}(t)dt^2} = \omega_{ij}^2 \tag{4.20}$$

where ω_{ij} is constant and it is ith link jth natural frequency of vibration. From (4.20),

$$(EI)_i \frac{d^4\phi_{ij}(w_i)}{\phi_{ij}(w_i)\rho_i dw_i^4} = \omega_{ij}^2 \tag{4.21}$$

$$(EI)_i \frac{d^4\phi_{ij}(w_i)}{dw_i^4} - \phi_{ij}(w_i)\rho_i\omega_{ij}^2 = 0 \tag{4.22}$$

$$\frac{d^2}{dw_i^2}\left[(EI)_i \frac{d^2\phi_{ij}(w_i)}{dw_i^2}\right] - \phi_{ij}(w_i)\rho_i\omega_{ij}^2 = 0 \tag{4.23}$$

Again from (4.20),

$$\frac{d^2\delta_{ij}(t)}{dt^2} + \omega_{ij}^2\delta_{ij}(t) = 0 \tag{4.24}$$

To find out the solution of $\delta_{ij}(t)$ from (4.24).

$$\lambda^2 + \omega_{ij}^2 = 0$$

$$\lambda = \pm\, \iota\, \omega_{ij}$$

$$\delta_{ij}(t) = \exp(\iota\, \omega_{ij}\, t) \tag{4.25}$$

From (4.22), finding solution of $\phi_{ij}\,(w_i)$.

$$(EI)_i \frac{d^4\phi_{ij}\,(w_i)}{dw_i^4} - \phi_{ij}\,(w_i)\,\rho_i\omega_{ij}^2 = 0 \tag{4.26}$$

Let $\breve{z} = \phi_{ij}\,(w_i)$ and place this in (4.26).

$$(EI)_i \frac{d^4\breve{z}}{dw_i^4} - \breve{z}\rho_i\omega_{ij}^2 = 0 \tag{4.27}$$

Let $\breve{z} = e^{\lambda w}$

$$(EI)_i \frac{d^4 e^{\lambda w}}{dw_i^4} - e^{\lambda w}\rho_i\omega_{ij}^2 = 0 \tag{4.28}$$

$$\frac{d^4 e^{\lambda w}}{dw^4} = \lambda^4 e^{\lambda w} \tag{4.29}$$

$$(EI)_i\lambda^4 e^{\lambda w} - e^{\lambda w}\rho_i\omega_{ij}^2 = 0 \tag{4.30}$$

$$(EI)_i\lambda^4 - \rho_i\omega_{ij}^2 = 0 \tag{4.31}$$

From (4.31), we get $\lambda_1 = -\frac{\sqrt[4]{\rho}_i\sqrt{\omega_{ij}}}{\sqrt[4]{(EI)_i}}$, $\lambda_2 = -j\,\frac{\sqrt[4]{\rho}_i\sqrt{\omega_{ij}}}{\sqrt[4]{(EI)_i}}$, $\lambda_3 = j\,\frac{\sqrt[4]{\rho}_i\sqrt{\omega_{ij}}}{\sqrt[4]{(EI)_i}}$, $\lambda_4 = \frac{\sqrt[4]{\rho}_i\sqrt{\omega_{ij}}}{\sqrt[4]{(EI)_i}}$

So the solution is

$$\phi_{ij}\,(w_i) = C_{1,ij}\sin(\beta_{ij}w_i) + C_{2,ij}\cos(\beta_{ij}w_i) + C_{3,ij}\sinh(\beta_{ij}w_i) + C_{4,ij}\cosh(\beta_{ij}w_i) \tag{4.32}$$

where,

$$\beta_{ij} = \frac{\sqrt[4]{\rho}_i\sqrt{\omega_{ij}}}{\sqrt[4]{(EI)_i}} \qquad \text{or} \qquad \beta_{ij}^4 = {}^{\omega_{ij}^2\rho_i}/_{(EI)_i} \tag{4.33}$$

So from above derivations, the solutions for $\delta_{ij}(t)$ i.e. (4.25) and $\phi_{ij}\,(w_i)$ i.e. (4.32) is obtained.

To get value of unknown coefficients in (4.32), applying the base conditions (4.13) produces

$$C_{3,ij} = -C_{1,ij} \quad \text{and} \qquad C_{4,ij} = -C_{2,ij} \tag{4.34}$$

Applying boundary conditions (4.14) with (4.34) and taking $(MD) = 0$ gives homogeneous solution (4.35) [2]. Researchers [2, 136, 139, 142] argue that making $(MD) = 0$ for modeling does not put remarkable effect on the performance of modeling of system.

$$[F(\beta_{ij})] \begin{bmatrix} C_{1,ij} \\ C_{2,ij} \end{bmatrix} = 0 \tag{4.35}$$

where $F(\beta_{ij})$, given in (4.35), is hugely dependent on M_{Li} and J_{Li} and is defined in (4.36).

$$\begin{aligned} &(1 + \cos(\beta_{ij} l_i) \cosh(\beta_{ij} l_i)) - \frac{M_{Li}\beta_{ij}}{\rho_i} (\sin(\beta_{ij} l_i) \cosh(\beta_{ij} l_i) - \cos(\beta_{ij} l_i) \sinh(\beta_{ij} l_i)) \\ &- \frac{J_{Li}\beta_{ij}^3}{\rho_i} (\sin(\beta_{ij} l_i) \cosh(\beta_{ij} l_i) + \cos(\beta_{ij} l_i) \sinh(\beta_{ij} l_i)) + \frac{M_{Li} J_{Li} \beta_{ij}^4}{\rho_i^2} \\ &(1 - \cos(\beta_{ij} l_i) \cosh(\beta_{ij} l_i)) = 0 \end{aligned} \tag{4.36}$$

Closed form equation of motion

After the model is discretized, there is possibility of getting finite number of solutions. Next step is to use Lagrangian equation to get closed form of equations. Lagrange-Euler equation will give N generalized coordinate q_i solutions.

$$\frac{d}{dt}\left(\frac{\partial L}{\partial \dot{w}_i}\right) - \frac{\partial L}{\partial w_i} = f_i, \qquad i = 1, \ldots, N \tag{4.37}$$

Here, $L = T - U$. w_i is the generalized coordinate and f_i is the force performing work on w_i.

From the Lagrange-Euler equation, flexible manipulator can be written in the form shown in (4.38).

$$M(w)\ddot{w} + h(w, \dot{w}) + Kw = Qu \tag{4.38}$$

where M is the inertia positive definite matrix, h is vector of centrifugal and coriolis forces, K is the stiffness matrix, and Q is input weighting matrix.

Now from hereafter, terms are defined for the specific TLFM case with two modes of vibrations for each link. TLFM with two modes of deflection for each link is considered in this research. This is the preferable general case of a multi-link flexible manipulator. TLFM possesses all the necessary multi-link flexible manipulator characteristics like infinite degrees of freedom, complex dynamic interactions, and coupled linking effects. More links or modes require the use of symbolic manipulation programs since it is difficult to derive the closed-form equations for those cases due to complications of the systems. Hastings and Book [141] considered two modes and five modes of vibration for a flexible manipulator system. They observed that an increased number of modes does not necessarily increase the performance of the system, but increases the complexity of the system resulting in degraded performance of the system. Furthermore, it is also difficult to find stiffness constants for higher modes. Orthonormalization is performed by choosing value of $C_{1,ij}$ that normalizes the mode shape function, so that:

$$\int_0^{l_i} \phi_{ij}^2 (w_i) dw_i = m_i \tag{4.39}$$

Furthermore, (4.40-4.43) are induced after normalization [2].

$$m_i = \int_0^{l_i} \rho_i dw_i = \rho_i l_i \tag{4.40}$$

$$d_i = \frac{1}{m_i} \int_0^{l_i} \rho_i w_i dw_i = \frac{1}{2} l_i \tag{4.41}$$

$$J_{oi} = \int_0^{l_i} \rho_i w_i^2 dw_i = \frac{1}{3} m_i l_i^2 \tag{4.42}$$

$$v_{ij} = \int_0^{l_i} \rho_i \phi_{ij} (w_i) \, dw_i \tag{4.43}$$

where m_i is mass of link i, d_i is distance of center of mass of link i from joint i, J_{oi} is inertia of link i, and v_{ij} is deformation moment of order 0 of mode j of link i.

Orthornomalization of mode functions simplify the inertia matrix and makes stiffness matrix a diagonal matrix. Luca and Siciliano [2], considered (4.44-4.48) to be used in (4.14).

$$M_{L1} = m_2 + m_{h2} + m_p \tag{4.44}$$

$$J_{L1} = J_{o2} + J_{h2} + J_p + m_p l_2^2 \tag{4.45}$$

$$(MD)_1 = (m_2 d_2 + m_p l_2)\cos\theta_2 - \left[(v_{21} + m_p \phi_{21,e})\,\delta_{21} + (v_{22} + m_p \phi_{22,e})\,\delta_{22}\right]\sin\theta_2 \tag{4.46}$$

$$M_{L2} = m_p \tag{4.47}$$

$$J_{L2} = J_p \tag{4.48}$$

M_{Li} is the sum of all the masses beyond link i, whereas J_{Li} and $(MD)_i$ depends on the successive link. For the TLFM case, (4.38) becomes.

$$M_{11}\ddot{\theta}_1 + M_{12}\ddot{\theta}_2 + M_{13}\ddot{\delta}_{11} + M_{14}\ddot{\delta}_{12} + M_{15}\ddot{\delta}_{21} + M_{16}\ddot{\delta}_{22} + h_1 = U_1 \tag{4.49}$$

$$M_{21}\ddot{\theta}_1 + M_{22}\ddot{\theta}_2 + M_{23}\ddot{\delta}_{11} + M_{24}\ddot{\delta}_{12} + M_{25}\ddot{\delta}_{21} + M_{26}\ddot{\delta}_{22} + h_2 = U_2 \tag{4.50}$$

$$M_{31}\ddot{\theta}_1 + M_{32}\ddot{\theta}_2 + M_{33}\ddot{\delta}_{11} + M_{34}\ddot{\delta}_{12} + M_{35}\ddot{\delta}_{21} + M_{36}\ddot{\delta}_{22} + h_3 + K_3\delta_{11} = 0 \tag{4.51}$$

$$M_{41}\ddot{\theta}_1 + M_{42}\ddot{\theta}_2 + M_{43}\ddot{\delta}_{11} + M_{44}\ddot{\delta}_{12} + M_{45}\ddot{\delta}_{21} + M_{46}\ddot{\delta}_{22} + h_4 + K_4\delta_{12} = 0 \tag{4.52}$$

$$M_{51}\ddot{\theta}_1 + M_{52}\ddot{\theta}_2 + M_{53}\ddot{\delta}_{11} + M_{54}\ddot{\delta}_{12} + M_{55}\ddot{\delta}_{21} + M_{56}\ddot{\delta}_{22} + h_5 + K_5\delta_{21} = 0 \tag{4.53}$$

$$M_{61}\ddot{\theta}_1 + M_{62}\ddot{\theta}_2 + M_{63}\ddot{\delta}_{11} + M_{64}\ddot{\delta}_{12} + M_{65}\ddot{\delta}_{21} + M_{66}\ddot{\delta}_{22} + h_6 + K_6\delta_{22} = 0 \tag{4.54}$$

where,

$$K = diag\left\{0, 0, \omega_{11}^2 m_1, \omega_{12}^2 m_1, \omega_{21}^2 m_2, \omega_{22}^2 m_2\right\} \tag{4.55}$$

and h_i is evaluated by Chrisoffel symbol [2]

$$h_i = \sum_{j=1}^{N}\sum_{k=1}^{N}\left(\frac{\partial M_{ij}}{\partial w_k} - \frac{1}{2}\frac{\partial M_{jk}}{\partial w_i}\right)\dot{w}_j\dot{w}_k \tag{4.56}$$

Even for TLFM, considering two modes for each link made the problem difficult for calculation. Increasing the modes will increase the complexity and will be very difficult to find out the solution by hand, if not impossible. For two link problem

finding out solutions of $\ddot{\theta}_1$, $\ddot{\theta}_2$, $\ddot{\delta}_{11}$, $\ddot{\delta}_{12}$, $\ddot{\delta}_{21}$ and $\ddot{\delta}_{22}$ from (4.49-4.54) are very complicated, so Matlab is used to find the desired solution. Detailed solutions take too much space and so they are not included in here. Please refer [2] for the closed form equations of TLFM.

Using the AMM and the Euler-Lagrange equation, TLFM closed form of equations can be written in the form as (4.57) in accordance with this study.

$$M_T\ddot{w}_T + K_T w_T + C_T = Q_T u \tag{4.57}$$

Where $w_T = (\theta_1\ \theta_2\ \delta_{11}\ \ldots \delta_{1r}\ \delta_{21}\ \ldots \delta_{2r})^T$, θ_1 and θ_2 are the TLFM $1st$ and $2nd$ link position angles respectively, $M_T \in R^{s\times s}$ is the inertia positive definite matrix, $C_T \in R^s$ is the vector of centrifugal and Coriolis forces, $K_T \in R^{s\times s}$ is the stiffness matrix, u is the input vector, and Q_T is the input weighting matrix. In addition, $s = \grave{L} + \sum_i r_i$, $\grave{L}$ represents the number of links, and r_i represents the modes considered for each link.

4.2 Summary

This chapter introduces the third nonlinear system, a TLFM, belonging to the same class of nonlinear systems that are discussed in the previous chapter. Flexible manipulators are coupled, nonlinear, continuous dynamic systems having infinite degrees of freedom defined by ordinary, partial and integral differential equations. Mathematical modeling of the TLFM is presented in this chapter. Dynamic equations of the system is truncated into finite dimensions by AMM, which represents flexible manipulator dynamic model by a truncated finite modal series comprises eigenmode functions and time-varying mode amplitudes.

CHAPTER 5

SIMULATION RESULTS AND DISCUSSION

A thorough analysis of the proposed control scheme is provided by comparing it with the above-mentioned varieties of intelligent control schemes. A complex and difficult desired trajectory (5.1) is considered for both systems to ascertain the effectiveness of the proposed control scheme. This trajectory involves step, sinusoidal, and pulse behavior.

$$\theta_{ref}(\iota) = \begin{cases} -D & \iota < 20 \\ D \sin\left(\frac{\pi\iota}{5}\right) & 20 \leq \iota < 40 \\ D & 40 \leq \iota \leq 60 \end{cases} \tag{5.1}$$

where D in here is 57^o or approximately equivalent to 1 rad. The desired response simulation model is shown in Figure C.5. The SMANFC-2 parameter ρ should be large, making the transition between cases in (2.36) less frequent and therefore the convergence speed will not be compromised. The parameter ρ is hence selected to be 10^6. In addition, as demonstrated in the sufficient descent condition of the MHS algorithm shown in Appendix B.1, the value of the τ parameter should be greater than 0.25. The SMANFC-2 gives optimum performance, when the parameter τ is selected to be 2, which is the same value used by the Hager and Zang algorithm [85].

The performance of the proposed control scheme (referred to as SMANFC-2 henceforth) is compared with several other intelligent control schemes. These schemes are:

- APID: This is an adaptive PID control scheme [143].

- ANFC-1: This is a simple direct type-1 ANFC scheme. The parameters of the control scheme are adapted by the SD algorithm [144].
- ANFC-2: This is a simple direct ANFC type-2 scheme. The design of the control scheme is almost the same as described in Section 2.2.2, except that the tuning algorithm is SD [145].
- SMC: This is a conventional SMC [146].
- Hybrid of SMC and ANFC (SMNFC): This is the SMC and the ANFC hybrid scheme. Type-1 ANFC estimates the parameters and provides them to the SMC control law. The basic SMC switching control is used [147].
- Hybrid of SMC and type-1 ANFC (SMANFC-1): This is the SMC and the ANFC hybrid scheme. Type-1 ANFC estimates the parameters and provides them to the SMC control law. A separate type-1 ANFC scheme is used instead of the basic SMC switching control function.

In the figures, θ denotes the position angle, e denotes the trajectory error, and deflections are denoted by z. The most commonly used performance indices such as integral absolute error (IAE), integral squared error (ISE), integral time squared error (ITSE) and integral time absolute error (ITAE) are also evaluated in order to better illustrate the superiority of the proposed control scheme. The following section discusses the results of the studied nonlinear systems considered for the validation of the proposed control scheme in this study.

5.1 Analysis of the First Studied System

The first system that is considered is the RSTFA system, the detailed modeling of the system is explained in Section 3.2.1. Figure C.1 shows the simulation model diagram. Variable names may differ from what is presented in the main text of the thesis.

In this study, to indicate the appendage deflections two AMM modes are considered for each appendage. In (3.17): This implies that $w_S = \{\theta_S\ \bar{\delta}_1\ \bar{\delta}_2\}^T$; where, θ_S is rigid hub rotation angle, $\bar{\delta}_1$ and $\bar{\delta}_2$ are the generalized coordinates for the appendage. Furthermore, in (3.17): $M_S \in R^{3\times3}$, $w_S \in R^{3\times1}$, $K_S \in R^{3\times3}$, $Q_S \in R^{3\times1}$ and $u \in R^{1\times1}$. The control system generates the torque u that operates at the rigid hub of the satellite. The parameters of the RSTFA system are shown in Table 5.1. The units are modified in conformance with the metric system in this paper.

Figure 5.1 shows the results of the RSTFA system with the control schemes. Figure 5.1a shows the hub rotation angle of the RSTFA system for the desired profile trajectory (5.1). This is an under-actuated problem, where there is only one control actuator providing torque at the rigid hub of the RSTFA system. The results show that the SMANFC-2 has less overshoot, better transient and quicker settling time than all the other control schemes. This is also apparent in Figure 5.1b, which demonstrates the trajectory errors of all the control schemes. Figure 5.1c shows the deflections of appendages, which are calculated by (3.10). It is evident from these results that the SMANFC-2 not only accomplished faster tracking but also rapidly dissipated the deflections from the appendages. Table

Table 5.1 Parameters of RSTFA & RSFFA system [1]

Parameters Names	Symbols	Values
Rotary inertia of hub (kgm^2)	I_{hub}	10.85
Mass density of beams (kgm^{-1})	ρ	1.30
Arm length (m)	L	1.22
Hub radius (m)	r	0.30
Flexural rigidity of links (Nm^2)	EI	30.83
Tip mass (kg)	m_{tip}	2.29
Rotary inertia of tip mass (kgm^2)	I_{tip}	0.002

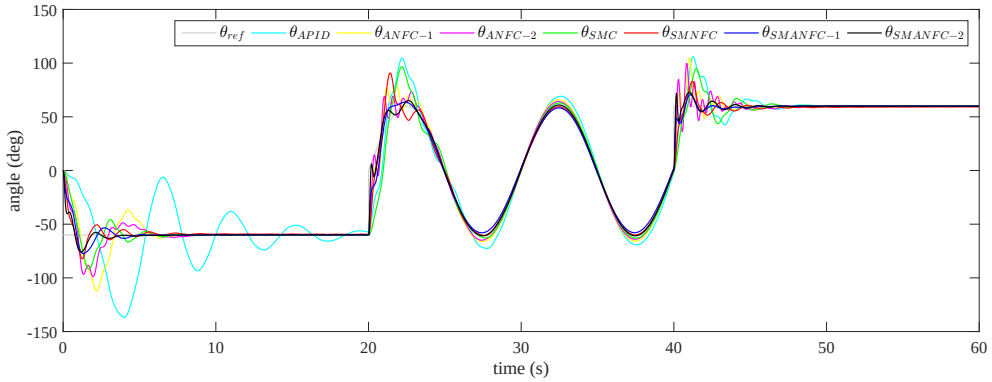

(a) Hub rotation angles

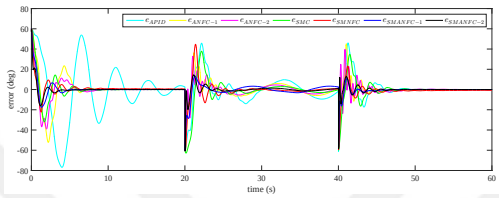

(b) Trajectory errors

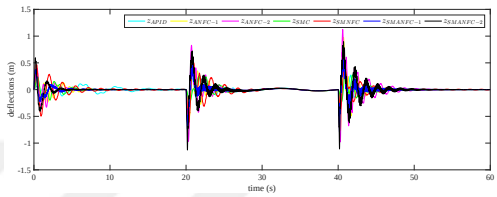

(c) Appendage deflections

Figure 5.1 Plots of the RSTFA system with the control schemes

5.2 offers a more detailed analysis of all the control schemes. The analysis shows that the SMANFC-2 is better than all the other control schemes in every aspect of the performance index.

Table 5.2 Performance indices for the RSTFA system

Control Scheme	IAE	ISE	ITAE	ISTE
APID	1273.2	771.1	20540.5	8611.3
ANFC-1	537.8	235.6	9512.4	2871.4
ANFC-2	424.9	152.5	8283.2	2134.1
SMC	513.2	252.3	11440.1	5006.3
SMNFC	322.7	115.0	7553.9	2274.7
SMANFC-1	253.3	74.4	5133.6	1041.7
SMANFC-2	168.5	45.5	3483.3	683.5

5.2 Analysis of the Second Studied System

A RSFFA system is considered for control purposes comprising a rigid hub and four identical cantilevered flexible appendages with tip masses. Figure C.2 shows the RSTFA simulation model diagram. Using the Lagrangian approach and expressing the appendage deflections by the AMM (3.22), the equations of motion can be expressed as (3.31). The parameters of the RSFFA system are given in Table 5.1. The detail mathematical modeling of the RSFFA system is presented in Section 3.3.1. In this study, to indicate the appendage deflections two AMM modes are considered for each appendage. In (3.31): This implies that $w_R = \{\theta_R \ \underline{\delta}_{11} \ \underline{\delta}_{21} \ \underline{\delta}_{12} \ \ \underline{\delta}_{22}\}^T$; where, θ_R is rigid hub rotation angle, $\underline{\delta}_{11}$ and $\underline{\delta}_{21}$ are the generalized coordinates for the first set of appendages, and $\underline{\delta}_{12}$ and $\underline{\delta}_{22}$ are the generalized coordinates for the second set of appendages. Furthermore, in (3.31): $M_R \in R^{5\times5}$, $w_R \in R^{5\times1}$, $K_R \in R^{5\times5}$, $Q_R \in R^{5\times3}$ and $u \in R^{3\times1}$. The control system generates the torque u_1 that operates at the rigid hub of the spacecraft, the torque u_2 that operates at the ends of the first and third appendages, and the torque u_3 that operates at the ends of second and fourth appendages. Spatial mode function variables are calculated to be 2.23 and -2.93 from the admissible function considered for the RSFFA (3.11) [1].

Figure 5.2 shows the results of the RSFFA system with the control schemes. Figure 5.2a shows the hub rotation angle of the RSFFA for the desired profile trajectory (5.1). The results clearly demonstrate that the SMANFC-2 has less overshoot, better transient and quicker settling time than all the other control schemes. This is also apparent in Figure 5.2b, which demonstrates the trajectory errors of all the control schemes. Figure 5.2c and Figure 5.2d show the deflections of both set of appendages, which are calculated by (3.22). The rapid movement of the spacecraft's rotation angle of the hub obviously tends to result in more appendage deflections, but the appendage deflections for the SMANFC-2 are well settled. It is evident from these results that the SMANFC-2 not only

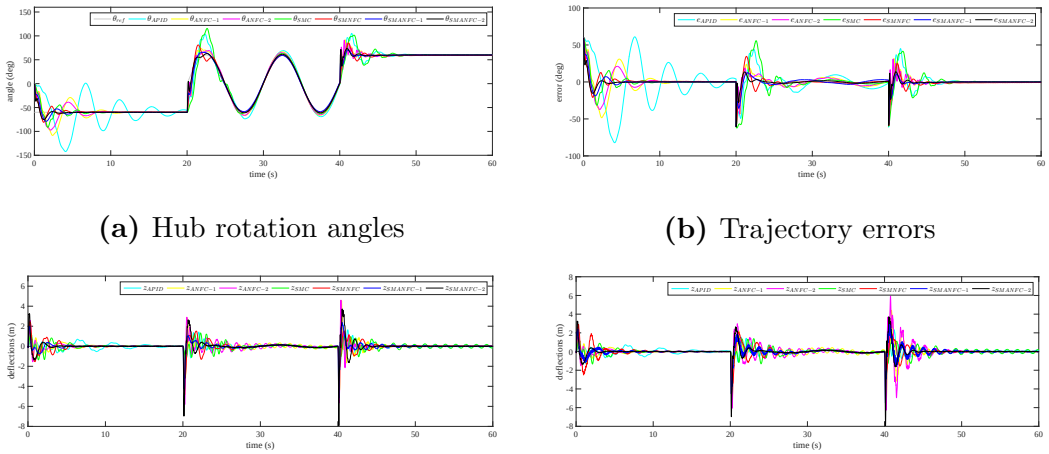

(a) Hub rotation angles

(b) Trajectory errors

(c) 1*st* set of appendage deflections

(d) 2*nd* set of appendage deflections

Figure 5.2 Plots of RSFFA system with the control schemes

accomplished faster tracking but also rapidly dissipated the deflections from the appendages. Table 5.3 offers a more detailed analysis of all the control schemes. The analysis shows that the SMANFC-2 is better than all the other control schemes in every aspect of the performance index. Besides SMANFC-2, SMNFC and SMANFC-1 are better than other control schemes. This indicates that the integration of SMC and ANFC has improved the efficiency of the control schemes compared to others.

Table 5.3 Performance indices for RSFFA system

Control Scheme	IAE	ISE	ITAE	ISTE
APID	1378.4	879.3	22011.6	9476.1
ANFC-1	603.0	248.7	9933.7	2650.0
ANFC-2	485.0	165.2	8663.8	1958.4
SMC	667.6	364.4	16123.1	8243.6
SMNFC	331.0	111.5	7891.0	2273.8
SMANFC-1	266.3	80.3	5277.8	1125.1
SMANFC-2	169.0	46.8	3413.5	705.5

5.3 Analysis of the Third Studied System

Table 5.4 Parameters of TLFM [2]

Parameters Names	Symbols	Values
Uniform density of $1st$ and $2nd$ link (kgm^{-1})	ρ_1 & ρ_2	0.2
Length of $1st$ and $2nd$ link (m)	l_1 & l_2	0.5
Distance of centre of mass of $2nd$ link from $2nd$ joint axis (m)	d_2	0.25
Mass of $1st$ link, $2nd$ link and payload (kg)	m_1, m_2 & m_p	0.1
Mass of $2nd$ hub (kg)	m_{h2}	1
Inertia of $1st$ link about $1st$ joint axis (kgm^2)	J_{o1}	0.0083
Inertia of $2nd$ link about $2nd$ joint axis (kgm^2)	J_{o2}	0.0083
Inertia of $1st$ hub and $2nd$ hub (kgm^2)	J_{h1} & J_{h2}	0.1
Inertia of payload (kgm^2)	J_p	0.0005
Flexural rigidity of $1st$ link and $2nd$ link (Nm^2)	EI_1 & EI_2	1

TLFM is a more complicated example because of the huge coupling effects between the two links. Figure C.3 shows the TLFM simulation model diagram. Figures C.4a, C.4b, C.4c, C.4d, C.4e and C.4f show the modules used in the TLFM. Variable names may differ from what is presented in the main text of the thesis. Variables and equations used in these modules can be found in [2]. Two AMM modes are considered for each TLFM link. In (4.57): The coordinates are

$w_T = (\theta_1\ \theta_2\ \delta_{11}\ \delta_{12}\ \delta_{21}\ \delta_{22})^T$; where θ_1 and θ_2 are $1st$ and $2nd$ link joint angle positions and δ_{11}, δ_{12}, δ_{21}, and δ_{22} are $1st$ link $1st$ mode, $1st$ link $2nd$ mode, $2nd$ link $1st$ mode and $2nd$ link $2nd$ mode modal displacements respectively. Furthermore, in (4.38): $M_T \in R^{6\times6}$, $C_T \in R^{6\times1}$, $K_T \in R^{6\times6}$, $u \in R^{2\times1}$ and $Q_T \in R^{6\times2}$. All the considered parameters are defined in Table 5.4 [2].

In order to further validate the robustness of the control system, the payload of TLFM is varied in order to check the robustness of the control system. The parameters of the control schemes are not changed and still, the control schemes should perform better for all the system variations in order to confirm better robust properties. Normal payload ($m_p = 0.1kg$), double payload ($m_p = 0.2kg$) and no payload ($m_p = 0kg$) are considered. It is understood that some parameters in (4.36) i.e., (4.44-4.48) depends on payload, that is the reason why changing the payload in TLFM affects the mode frequencies of the structure and changes the characteristics equation, which in returns changes the eigen values. This means for different payloads, derivations and calculations are again needed to be carried out, so to find out the values for the new changed payload. The calculations are carried out in following steps. $F(\beta_{ij})$ (4.36), is equated to zero and there is need to find out the values of β_{ij} from this equation. First m_i roots of this (4.36) will give positive values of β_{ij}. Then using these β_{ij}, values of w_{ij} (4.33) are evaluated. These values are then used in (4.32) to get values of $C_{1,ij}$ and $C_{2,ij}$, those are scale factors chosen by suitable normalization process that normalizes the mode shape function, so that (4.39) should satisfy.

5.3.1 TLFM with Normal Payloads

Figure 5.3 gives the root for TLFM with normal payloads. Figure 5.3a gives the root of $1st$ link $1st$ mode and $1st$ link $2nd$ mode that are $\beta_{11} = 1.16$ and $\beta_{12} = 2.25$, respectively. Figure 5.3b gives the root of $2nd$ link $1st$ mode and $2nd$ link $2nd$ mode that are $\beta_{21} = 2.47$ and $\beta_{22} = 6.69$, respectively. The mode

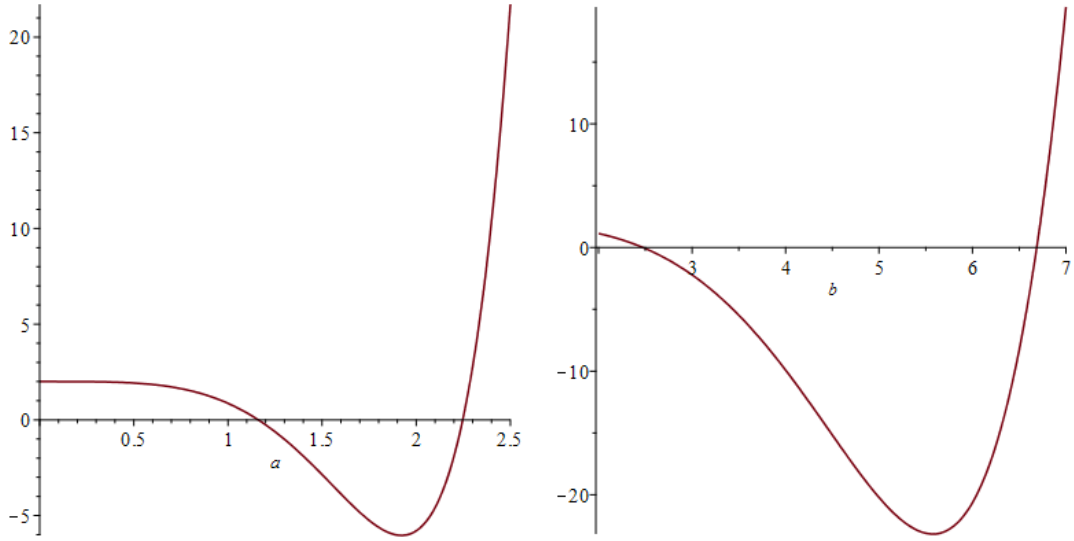

(a) 1*st* link roots **(b)** 2*nd* link roots

Figure 5.3 Roots for normal payload manipulator

shapes (4.32) evaluated for the TLFM with normal payload are $\phi_{11} = 0.143$, $\phi'_{11} = 0.507$, $\phi_{12} = 0.092$, $\phi'_{12} = -0.233$, $\phi_{21} = 0.137$, $\phi'_{21} = 0.411$, $\phi_{22} = -0.007$ and $\phi'_{22} = -1.135$.

Figure 5.4 shows the results of the TLFM with the control schemes. The deflections and angular positions of the two links are shown separately for a better view of the results. Figure 5.4a and Figure 5.4b show the angular positions of 1*st* and 2*nd* links respectively. The results indicate that the SMANFC-2 has faster convergence and superior performance in terms of fewer oscillations, better settling time, and less steady-state errors. This superiority of the SMANFC-2 is also apparent by the trajectory errors shown in Figure 5.4c and Figure 5.4d. Figure 5.4e and Figure 5.4f show the deflections of both links. TLFM has huge coupling effects, and therefore fluctuations in one link have a significant impact on the other, as shown in the figures. The sudden massive torque of the control systems to reach the target quickly induces further link deflections, which can then affect the accuracy of the link position. The angular positions of the SMANFC-2 are quickly following the desired trajectory and the deflections are well handled. The performance indices for both TLFM links are shown in Table 5.5. These perfor-

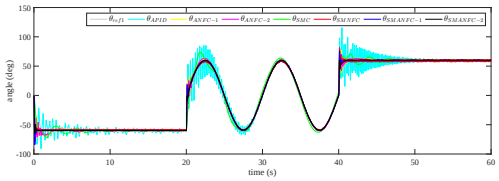

(a) 1*st* link angular positions

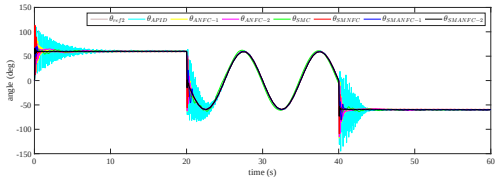

(b) 2*nd* link angular positions

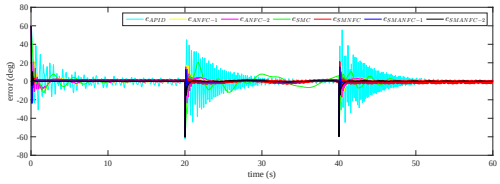

(c) 1*st* link trajectory errors

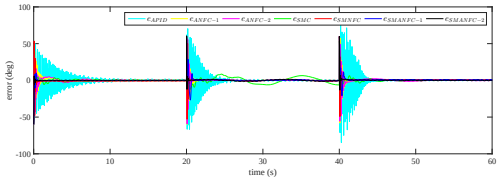

(d) 2*nd* link trajectory errors

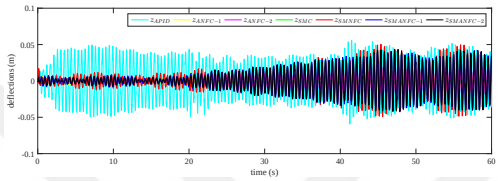

(e) 1*st* link deflections

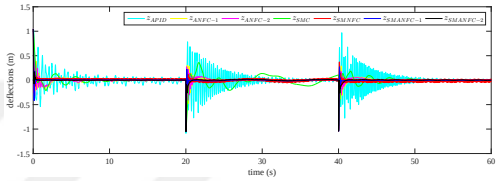

(f) 2*nd* link deflections

Figure 5.4 Plots of TLFM with the control schemes (normal payloads)

mance indices clearly indicate the superiority of the SMANFC-2 for both links compared to all other control schemes. Apart from SMANFC-2, the performance of SMNFC and SMANFC-1 is better than other control schemes.

5.3.2 TLFM with No Payloads

Figure 5.5 gives the root for TLFM with no payloads. Figure 5.5a gives the root of 1*st* link 1*st* mode and 1*st* link 2*nd* mode that are $\beta_{11} = 1.206$ and $\beta_{12} = 2.325$, respectively. Figure 5.5b gives the root of 2*nd* link 1*st* mode and 2*nd* link 2*nd* mode that are $\beta_{21} = 3.6$ and $\beta_{22} = 6.72$, respectively. With these values and using the procedure that is discussed above, we get values of mode shapes from (4.32) i.e., $\phi_{11} = 0.143$, $\phi'_{11} = 0.501$, $\phi_{12} = 0.090$, $\phi'_{12} = -0.267$, $\phi_{21} = 0.136$, $\phi'_{21} = 0.402$, $\phi_{22} = -0.0389$ and $\phi'_{22} = -1.441$.

Figure 5.6a and Figure 5.6b show the angular positions of 1*st* and 2*nd* links

Table 5.5 Performance indices for TLFM (normal payloads)

Control Schemes	1*st* link				2*nd* link			
	IAE	ISE	ITAE	ITSE	IAE	ISE	ITAE	ITSE
APID	536.3	152.3	13452.6	3569.9	495.3	254.6	11197.1	6468.2
ANFC-1	150.6	28.8	3277.5	479.6	121.4	44.4	2559.0	941.6
ANFC-2	133.2	25.1	2824.7	404.5	129.9	39.6	3068.5	867.1
SMC	342.3	73.9	8692.2	1496.9	215.5	33.4	5772.4	705.9
SMNFC	136.0	17.3	4111.0	391.7	112.4	26.5	3045.5	496.5
SMANFC-1	64.0	17.1	1578.2	334.6	88.9	26.1	2364.6	575.9
SMANFC-2	55.3	15.1	1549.6	315.2	52.5	9.1	1494.3	187.2

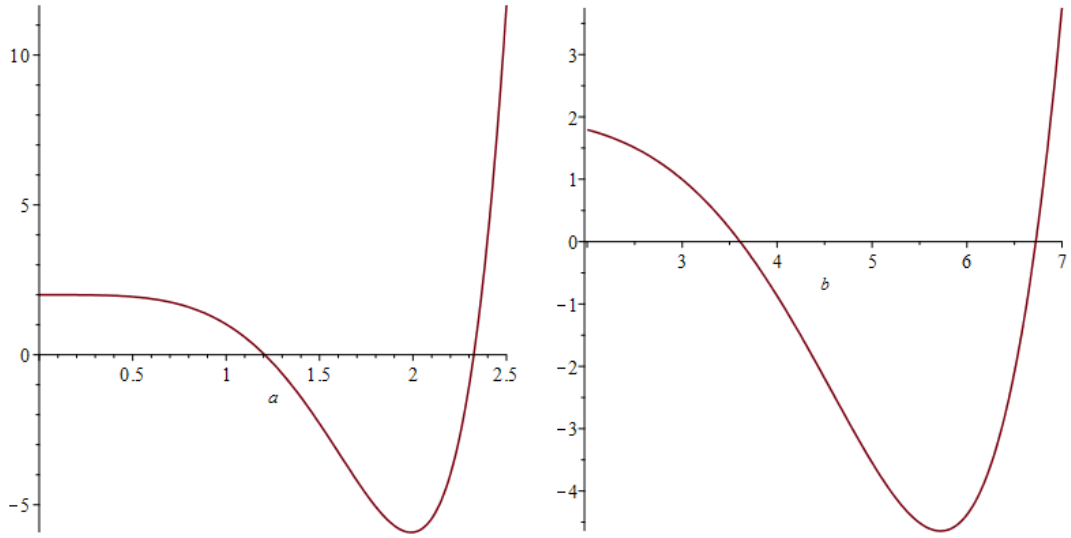

(a) 1*st* link roots **(b)** 2*nd* link roots

Figure 5.5 Roots for no payload manipulator

respectively. The results indicate that the SMANFC-2 has faster convergence and superior performance in terms of fewer oscillations, better settling time, and less steady-state errors. This superiority of the SMANFC-2 is also apparent by the trajectory errors shown in Figure 5.6c and Figure 5.6d. This shows the robustness of SMANFC-2 control scheme, even without manually changing the parameters

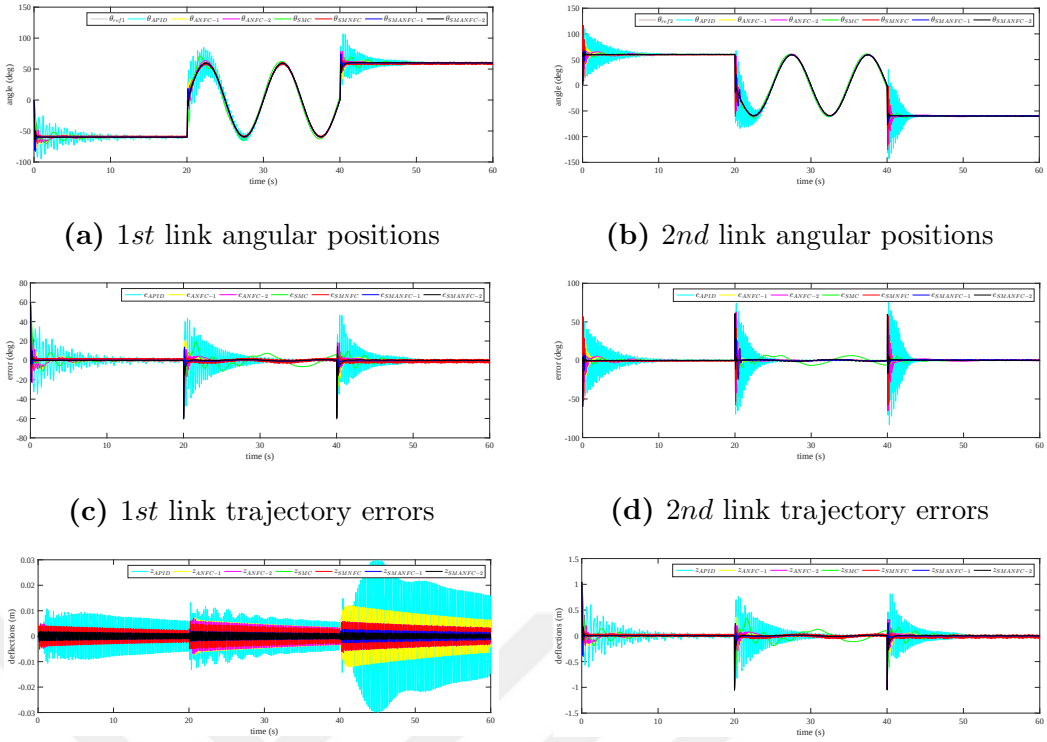

(a) 1*st* link angular positions

(b) 2*nd* link angular positions

(c) 1*st* link trajectory errors

(d) 2*nd* link trajectory errors

(e) 1*st* link deflections

(f) 2*nd* link deflections

Figure 5.6 Plots of TLFM with the control schemes (no payloads)

of the control scheme, still self-adapted against variation, and performed better than other control schemes. Figure 5.6e and Figure 5.6f show the deflections of both links. As expected with no payloads, the deflections of the links are less. SMANFC-2 has better deflection suppression as well as better angle tracking capability. The performance indices for both TLFM links are shown in Table 5.6. These performance indices clearly indicate the superiority of the SMANFC-2 for both links compared to all other control schemes.

5.3.3 TLFM with Double Payloads

Figure 5.7 shows the roots of frequency equation of TLFM with double payloads i.e., $\beta_{11} = 1.123$, $\beta_{12} = 2.183$, $\beta_{21} = 2.142$ and $\beta_{22} = 6.68$. Other parameters for the TLFM with double payloads are $\phi_{11} = 0.144$, $\phi'_{11} = 0.512$, $\phi_{12} = 0.0934$, $\phi'_{12} = -0.220$, $\phi_{21} = 0.137$, $\phi'_{21} = 0.410$, $\phi_{22} = -0.004$ and $\phi'_{22} = -1.103$.

Table 5.6 Performance indices for TLFM (no payloads)

Control Schemes	1*st* link				2*nd* link			
	IAE	ISE	ITAE	ITSE	IAE	ISE	ITAE	ITSE
APID	486.1	139.2	10735.6	2705.3	437.8	225.4	9099.0	5356.8
ANFC-1	141.3	27.8	2996.7	450.9	121.4	44.1	2404.3	927.9
ANFC-2	125.5	24.7	2562.2	387.6	140.9	44.9	3333.9	1054.8
SMC	326.2	71.0	8208.4	1418.3	203.4	31.9	5443.3	674.7
SMNFC	136.1	16.9	4111.7	391.3	114.4	29.7	3143.9	626.9
SMANFC-1	63.5	17.0	1576.2	333.6	74.5	22.0	1887.9	434.3
SMANFC-2	54.8	15.4	1540.2	322.4	51.6	9.0	1429.0	185.7

Figure 5.8a and Figure 5.8b show the angular positions of 1*st* and 2*nd* links respectively. The results indicate that the SMANFC-2 has faster convergence and superior performance in terms of fewer oscillations, better settling time, and less steady-state errors. This superiority of the SMANFC-2 is also apparent by the trajectory errors shown in Figure 5.8c and Figure 5.8d. Figure 5.8e and Figure 5.8f show the deflections of both links. With doubling of the payloads more deflections are expected as seen by the figures. Still, SMANFC-2 has performed better than other control schemes. It has shown great tracking capability as well as better deflection suppression. To further elaborate the performance, the performance indices for both TLFM links are shown in Table 5.7. These performance indices clearly indicate the superiority of the SMANFC-2 for both links compared to all other control schemes.

It is logical that the larger payload causes more TLFM fluctuations and is also seen in the results in this chapter. In addition, when more abrupt inputs were utilized, more TLFM fluctuations were observed. For all the cases, results depict that links are strongly coupled and the fluctuations introduced in one link affect

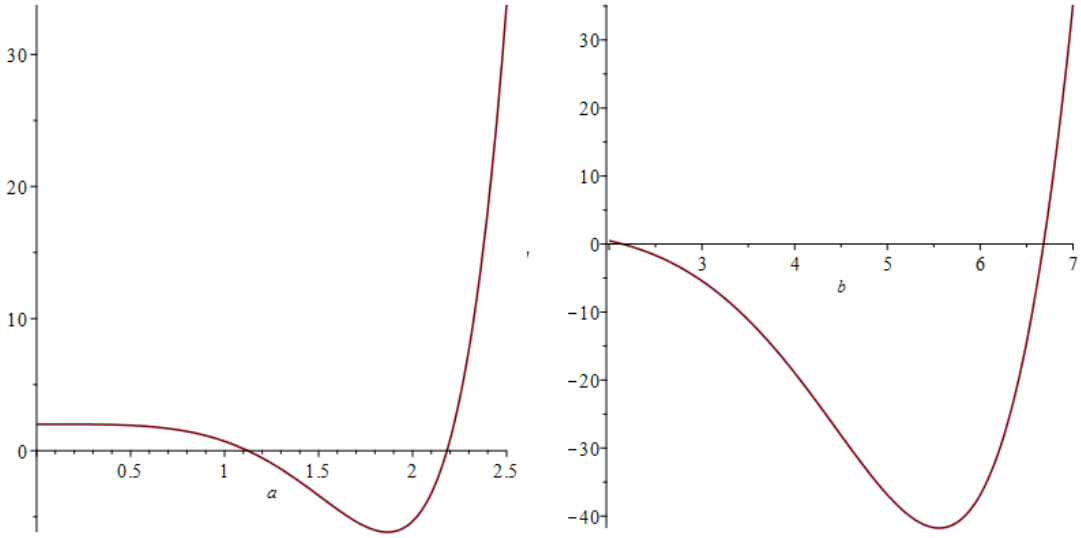

(a) 1*st* link roots **(b)** 2*nd* link roots

Figure 5.7 Roots for double payload manipulator

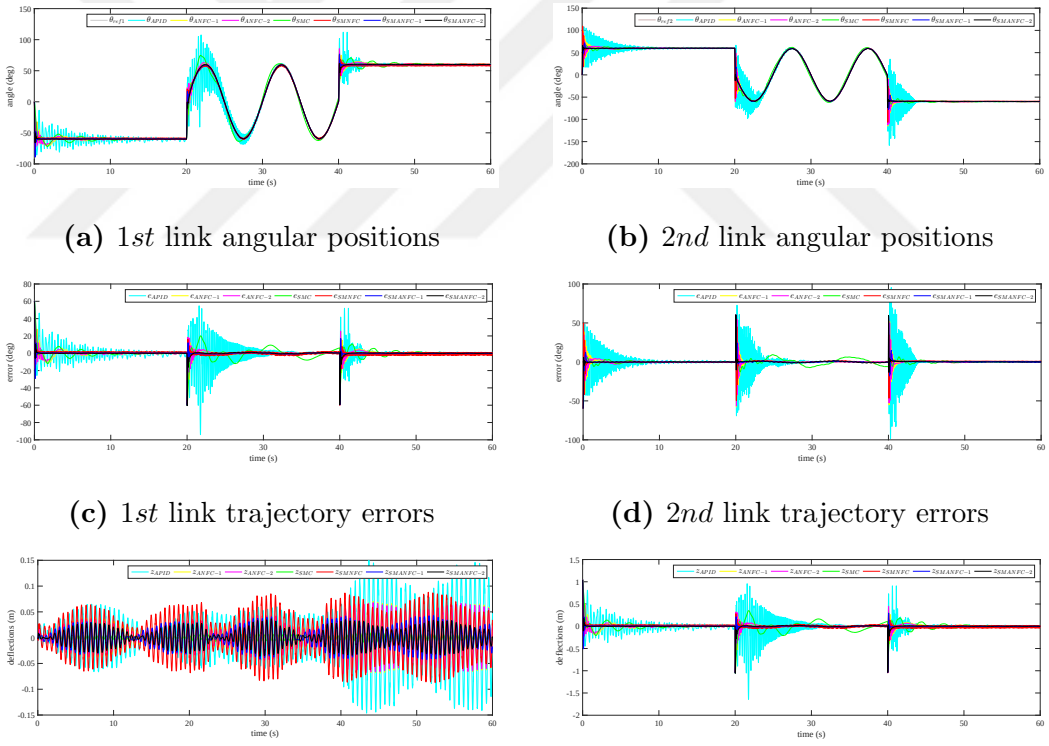

(a) 1*st* link angular positions **(b)** 2*nd* link angular positions

(c) 1*st* link trajectory errors **(d)** 2*nd* link trajectory errors

(e) 1*st* link deflections **(f)** 2*nd* link deflections

Figure 5.8 Plots of TLFM with the control schemes (double payloads)

other link modes also.

The results of all the studied nonlinear systems show that SMANFC-2 converges

Table 5.7 Performance indices for TLFM (double payloads)

Control Schemes	1st link				2nd link			
	IAE	ISE	ITAE	ITSE	IAE	ISE	ITAE	ITSE
APID	549.8	212.2	11061.6	4194.5	523.4	288.1	11852.4	7544.4
ANFC-1	171.9	32.2	3876.1	536.4	133.4	43.7	3030.5	912.3
ANFC-2	146.3	27.4	3078.1	449.6	126.7	38.0	2865.3	830.9
SMC	362.8	76.8	9229.8	1580.1	225.8	34.9	6053.4	738.6
SMNFC	131.3	17.1	3962.6	392.0	109.0	23.7	2961.1	449.0
SMANFC-1	65.1	17.3	1592.9	325.5	72.0	22.1	1888.4	458.7
SMANFC-2	52.2	15.0	1378.5	308.4	49.0	9.0	1337.0	183.9

quickly and thus does not have to make significant changes in each iteration and therefore the overall work done is less, while other control schemes constantly carry out heavy calculations to train the system in order to achieve the desired goal. Although the SMANFC-2 uses almost twice as many parameters as the type-1 ANFC, requiring more mathematical operations and more memory space, it provides more degrees of freedom and better ability to address uncertainty in the nonlinear systems. It thus delivers robust and fast performance compared to other control systems at a cost of slightly additional computational complexity, which is needed to better tackle the uncertainty in the nonlinear systems.

5.4 Summary

Simulation results of all three studied nonlinear systems that belong to the same class have been given in this chapter. For all three systems, which are RSTFA, RSFFA and TLFM, two modes for each appendage/link are considered to represent deflections in AMM. To further check the robustness of the control schemes,

TLFM is considered with three different payloads i.e., no payload, normal payload, and double payload. Changing the payload changes the entire dynamics of the system, and this is a challenging problem for the control scheme and is the best way to check the robustness of the control scheme. The detailed comparative analysis between the SMANFC-2 and other intelligent control schemes have been provided in this chapter for all the case studies. The results indicate that the SMANFC-2 performs best in every case and is, therefore, a better choice for the class of systems, which requires positional tracking while also keeping the fluctuations of the flexible appendages in control. It shows the advantages of both SMC and ANFCT2, which include faster response and robustness against uncertainties. This concludes that the scheme introduced in this study is well suited for a large class of single-body and multi-body systems.

CHAPTER 6

CONCLUSION

This chapter presents a summary of main results and contributions of the thesis with some conclusive remarks and future research directions. The study presents a new control scheme designated as the SMANFC-2, which is a hybrid of the ANFCT2 and the SMC, for the control of the class of nonlinear flexible systems. Flexible satellites, multi-link robotic systems, and several similar large flexible systems are part of the same class of nonlinear systems. The literature review, dynamic modeling, and implementation of three studied nonlinear systems of the same class, which are RSTFA, RSFFA and TLFM, are discussed in this thesis. These systems belong to the family of multi-body hybrid distributed parameter systems that are a combination of interconnected rigid and elastic bodies. The systems are highly nonlinear, infinite-dimensional, highly coupled systems described by the hybrid coordinate systems of ordinary, partial, and integral differential equations. The original systems have infinite solutions, so it is necessary to discretize the system in order to obtain the finite solutions. The AMM represents the system into time-varying mode amplitudes and spatially dependent eigenmode functions. It transforms the models into finite-dimensional models, but the truncated systems have arbitrarily defined dimensions and uncertainties, making it difficult to control them. Uncertain functions of the system are estimated by the ANFCT2 and provided to the SMC control law. In addition, another ANFCT2 aims to ensure that the system states reach the sliding surface more efficiently. The ANFCT2 uses a new modified CG optimization method that ensures global convergence and stability, which are not guaranteed by the widely used SD method. The stability of the SMANFC-2 is ensured by the Lya-

punov stability theorem. The SMANFC-2 is a model-free control scheme, since the control law does not depend on any dynamic parameters of the plant, which makes it suitable for a wide range of nonlinear systems of the same class. Furthermore, it provides the benefits of both the SMC and the ANFCT2 schemes and overcomes the deficiencies of both schemes. The proposed control scheme with its self-tuning mechanism has handled the problem efficiently and delivered an exceptional performance. It has effectively tracked the position and regulated the vibrations of the flexible nonlinear systems. By comparing the results with other intelligent control schemes, it is evident that the SMANFC-2 has the robustness to uncertainty as well as better setting time, less steady-state error, and less overshoot. As a conclusion of this study, it is revealed that the SMANFC-2 scheme is more reliable than other intelligent control schemes for control of a class of nonlinear flexible single-body and multi-body systems that requires simultaneous suppression of fluctuations.

There are many potential research possibilities for prospective research. The practical implementation of the proposed control scheme with nonlinear real-time systems could be considered. The control scheme could also be validated for a different class of nonlinear systems. The ANFCT2, discussed in this study, could be used in conjunction with other well-known control strategies to bring together a control scheme with combined advantages. The control system could be designed to be robust against unstructured uncertainties, such as external disturbances. It will bring a more robust control scheme that will be very useful as external disturbances can affect the performance of control schemes in practical systems.

REFERENCES

[1] Junkins, J. L. (1993). *Introduction to dynamics and control of flexible structures*, Aiaa.

[2] De Luca, A., Siciliano, B. (1991). Closed-form dynamic model of planar multilink lightweight robots, *IEEE Trans. Syst. Man Cybern.*, **21(4)**, 826–839.

[3] Grüne, L., Pannek, J. (2017). Nonlinear model predictive control, *Nonlinear Model Predictive Control*, 45–69.

[4] Wu, J., Fu, Q., Li, Z. (2017). $h\infty$ control via state observer feedback for the t–s fuzzy singular system, *International Journal of Machine Learning and Cybernetics*, **8(2)**, 619–626.

[5] Rigatos, G., Siano, P., Raffo, G. (2017). A nonlinear h-infinity control method for multi-dof robotic manipulators, *Nonlinear Dynamics*, **88(1)**, 329–348.

[6] Xiang, X., Yu, C., Lapierre, L., Zhang, J., Zhang, Q. (2018). Survey on fuzzy-logic-based guidance and control of marine surface vehicles and underwater vehicles, *International Journal of Fuzzy Systems*, **20(2)**, 572–586.

[7] Soliman, M. A., Hasanien, H. M., Azazi, H. Z., El-Kholy, E. E., Mahmoud, S. A. (2018). An adaptive fuzzy logic control strategy for performance enhancement of a grid-connected pmsg-based wind turbine, *IEEE Transactions on Industrial Informatics*, **15(6)**, 3163–3173.

[8] Li, Y., Tong, S. (2017). Adaptive neural networks prescribed performance control design for switched interconnected uncertain nonlinear systems,

IEEE transactions on neural networks and learning systems, **29(7)**, 3059–3068.

[9] Niu, B., Li, L. (2017). Adaptive backstepping-based neural tracking control for mimo nonlinear switched systems subject to input delays, *IEEE Transactions on Neural Networks and Learning Systems*, **29(6)**, 2638–2644.

[10] Incremona, G. P., Rubagotti, M., Ferrara, A. (2016). Sliding mode control of constrained nonlinear systems, *IEEE Transactions on Automatic Control*, **62(6)**, 2965–2972.

[11] Sira-Ramírez, H., Aguilar-Orduña, M., Zurita-Bustamante, E. (2019). On the sliding mode control of mimo nonlinear systems: An input-output approach, *International Journal of Robust and Nonlinear Control*, **29(3)**, 715–735.

[12] Sun, N., Wu, Y., Fang, Y., Chen, H. (2017). Nonlinear antiswing control for crane systems with double-pendulum swing effects and uncertain parameters: Design and experiments, *IEEE Transactions on Automation Science and Engineering*, **15(3)**, 1413–1422.

[13] Zeng, G.-Q., Xie, X.-Q., Chen, M.-R., Weng, J. (2019). Adaptive population extremal optimization-based pid neural network for multivariable nonlinear control systems, *Swarm and evolutionary computation*, **44**, 320–334.

[14] Wu, C., Liu, J., Jing, X., Li, H., Wu, L. (2017). Adaptive fuzzy control for nonlinear networked control systems, *IEEE Transactions on Systems, Man, and Cybernetics: Systems*, **47(8)**, 2420–2430.

[15] Aounallah, T., Essounbouli, N., Hamzaoui, A., Bouchafaa, F. (2018). Algorithm on fuzzy adaptive backstepping control of fractional order for doubly-fed induction generators, *IET Renewable Power Generation*, **12(8)**, 962–967.

[16] Utkin, V. (1977). Variable structure systems with sliding modes, *IEEE Transactions on Automatic control*, **22(2)**, 212–222.

[17] Utkin, V. I. (2013). *Sliding modes in control and optimization*, Springer Science & Business Media.

[18] Hamayun, M. T., Edwards, C., Alwi, H. (2016). Integral sliding mode control, *Fault Tolerant Control Schemes Using Integral Sliding Modes*, 17–37.

[19] Jedda, O., Ghabi, J., Douik, A. (2017). Sliding mode control of an inverted pendulum, *Applications of Sliding Mode Control*, 105–118.

[20] Utkin, V., Guldner, J., Shi, J. (2017). *Sliding mode control in electro-mechanical systems*, CRC press.

[21] Ho, H., Wong, Y.-K., Rad, A. B. (2009). Adaptive fuzzy sliding mode control with chattering elimination for nonlinear siso systems, *Simulation Modelling Practice and Theory*, **17(7)**, 1199–1210.

[22] Chang, W.-J., Hsu, F.-L. (2016). Sliding mode fuzzy control for takagi–sugeno fuzzy systems with bilinear consequent part subject to multiple constraints, *Information Sciences*, **327**, 258–271.

[23] Layeghi, H., Arjmand, M. T., Salarieh, H., Alasty, A. (2008). Stabilizing periodic orbits of chaotic systems using fuzzy adaptive sliding mode control, *Chaos, Solitons & Fractals*, **37(4)**, 1125–1135.

[24] Kumar, J., Azar, A. T., Kumar, V., Rana, K. P. S. (2018). Design of fractional order fuzzy sliding mode controller for nonlinear complex systems, *Mathematical Techniques of Fractional Order Systems*, 249–282.

[25] Chang, C.-W., Yang, C.-Y., Tao, C.-W. (2017). Interval fuzzy sliding-mode formation controller design, *Soft Computing*, **21(14)**, 4045–4054.

[26] Markazi, A. H. D., Maadani, M., Zabihifar, S. H., Doost-Mohammadi, N. (2018). Adaptive fuzzy sliding mode control of under-actuated nonlinear

systems, *International Journal of Automation and Computing*, **15(3)**, 364–376.

[27] Wen, S., Chen, M. Z., Zeng, Z., Huang, T., Li, C. (2017). Adaptive neural-fuzzy sliding-mode fault-tolerant control for uncertain nonlinear systems, *IEEE Transactions on Systems, Man, and Cybernetics: Systems*, **47(8)**, 2268–2278.

[28] Zadeh, L. A. (1965). Fuzzy sets, *Information and control*, **8(3)**, 338–353.

[29] Buckley, J. J. (1993). Sugeno type controllers are universal controllers, *Fuzzy sets and systems*, **53(3)**, 299–303.

[30] Castro, J. L. (1995). Fuzzy logic controllers are universal approximators, *IEEE transactions on systems, man, and cybernetics*, **25(4)**, 629–635.

[31] Saif, A.-W. A., Mudasar, M., Mysorewala, M., Elshafei, M. (2020). Observer-based interval type-2 fuzzy logic control for nonlinear networked control systems with delays, *International Journal of Fuzzy Systems*, **22(2)**, 380–399.

[32] Khater, A. A., El-Nagar, A. M., El-Bardini, M., El-Rabaie, N. M. (2019). Online learning of an interval type-2 tsk fuzzy logic controller for nonlinear systems, *Journal of the Franklin Institute*, **356(16)**, 9254–9285.

[33] El-Nagar, A. M. (2018). Nonlinear dynamic systems identification using recurrent interval type-2 tsk fuzzy neural network–a novel structure, *ISA transactions*, **72**, 205–217.

[34] Pratama, M., Lu, J., Lughofer, E., Zhang, G., Er, M. J. (2016). An incremental learning of concept drifts using evolving type-2 recurrent fuzzy neural networks, *IEEE Transactions on Fuzzy Systems*, **25(5)**, 1175–1192.

[35] Mendel, J., Hagras, H., Tan, W.-W., Melek, W. W., Ying, H. (2014). *Introduction to type-2 fuzzy logic control: theory and applications*, John Wiley & Sons.

[36] Castillo, O., Amador-Angulo, L., Castro, J. R., Garcia-Valdez, M. (2016). A comparative study of type-1 fuzzy logic systems, interval type-2 fuzzy logic systems and generalized type-2 fuzzy logic systems in control problems, *Inf. Sci.*, **354**, 257–274.

[37] Sarangapani, J. (2018). *Neural network control of nonlinear discrete-time systems*, CRC press.

[38] Siddique, N., Adeli, H. (2013). *Computational intelligence: synergies of fuzzy logic, neural networks and evolutionary computing*, John Wiley & Sons.

[39] Snyman, J. A., Wilke, D. N. (2018). Line search descent methods for unconstrained minimization, *Practical Mathematical Optimization*, 41–69.

[40] Mishra, S. K., Ram, B. (2019). Conjugate gradient methods, *Introduction to Unconstrained Optimization with R*, 211–244.

[41] Cottle, R. W., Thapa, M. N. (2017). Descent methods, *Linear and Nonlinear Optimization*, 317–368.

[42] Lin, C.-M., Le, T.-L., Huynh, T.-T. (2018). Self-evolving function-link interval type-2 fuzzy neural network for nonlinear system identification and control, *Neurocomputing*, **275**, 2239–2250.

[43] Han, H.-G., Lin, Z.-L., Qiao, J.-F. (2017). Modeling of nonlinear systems using the self-organizing fuzzy neural network with adaptive gradient algorithm, *Neurocomputing*, **266**, 566–578.

[44] Juang, C.-F., Juang, K.-J. (2016). Circuit implementation of data-driven tsk-type interval type-2 neural fuzzy system with online parameter tuning ability, *IEEE Transactions on Industrial Electronics*, **64(5)**, 4266–4275.

[45] Mai, S., Yang, C., Qiao, J. (2017). A recurrent rbf neural network based on adaptive optimum steepest descent learning algorithm, *2017 36th Chinese Control Conference (CCC)*, 3942–3947.

[46] Lin, C.-M., Le, T.-L. (2017). Pso-self-organizing interval type-2 fuzzy neural network for antilock braking systems, *International Journal of Fuzzy Systems*, **19(5)**, 1362–1374.

[47] Khanesar, M. A., Kayacan, E. (2017). A novel complexity reduced levenberge-marquardt algorithm: Application to the training of interval type-2 fuzzy systems, *2017 IEEE International Conference on Fuzzy Systems (FUZZ-IEEE)*, 1–6.

[48] Mathew, J., Griffin, J., Alamaniotis, M., Kanarachos, S., Fitzpatrick, M. E. (2018). Prediction of welding residual stresses using machine learning: Comparison between neural networks and neuro-fuzzy systems, *Applied Soft Computing*, **70**, 131–146.

[49] Heidari, H., Korayem, M., Haghpanahi, M., Batlle, V. F. (2013). Optimal trajectory planning for flexible link manipulators with large deflection using a new displacements approach, *Journal of Intelligent & Robotic Systems*, **72(3-4)**, 287–300.

[50] Pradhan, S. K., Subudhi, B. (2014). Nonlinear adaptive model predictive controller for a flexible manipulator: An experimental study, *IEEE Transactions on Control Systems Technology*, **22(5)**, 1754–1768.

[51] Qiu, Z.-c., Zhang, X.-m., Wang, Y.-c., Wu, Z.-w., et al. (2009). Active vibration control of a flexible beam using a non-collocated acceleration sensor

and piezoelectric patch actuator, *Journal of sound and vibration*, **326(3)**, 438–455.

[52] Sun, D., Mills, J. K., Shan, J., Tso, S. (2004). A pzt actuator control of a single-link flexible manipulator based on linear velocity feedback and actuator placement, *Mechatronics*, **14(4)**, 381–401.

[53] Mahamood, R. M., Pedro, J. O. (2011). Hybrid pd/pid controller design for two-link flexible manipulators, *IEEE Control Conference (ASCC), 2011 8th Asian*, 1358–1363.

[54] Miyasato, Y. (2010). Finite dimensional adaptive $h\infty$ control for flexible arms preceded by input nonlinearites, *Intelligent Control (ISIC), 2010 IEEE International Symposium on*, 2296–2301.

[55] Ho, M.-T., Tu, Y.-W. (2006). Position control of a single-link flexible manipulator using $h\infty$-based pid control, *IEE Proceedings-Control Theory and Applications*, **153(5)**, 615–622.

[56] Yanmin, W., Yuqing, C., Hongwei, X. (2015). Optimized continuous nonsingular terminal sliding mode control of uncertain flexible manipulators, *IEEE 34th Chinese Control Conference (CCC)*, 3392–3397.

[57] Zebin, T., Alam, M. (2010). Dynamic modeling and fuzzy logic control of a two-link flexible manipulator using genetic optimization techniques, *Computer and Information Technology (ICCIT), 2010 13th International Conference on*, 418–423.

[58] Chaoui, H., Gueaieb, W., Yagoub, M. C., Sicard, P. (2006). Hybrid neural fuzzy sliding mode control of flexible-joint manipulators with unknown dynamics, *IEEE Industrial Electronics, IECON 2006-32nd Annual Conference on*, 4082–4087.

[59] Sanz, A., Etxebarria, V. (2006). Experimental control of a two-dof flexible robot manipulator by optimal and sliding methods, *Journal of Intelligent & Robotic Systems*, **46(2)**, 95–110.

[60] Pradhan, S. K., Subudhi, B. (2013). Fuzzy learning based adaptive control for a two-link flexible manipulator, *Control Applications (CCA), 2013 IEEE International Conference on*, 282–287.

[61] Li, Y., Tong, S., Li, T. (2013). Adaptive fuzzy output feedback control for a single-link flexible robot manipulator driven dc motor via backstepping, *Nonlinear Analysis: Real World Applications*, **14(1)**, 483–494.

[62] Su, Z., Khorasani, K. (2001). A neural-network-based controller for a single-link flexible manipulator using the inverse dynamics approach, *IEEE Transactions on Industrial Electronics*, **48(6)**, 1074–1086.

[63] Neto, A. D. A., Goes, L. C. S., Nascimento, C. L. (2010). Accumulative learning using multiple ann for flexible link control, *IEEE Transactions on Aerospace and Electronic Systems*, **46(2)**, 508–524.

[64] Zhang, Y., Yang, T., Sun, Z. (2009). Neuro-sliding-mode control of flexible-link manipulators based on singularly perturbed model, *Tsinghua Science & Technology*, **14(4)**, 444–451.

[65] Ross, T. J. (2009). *Fuzzy logic with engineering applications*, John Wiley & Sons.

[66] Demuth, H. B., Beale, M. H., De Jess, O., Hagan, M. T. (2014). *Neural network design*, Martin Hagan.

[67] Passino, K. M., Yurkovich, S. (1997). *Fuzzy Control*, Addison-Wesley Longman Publishing Co., Inc.:USA.

[68] Tinkir, M., Önen, Ü., Kalyoncu, M. (2010). Modelling of neurofuzzy control of a flexible link, *Proceedings of the Institution of Mechanical Engineers, Part I: Journal of Systems and Control Engineering*, **224(5)**, 529–543.

[69] Önen, Ü., Kalyoncu, M., Tinkir, M., Botsali, F. M. (2011). Application of adaptive neural network based interval type-2 fuzzy logic control on a nonlinear system, *Computer Research and Development (ICCRD), 2011 3rd International Conference on*, volume 4, 104–108.

[70] Subudhi, B., Morris, A. S. (2009). Soft computing methods applied to the control of a flexible robot manipulator, *Applied Soft Computing*, **9(1)**, 149–158.

[71] Sotiropoulos, D., Kostopoulos, A., Grapsa, T. (2002). A spectral version of perry's conjugate gradient method for neural network training, *Proceedings of 4th GRACM Congress on Computational Mechanics*, volume 1, 291–298.

[72] Khan, L., Qamar, S., Khan, M. U. (2014). Comparative analysis of adaptive neurofuzzy control techniques for full car active suspension system, *Arabian Journal for Science and Engineering*, **39(3)**, 2045–2069.

[73] Riaz, S., Khan, L. (2015). Neurofuzzy adaptive control for full-car nonlinear active suspension with onboard antilock braking system, *Arabian Journal for Science and Engineering*, **40(12)**, 3483–3505.

[74] Fletcher, R., Powell, M. J. (1963). A rapidly convergent descent method for minimization, *The computer journal*, **6(2)**, 163–168.

[75] Wright, S., Nocedal, J. (1999). Numerical optimization, *Springer Science*, **35**, 67–68.

[76] Bertsekas, D. P. (1999). *Nonlinear programming*, Athena scientific Belmont.

[77] Fletcher, R., Reeves, C. M. (1964). Function minimization by conjugate gradients, *The computer journal*, **7(2)**, 149–154.

[78] Hestenes, M. R., Stiefel, E. (1952). *Methods of conjugate gradients for solving linear systems*, volume 49, NBS.

[79] Slotine, J.-J. E., Li, W., et al. (1991). *Applied nonlinear control*, volume 199, Prentice hall Englewood Cliffs, NJ.

[80] Wang, J., Rad, A. B., Chan, P. T. (2001). Indirect adaptive fuzzy sliding mode control: Part I: fuzzy switching, *Fuzzy Sets and Systems*, **122(1)**, 21–30.

[81] Takagi, T., Sugeno, M. (1993). Fuzzy identification of systems and its applications to modeling and control, *Readings in Fuzzy Sets for Intelligent Systems*, 387–403, Elsevier.

[82] Sugeno, M., Yasukawa, T. (1993). A fuzzy-logic-based approach to qualitative modeling, *IEEE T. Fuzzy Syst.*, **1**, 7.

[83] Takagi, T., Sugeno, M. (1985). Fuzzy identification of systems and its applications to modeling and control, *IEEE Trans. Syst. Man Cybern.*, **(1)**, 116–132.

[84] Mitaim, S., Kosko, B. (1996). What is the best shape for a fuzzy set in function approximation?, *Fuzzy Systems, 1996., Proceedings of the Fifth IEEE International Conference on*, volume 2, 1237–1243.

[85] Hager, W. W., Zhang, H. (2005). A new conjugate gradient method with guaranteed descent and an efficient line search, *SIAM J. Optimiz.*, **16**, 170–192.

[86] Hestenes, M. R., Stiefel, E. (1952). *Methods of conjugate gradients for solving linear systems*, volume 49, NBS: Washington.

[87] Dong, X. L., Liu, H., Xu, Y. L., Yang, X. M. (2015). Some nonlinear conjugate gradient methods with sufficient descent condition and global convergence, *Optim. Lett.*, **9(7)**, 1421–1432.

[88] Dai, Y.-H., Yuan, Y. (1999). A nonlinear conjugate gradient method with a strong global convergence property, *SIAM J. Optimiz.*, **10**, 177–182.

[89] Wolfe, P. (1969). Convergence conditions for ascent methods, *SIAM Rev.*, **11(2)**, 226–235.

[90] Dong, X., Liu, H., He, Y. (2015). A self-adjusting conjugate gradient method with sufficient descent condition and conjugacy condition, *J. Optimiz. Theory App.*, **165(1)**, 225–241.

[91] Zoutendijk, G. (1970). Nonlinear programming, computational methods, *Integer and nonlinear programming*, 37–86.

[92] Yuan, G. (2009). Modified nonlinear conjugate gradient methods with sufficient descent property for large-scale optimization problems, *Optim. Lett.*, **3**, 11–21.

[93] Dai, Z.-f., Tian, B.-S. (2011). Global convergence of some modified prp nonlinear conjugate gradient methods, *Optim. Lett.*, **5(4)**, 615–630.

[94] Suresh M, J., Atul G, K., Peiman G, M. (1995). *A Class of Stabilizing Controllers for Flexible Multibody Systems*, NASA: Langley.

[95] Jonker, B. (1989). A finite element dynamic analysis of spatial mechanisms with flexible links, *Computer Methods in Applied Mechanics and Engineering*, **76(1)**, 17–40.

[96] Morris, A. S., Madani, A. (1998). Quadratic optimal control of a two-flexible-link robot manipulator, *Robotica*, **16(1)**, 97–108.

[97] Kim, J.-S., Uchiyama, M. (2000). Dynamic modeling of two cooperating flexible manipulators, *Journal of Mechanical Science and Technology*, **14(2)**, 188–196.

[98] Yoshikawa, T., Hosoda, K. (1996). Modeling of flexible manipulators using virtual rigid links and passive joints, *The International Journal of Robotics Research*, **15(3)**, 290–299.

[99] Nadira, R., Mahil, S. (1986). A finite element/lagrange approach to modeling lightweight flexible manipulators, *Journal of dynamic systems, measurement, and control-Transactions of the ASME*, **108**, 199.

[100] Chung, J., Yoo, H. H. (2002). Dynamic analysis of a rotating cantilever beam by using the finite element method, *Journal of Sound and Vibration*, **249(1)**, 147–164.

[101] Gaultier, P. E., Cleghorn, W. L. (1991). Modelling of multi-link spatial flexible manipulators employing the finite element method, *13th Canadian Congress of Applied Mechanics*, volume 1, 648–649.

[102] Jonker, B. (1989). A finite element dynamic analysis of spatial mechanisms with flexible links, *Computer Methods in Applied Mechanics and Engineering*, **76(1)**, 17–40.

[103] Rahimi, H., Nazemizadeh, M. (2014). Dynamic analysis and intelligent control techniques for flexible manipulators: a review, *Advanced Robotics*, **28(2)**, 63–76.

[104] Castri, C. d., Messina, A. (2012). Exact modeling for control of flexible manipulators, *Journal of Vibration and Control*, **18(10)**, 1526–1551.

[105] Thomson, W. (2018). *Theory of vibration with applications*, CrC Press.

[106] Korayem, M., Rahimi, H. (2011). Nonlinear dynamic analysis for elastic robotic arms, *Frontiers of Mechanical Engineering*, **6(2)**, 219–228.

[107] Karray, F., Grewal, A., Glaum, M., Modi, V. (1997). Stiffening control of a class of nonlinear affine systems, *IEEE Trans. Aerosp. Electron. Syst.*, **33**, 473–484.

[108] Grewal, A., Modi, V. (1996). Robust attitude and vibration control of the space station, *Acta Astronautica*, **38(3)**, 139–160.

[109] Gorinevsky, D., Vukovich, G. (1998). Nonlinear input shaping control of flexible spacecraft reorientation maneuver, *Journal of Guidance, Control, and Dynamics*, **21(2)**, 264–270.

[110] Singh, S. N., Zhang, R. (2004). Adaptive output feedback control of spacecraft with flexible appendages by modeling error compensation, *Acta Astronaut.*, **54**, 229–243.

[111] Singh, S. N., de Araujo, A. D. (1999). Adaptive control and stabilization of elastic spacecraft, *IEEE Trans. Aerosp. Electron. Syst.*, **35(1)**, 115–122.

[112] Annaswamy, A. M., Clancy, D. J. (1996). Adaptive control strategies for flexible space structures, *IEEE Trans. Aerosp. Electron. Syst.*, **32**, 952–966.

[113] Maganti, G. B., Singh, S. N. (2007). Simplified adaptive control of an orbiting flexible spacecraft, *Acta Astronaut.*, **61**, 575–589.

[114] Azadi, M., Fazelzadeh, S., Eghtesad, M., Azadi, E. (2011). Vibration suppression and adaptive-robust control of a smart flexible satellite with three axes maneuvering, *Acta Astronaut.*, **69**, 307–322.

[115] Nayeri, M. R. D., Alasty, A., Daneshjou, K. (2004). Neural optimal control of flexible spacecraft slew maneuver, *Acta Astronautica*, **55(10)**, 817–827.

[116] Hovakimyan, N., Cao, C. (2010). *L1 adaptive control theory: guaranteed robustness with fast adaptation*, volume 21, SIAM-Society for Industrial and Applied Mathematics.

[117] Lee, K. W., Singh, S. N. (2012). L1 adaptive control of flexible spacecraft despite disturbances, *Acta Astronaut.*, **80**, 24–35.

[118] Hu, Q. (2010). Sliding mode attitude control with l2-gain performance and vibration reduction of flexible spacecraft with actuator dynamics, *Acta Astronaut.*, **67**, 572–583.

[119] Bang, H., Ha, C.-K., Kim, J. H. (2005). Flexible spacecraft attitude maneuver by application of sliding mode control, *Acta Astronaut.*, **57**, 841–850.

[120] Dong, C., Xu, L., Chen, Y., Wang, Q. (2009). Networked flexible spacecraft attitude maneuver based on adaptive fuzzy sliding mode control, *Acta Astronaut.*, **65**, 1561–1570.

[121] Hu, Q.-l., Wang, Z., Gao, H. (2008). Sliding mode and shaped input vibration control of flexible systems, *IEEE Transactions on Aerospace and Electronic systems*, **44(2)**, 503–519.

[122] Lupi, V. D., Chun, H. M., Turner, J. D. (1992). Distributed control and simulation of a bernoulli-euler beam, *J. Guid. Control Dyn.*, **15**, 727–734.

[123] Meirovitch, L., Quinn, R. (1987). Equations of motion for maneuvering flexible spacecraft, *J. Guid. Control Dyn.*, **10**, 453–465.

[124] Meirovitch, L., Stemple, T. (1995). Hybrid equations of motion for flexible multibody systems using quasicoordinates, *J. Guid. Control Dyn.*, **18**, 678–688.

[125] Elgohary, T. A., Turner, J. D. (2013). Generalized frequency domain modeling and analysis for a flexible rotating spacecraft, *AIAA Modeling and Simulation Technologies (MST) Conference*, 4914.

[126] Elgohary, T. A., Turner, J. D., Junkins, J. (2014). Dynamics and controls of a generalized frequency domain model flexible rotating spacecraft, *SpaceOps 2014 Conference*, 1797.

[127] Elgohary, T. A., Turner, J. D., Junkins, J. L. (2015). Analytic transfer functions for the dynamics & control of flexible rotating spacecraft performing large angle maneuvers, *J. Astronaut. Sci.*, **62**, 168–195.

[128] Junkins, J. L., Kim, Y. (1993). Mathematical models of flexible structures, *Introduction to Dynamics and Control of Flexible Structures*, 139–234.

[129] Kim, Y., Junkins, J., Kurdila, A. (1992). On the consequences of certain modeling approximations in dynamics and control of flexible space structures, *33rd Structures, Structural Dynamics and Materials Conference*, 2206.

[130] Zhang, X., Xu, W., Nair, S. (2004). Comparison of some modeling and control issues for a flexible two link manipulator, *ISA transactions*, **43(4)**, 509–525.

[131] Chen, W., Yu, Y., Zhao, X., Zhao, L., Sun, Q. (2011). Position control of a 2dof underactuated planar flexible manipulator, *Mechatronics and Automation (ICMA), 2011 International Conference on*, 464–469.

[132] Tokhi, M. O., Mohammed, Z. (2001). Dynamic characterisation of a flexible manipulator system, *Cambridge University Press*, **19(5)**, 571–580.

[133] Kanoh, H., Tzafestas, S., Lee, H. G., Kalat, J. (1986). Modelling and control of flexible robot arms, *Decision and Control, 1986 25th IEEE Conference on*, volume 25, 1866–1870.

[134] Zhang, X., Xu, W., Nair, S. (2004). Comparison of some modeling and control issues for a flexible two link manipulator, *ISA transactions*, **43(4)**, 509–525.

[135] Khorrami, F., Jain, S. (1993). Nonlinear control with end-point acceleration feedback for a two-link flexible manipulator: Experimental results, *Journal of Field Robotics*, **10(4)**, 505–530.

[136] Subudhi, B., Morris, A. S. (2002). Dynamic modelling, simulation and control of a manipulator with flexible links and joints, *Robot. Auton. Syst.*, **41(4)**, 257–270.

[137] Meirovitch, L. (1975). *Elements of vibration analysis*, McGraw-Hill.

[138] Fraser, A. R., Daniel, R. W. (2012). *Perturbation techniques for flexible manipulators*, volume 138, Springer Science & Business Media.

[139] Theodore, R. J., Ghosal, A. (1995). Comparison of the assumed modes and finite element models for flexible multilink manipulators, *Int. J. Robotics Res.*, **14(2)**, 91–111.

[140] Barbieri, E., Ozguner, U. (1988). Unconstrained and constrained mode expansions for a flexible slewing link, *American Control Conference, 1988*, 83–88.

[141] Hastings, G., Book, W. (1986). Verification of a linear dynamic model for flexible robotic manipulators, *Robotics and Automation. Proceedings. 1986 IEEE International Conference on*, volume 3, 1024–1029.

[142] Khairudin, M., Mohamed, Z., Husain, A., Mamat, R. (2014). Dynamic characterisation of a two-link flexible manipulator: theory and experiments, *Advances in robotics research*, **1(1)**, 61–79.

[143] Khan, L., Qamar, S., Khan, U. (2016). Adaptive pid control scheme for full car suspension control, *J. Chin. Inst. Eng.*, **39**, 169–185.

[144] Khan, L., Khan, M. U., Qamar, S. (2012). Comparative analysis of suspension systems using adaptive fuzzy control, *2012 4th International Conference on Intelligent and Advanced Systems (ICIAS2012)*, volume 1, 22–27.

[145] Khan, M. U., Kara, T. (2020). Adaptive control of a two-link flexible manipulator using a type-2 neural fuzzy system, *Arabian Journal for Science and Engineering*, **45(3)**, 1949–1960.

[146] Utkin, V., Guldner, J., Shi, J. (2009). *Sliding mode control in electro-mechanical systems*, CRC press.

[147] Liu, J. (2017). *Sliding Mode Control Using MATLAB*, Academic Press.

APPENDICES

APPENDIX A

STABILITY ANALYSIS OF SMANFC-2

Stability analysis of the control law is presented in this appendix. Using (2.7) in (2.8), (A.1) is obtained.

$$\dot{V} = S[f(\chi) + \frac{g(\chi)}{\hat{g}(\chi)}[-\hat{f}(\chi) - \sum_{i=1}^{n-1} \lambda_i e_{n-i+1} + \dot{\chi}_{dn} + \Upsilon] - \dot{\chi}_{dn} + \sum_{i=1}^{n-1} \lambda_i e_{n-i+1}] \tag{A.1}$$

Using $-\hat{f}(\chi) + \hat{f}(\chi)$ in (A.1) gives,

$$\begin{aligned}\dot{V} =& S[f(\chi) - \hat{f}(\chi) + \hat{f}(\chi) + \frac{g(\chi)}{\hat{g}(\chi)}[-\hat{f}(\chi) - \sum_{i=1}^{n-1} \lambda_i e_{n-i+1} + \dot{\chi}_{dn} + \Upsilon] - \dot{\chi}_{dn} \\ &+ \sum_{i=1}^{n-1} \lambda_i e_{n-i+1}]\end{aligned} \tag{A.2}$$

and

$$\begin{aligned}=& S[f(\chi) - \hat{f}(\chi) + \hat{f}(\chi) - \frac{g(\chi)}{\hat{g}(\chi)}\hat{f}(\chi) - \frac{g(\chi)}{\hat{g}(\chi)} \sum_{i=1}^{n-1} \lambda_i e_{n-i+1} + \frac{g(\chi)}{\hat{g}(\chi)}\dot{\chi}_{dn} \\ &+ \frac{g(\chi)}{\hat{g}(\chi)}\Upsilon - \dot{\chi}_{dn} + \sum_{i=1}^{n-1} \lambda_i e_{n-i+1}\end{aligned} \tag{A.3}$$

$$\begin{aligned}&= S[f(\chi) - \hat{f}(\chi) + \frac{\hat{f}(\chi)}{\hat{g}(\chi)}[\hat{g}(\chi) - g(\chi)] + \frac{\dot{\chi}_{dn} - \sum_{i=1}^{n-1} \lambda_i e_{n-i+1}}{\hat{g}(\chi)}(g(\chi) - \hat{g}(\chi)) \\ &+ \frac{g(\chi)}{\hat{g}(\chi)}\Upsilon]\end{aligned} \tag{A.4}$$

The purpose of the above mathematical steps are to write equation in form of $f(\chi) - \hat{f}(\chi)$ and $g(\chi) - \hat{g}(\chi)$. From the Remark 2.2.3,

$$\left| f - \hat{f} \right| < F, \quad |g - \hat{g}| < G \tag{A.5}$$

Considering (A.5) and $\Upsilon = -K\ |u^*|\ sgn(S)$, (A.4) is reformulated as,

$$\dot{V} \leq S \left[F + \frac{\hat{f}}{\hat{g}} G + \frac{\dot{\chi}_{dn} - \sum_{i=1}^{n-1} \lambda_i e_{n-i+1}}{\hat{g}} G - \frac{g}{\hat{g}} K\ |u^*|\ sgn(S) \right] \tag{A.6}$$

and

$$\dot{V} \leq |S| \left[F + \left| \frac{\hat{f}}{\hat{g}} \right| G + \frac{\left| \dot{\chi}_{dn} - \sum_{i=1}^{n-1} \lambda_i e_{n-i+1} \right|}{|\hat{g}|} G - \frac{g}{\hat{g}} K\ |u^*| \right] \tag{A.7}$$

Given that the identification errors are adequately small (A.5), the strictly positive definite assumption of g (Assumption 2.2.1), and that $K\ |u^*|$ is positive and greater than the other terms in (A.7), ensures that $\dot{V}$ is negative definite.

$$\dot{V} \leq -\varpi\, |S| \tag{A.8}$$

where ϖ is a positive number. The equation (A.8) implies that, by the Lyapunov stability theory, the process trajectories reach the sliding surface at a finite time and, taking into account the sliding surface (2.3), the tracking error asymptotically converges to zero and, as a result, the system's state variables follow the desired trajectory.

APPENDIX B

MHS ALGORITHM MATHEMATICAL PROOFS

This appendix presents sufficient descent condition, global convergence and result of the proposed control scheme algorithm.

B.1 Sufficient Descent Condition

Proof of Theorem 2.2.1 For all $\kappa > 1$, the following two cases are considered from (2.36),

Case (i):

If $\frac{\varphi(k)^T\psi(\kappa-1)}{\eta(k-1)^T\psi(\kappa-1)} \leq \iota\frac{\varphi(k)^T\eta(\kappa-1)}{\|\eta(\kappa-1)\|^2}$, then $\beta(\kappa) = 0$ (2.37) and therefore $\eta(\kappa)^T\varphi(\kappa) = -\|\varphi(\kappa)\|^2$.

Case (ii):

If $\frac{\varphi(k)^T\psi(\kappa-1)}{\eta(k-1)^T\psi(\kappa-1)} > \iota\frac{\varphi(k)^T\eta(\kappa-1)}{\|\eta(\kappa-1)\|^2}$, then using this condition, multiplying (2.36) by $\varphi(\kappa)^T$ and using (2.37) gives,

$$\varphi(\kappa)^T\eta(\kappa) = -\|\varphi(\kappa)\|^2 + \beta(\kappa)\varphi(\kappa)^T\eta(\kappa-1) \tag{B.1}$$

$$= -\|\varphi(\kappa)\|^2 + \frac{\varphi(k)^T\psi(\kappa-1)}{\eta(k-1)^T\psi(\kappa-1)}\varphi(\kappa)^T\eta(\kappa-1) - \iota\frac{\varphi(k)^T\eta(\kappa-1)}{\|\eta(\kappa-1)\|^2}\varphi(\kappa)^T\eta(\kappa-1) \tag{B.2}$$

It is observed that, (B.2) can be written in the form of the quadratic formula.

For this purpose putting $\frac{\|\varphi(k)\|^2}{4\iota}$ in (B.2). Consider (B.2),

$$= - \|\varphi(\kappa)\|^2 + \frac{\|\varphi(k)\|^2}{4\iota} - \frac{\|\varphi(k)\|^2}{4\iota} + \frac{\varphi(k)^T\psi(\kappa-1)}{\eta(k-1)^T\psi(\kappa-1)}\varphi(\kappa)^T\eta(\kappa-1)$$
$$- \iota\frac{\varphi(k)^T\eta(\kappa-1)}{\|\eta(\kappa-1)\|^2}\varphi(\kappa)^T\eta(\kappa-1) \tag{B.3}$$

and

$$= - \left(1 - \frac{1}{4\iota}\right)\|\varphi(\kappa)\|^2 - \frac{\|\varphi(k)\|^2}{4\iota} + \frac{\varphi(k)^T\psi(\kappa-1)}{\eta(k-1)^T\psi(\kappa-1)}\varphi(\kappa)^T\eta(\kappa-1)$$
$$- \iota\frac{\varphi(k)^T\eta(\kappa-1)}{\|\eta(\kappa-1)\|^2}\varphi(\kappa)^T\eta(\kappa-1) \tag{B.4}$$

Using $\hbar = \sqrt{\iota}\frac{\left(\varphi(k)^T\eta(k-1)\right)}{\|\eta(k-1)\|}$ and $\bar{\psi} = \frac{\|\varphi(k)\|}{2\sqrt{\iota}}$. This gives, from (B.4)

$$\eta(\kappa)^T\varphi(\kappa) \leq - \left(1 - \frac{1}{4\iota}\right)\|\varphi(\kappa)\|^2 + (-\bar{\psi}^2 + 2\bar{\psi}\hbar - \hbar^2) \tag{B.5}$$

The inequality $\bar{\psi}^2 + \hbar^2 \geq 2\bar{\psi}\hbar$ ensures that (B.5) is satisfied and it completes the proof.

B.2 Global Convergence

Proof of Theorem 2.2.2 From (2.36), the following two cases are considered to prove the theorem.

Case (i):

If $\left|\varphi(k)^T\psi(k-1)\right| \geq \rho\|\varphi(k)\|$, then $\|\eta_\kappa\| = \|\varphi_\kappa\|$ holds.

Case (ii):

If $\left|\varphi(k)^T\psi(k-1)\right| < \rho\|\varphi(k)\|$,

From (2.37)

$$\bar{\beta}(\kappa) = \frac{\varphi(\kappa)^T\psi(\kappa-1)}{\eta(k-1)^T\psi(\kappa-1)} + \iota\frac{\varphi(\kappa)^T\eta(\kappa-1)}{\|\eta(\kappa-1)\|^2} \tag{B.6}$$

then using $\left|\varphi(k)^T\psi(k-1)\right| < \rho\left\|\varphi(k)\right\|$, (B.6) and the Cauchy-Schwarz inequality [87] gives,

$$|\beta(\kappa)| \leq \bar{\beta}(\kappa) \tag{B.7}$$

$$\leq \frac{\varphi(\kappa)^T\psi(\kappa-1)}{\eta(k-1)^T\psi(\kappa-1)} + \iota\frac{\varphi(\kappa)^T\eta(\kappa-1)}{\left\|\eta(\kappa-1)\right\|^2} \tag{B.8}$$

$$\leq \frac{\left\|\varphi(\kappa)\right\|}{\left\|\eta(\kappa-1)\right\|}\left[1+\iota\right] \tag{B.9}$$

Using (2.36) and (B.9) gives,

$$\left\|\eta(\kappa)\right\| \leq \left\|\varphi(\kappa)\right\| + |\beta(\kappa)|\left\|\eta(\kappa-1)\right\| \tag{B.10}$$

$$\leq \left\|\varphi(\kappa)\right\| + \left|\frac{\varphi(\kappa)}{\left\|\eta(\kappa-1)\right\|}\left[1+\iota\right]\right|\left\|\eta(\kappa-1)\right\| \tag{B.11}$$

$$\leq \left\|\varphi(\kappa)\right\|\left[2+\iota\right] \tag{B.12}$$

Letting $\bar{o} = 2+\iota$, the proof is completed.

B.3 Convergence Result

Proof of Theorem 2.2.3 The Zoutendijk condition defined by (B.13) is used to prove the theorem.

$$\sum_{\kappa\geq 1}\frac{\left(\varphi(\kappa)^T\eta(\kappa)\right)^2}{\left\|\eta(\kappa)\right\|^2} < \infty \tag{B.13}$$

Suppose if (2.41) does not hold, then there exists a constant $\varepsilon > 0$, so that

$$\left\|\varphi(\kappa)\right\| \geq \varepsilon, \forall\ \kappa \in N \tag{B.14}$$

Using the inequalities from (2.39), (2.40) and (B.13) gives (B.15),

$$\sum_{\kappa\geq 1}(\bar{o})^{-2}\left\|\varphi(\kappa)\right\|^2 \leq \sum_{\kappa\geq 1}\frac{\left\|\varphi(\kappa)\right\|^4}{\left\|\eta(\kappa)\right\|^2} < \bar{h}^{-2}\sum_{\kappa\geq 1}\frac{\left(\varphi(\kappa)^T\eta(\kappa)\right)^2}{\left\|\eta(\kappa)\right\|^2} < \infty \tag{B.15}$$

Where $\bar{h} = \left(1-\frac{1}{4\iota}\right)$. Using (2.39) in (B.13), the middle term is evaluated and later with (2.40) the left most term. This is general CG algorithm proof [87, 90], which is valid if the algorithm satisfies the sufficient descent condition and global convergence properties. Taken into account the Assumption 2.2.2, (B.15) states that $\lim_{\kappa\to\infty}\left\|\varphi(\kappa)\right\| = 0$, which contradicts (B.14), and therefore proves the theorem.

APPENDIX C

SIMULATION MODELS

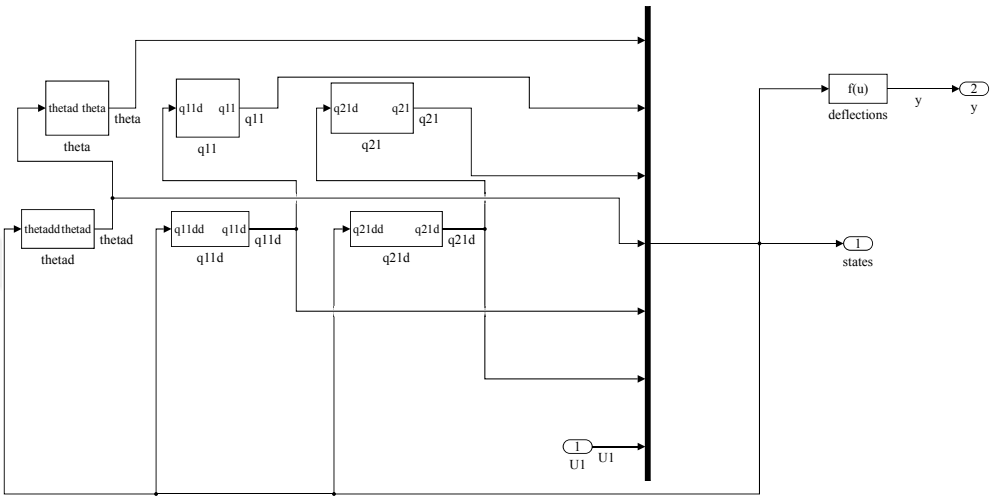

Figure C.1 RSTFA in simulation model diagram

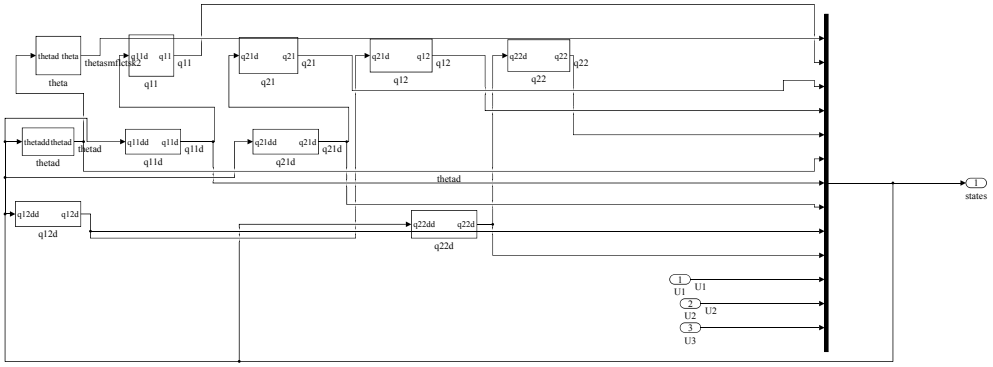

Figure C.2 RSFFA in simulation model diagram

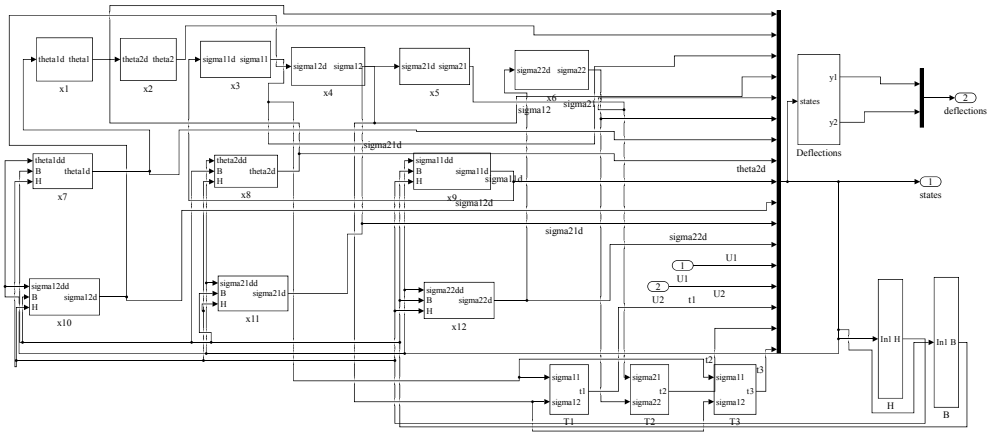

Figure C.3 TLFM in simulation model diagram

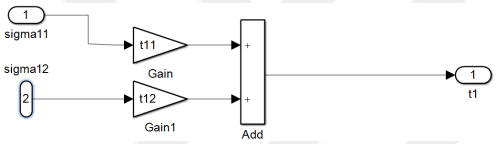

(a) T1 module of TLFM

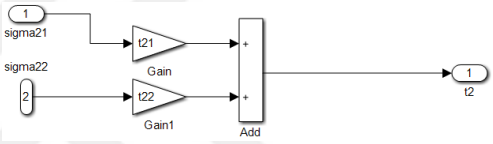

(b) T2 module of TLFM

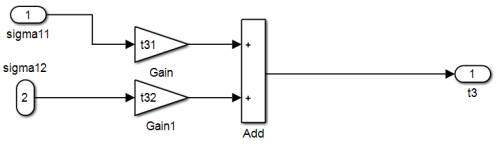

(c) T3 module of TLFM

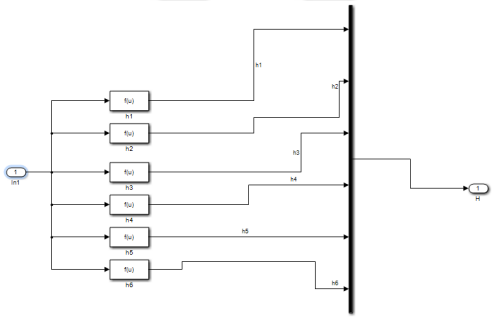

(d) H module of TLFM

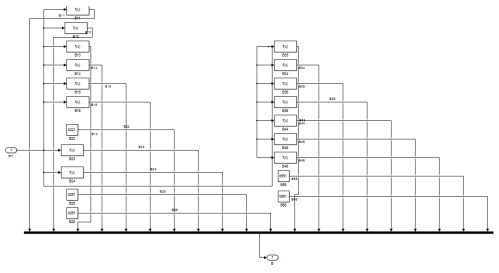

(e) B module of TLFM

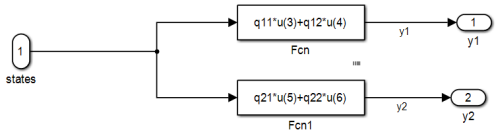

(f) Deflections module of TLFM

Figure C.4 Modules used in TLFM

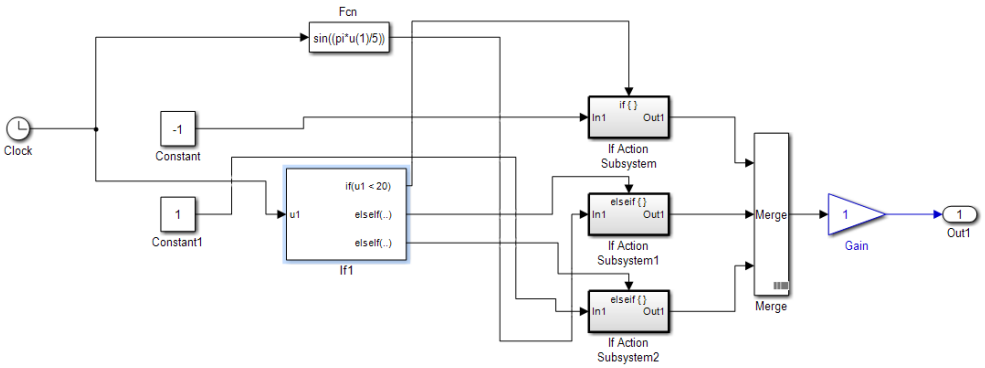

Figure C.5 Desired response

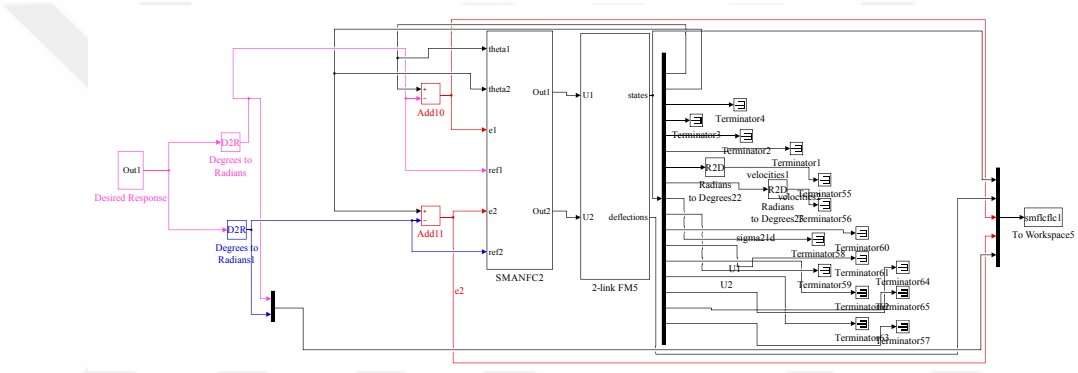

Figure C.6 Control scheme with the nonlinear system

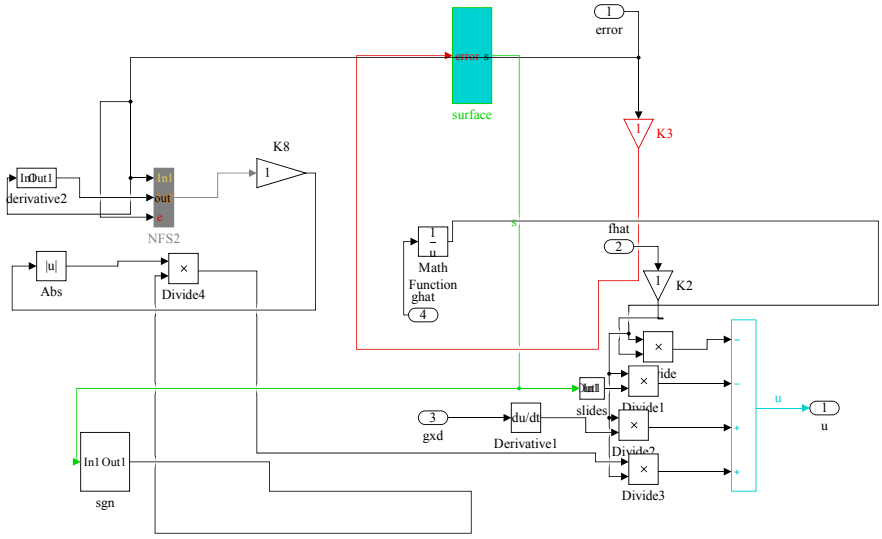

Figure C.7 Control law module

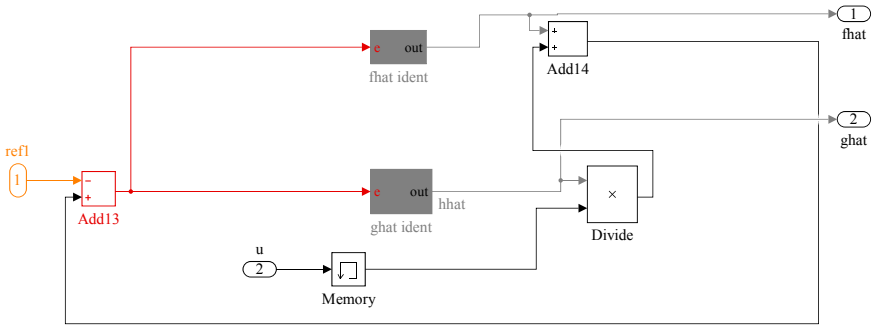

Figure C.8 Identification module

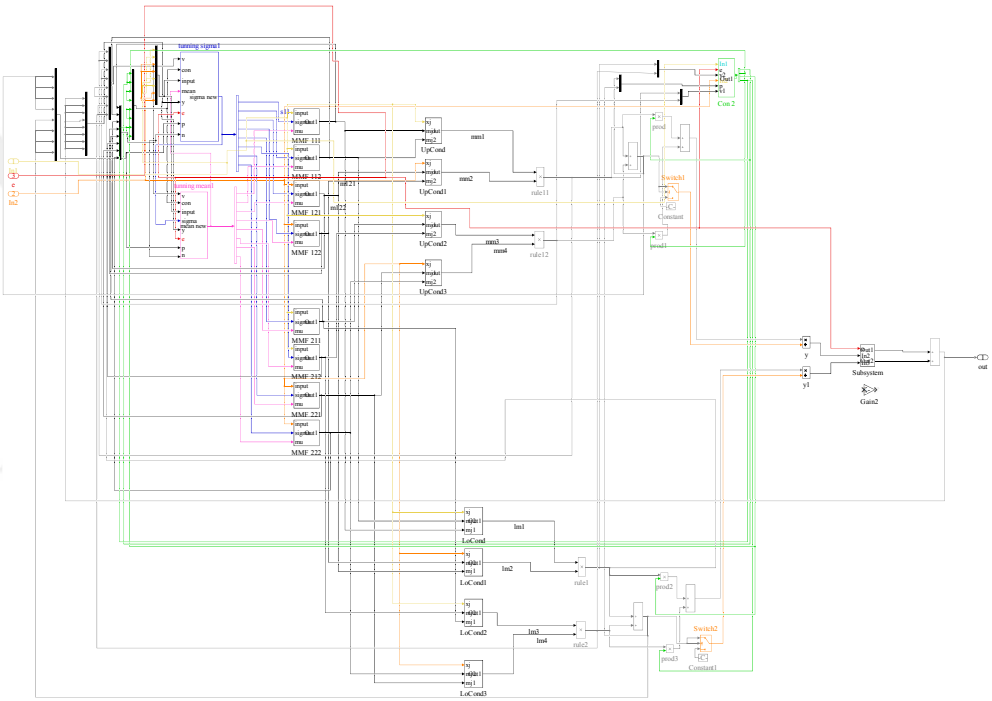

Figure C.9 ANFCT2 internal structure

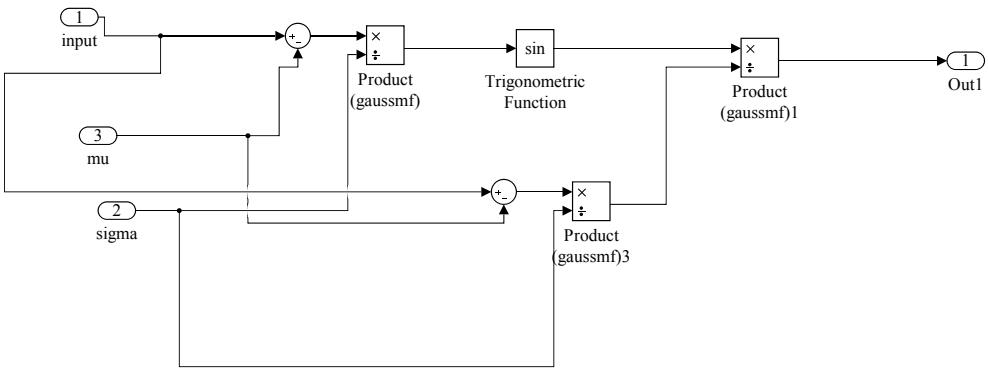

Figure C.10 Sinc membership function

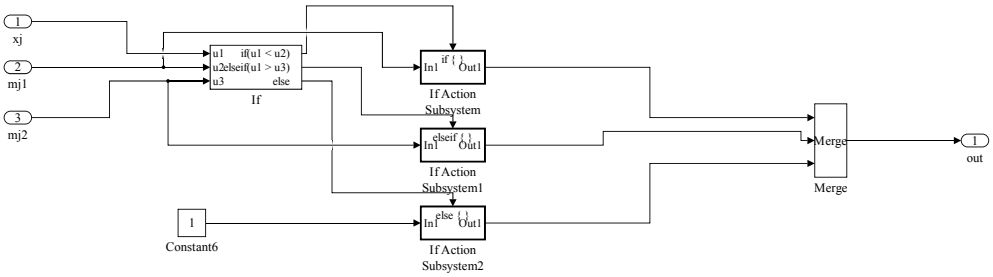

Figure C.11 Membership switching

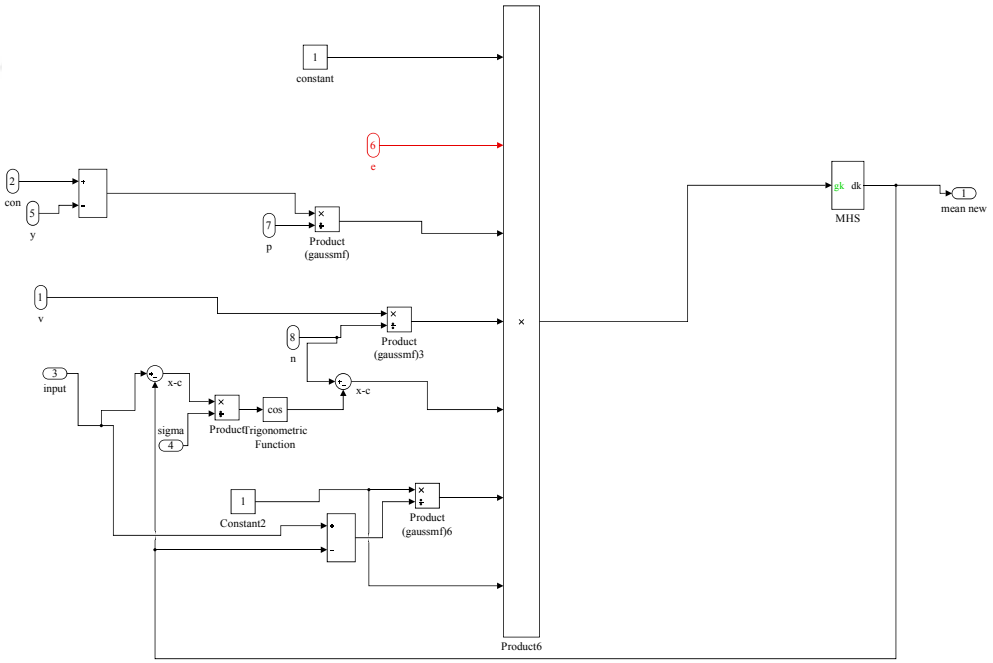

Figure C.12 Membership mean update module

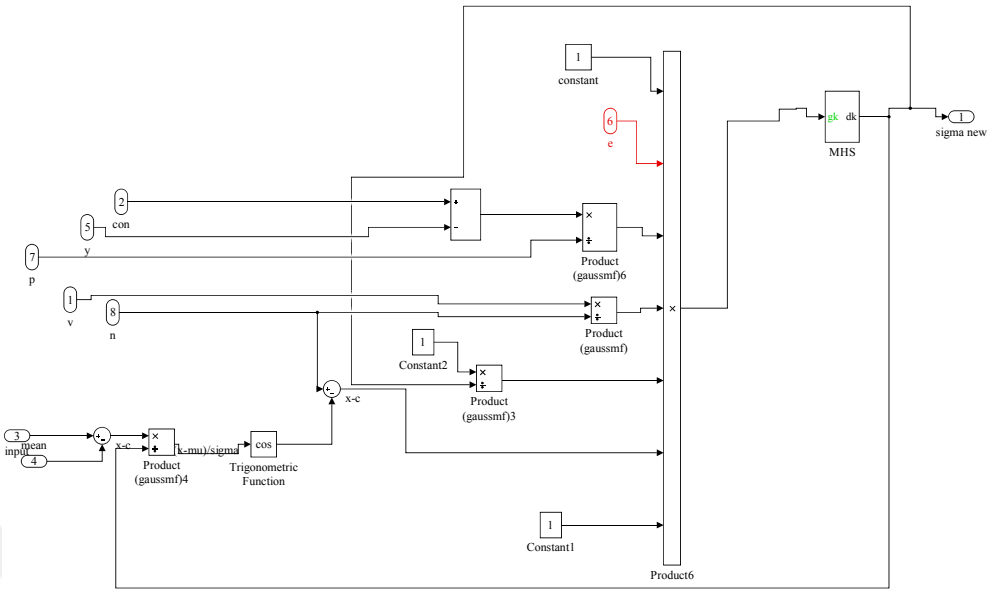

Figure C.13 Membership variance update module

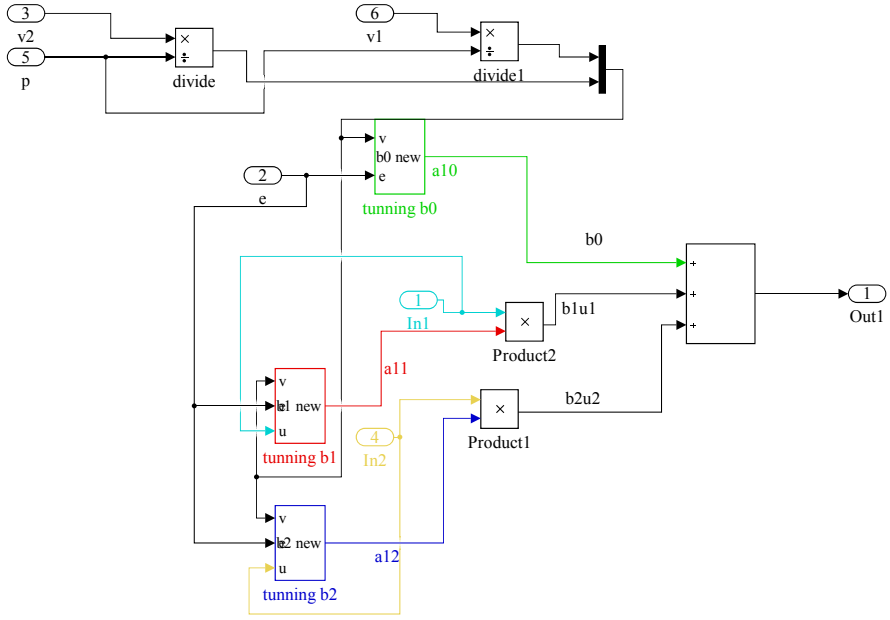

Figure C.14 Consequent parameters update module

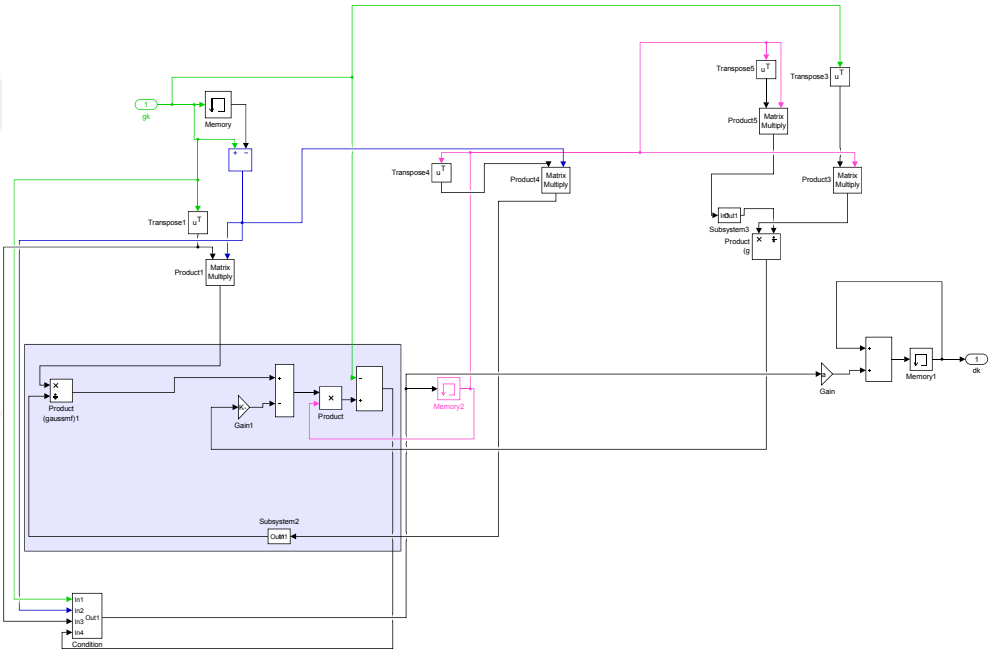

Figure C.15 MHS algorithm

CURRICULUM VITAE

PERSONAL INFORMATION

Surname, Name	KHAN, Muhammad Umair
Nationality	Pakistan
Date and Place of Birth	20 August 1987, Pakistan
Phone	+905538015446
Email	engr.m.umair.khan@gmail.com
Foreign Languages	English, Urdu/Hindi, Turkish

EDUCATION

Degree	University	Year of Graduation
MS	COMSATS University Islamabad, Abbottabad Campus, Pakistan	2010
BS	COMSATS University Islamabad, Abbottabad Campus, Pakistan	2008

WORK EXPERIENCE

Position	Place	Year
Lecturer	COMSATS University Islamabad, Abbottabad Campus, Pakistan	2011–2014

PUBLICATIONS

- Khan, M. U. , Kara, T. (2020). Adaptive type-2 neural fuzzy sliding mode control of a class of nonlinear systems, *Nonlinear Dynamics, Springer*, https://doi.org/10.1007/s11071-020-05877-z. (From Ph.D. study).

- Khan, M. U., Kara, T. (2020). Adaptive control of a two-link flexible manipulator using a type-2 neural fuzzy system, *Arabian Journal for Science and Engineering, Springer*, **45(3)**, 1949-1960, (From Ph.D. study).

- Khan, M. U., Kara, T. (2019). An adaptive neural fuzzy sliding mode control scheme for rotational maneuvering and vibration suppression of a flexible spacecraft, *3rd International Symposium on Multidisciplinary Studies and Innovative Technologies (ISMSIT)*, 1-6, (From Ph.D. study).

- Khan, M. U., Kara, T. (2019). An adaptive neural fuzzy control scheme for rotational maneuvering and vibration suppression of a flexible satellite system, *International Artificial Intelligence and Data Processing Symposium (IDAP)*, 1-6, (From Ph.D. study).

- Khan, L., Qamar, S., Khan, M. U. (2016). Adaptive PID control scheme for full car suspension control, *Journal of the Chinese Institute of Engineers, Taylor & Francis*, **39(2)**, 169–185, (Before Ph.D. study).

- Khan, L., Qamar, S., Khan, M. U. (2014). Comparative analysis of adaptive NeuroFuzzy control techniques for full car active suspension system, *Arabian Journal for Science and Engineering, Springer*, **39(3)**, 2045–2069, (Before Ph.D. study).

- Khan, L., Khan, M. U., Qamar, S. (2012). Comparative analysis of sus-

pension systems using adaptive fuzzy control, *4th International Conference on Intelligent , Advanced Systems (ICIAS), IEEE*, 22–27, (Before Ph.D. study).

- Khan, L., Qamar, S., Khan, M. U. (2012). Active suspension control based on adaptive wavelets neuro-fuzzy strategy, *15th International Multitopic Conference (INMIC), IEEE*, 89–96, (Before Ph.D. study).

- Khan, L., Qamar, S., Khan, M. U. (2012). Neuro-fuzzy wavelets based network for full car active suspension system, *International Conference on Emerging Technologies (ICET), IEEE*, 1–6, (Before Ph.D. study).

- Khan, L., Qamar, S., Khan, M. U. (2012). Adaptive wavelets based fuzzy nn control for active suspension model, *International Multi Topic Conference, IEEE*, 249–260, (Before Ph.D. study).

INDEX